



TECHNICAL REPORT

**Smart Body Area Network (SmartBAN);
Measurements and modelling of SmartBAN
Radio Frequency (RF) environment**

Reference

RTR/SmartBAN-0020

Keywords

MAC, measurement, network

ETSI

650 Route des Lucioles
F-06921 Sophia Antipolis Cedex - FRANCE

Tel.: +33 4 92 94 42 00 Fax: +33 4 93 65 47 16

Siret N° 348 623 562 00017 - APE 7112B
Association à but non lucratif enregistrée à la
Sous-Préfecture de Grasse (06) N° w061004871

Important notice

The present document can be downloaded from:

<http://www.etsi.org/standards-search>

The present document may be made available in electronic versions and/or in print. The content of any electronic and/or print versions of the present document shall not be modified without the prior written authorization of ETSI. In case of any existing or perceived difference in contents between such versions and/or in print, the prevailing version of an ETSI deliverable is the one made publicly available in PDF format at www.etsi.org/deliver.

Users of the present document should be aware that the document may be subject to revision or change of status.

Information on the current status of this and other ETSI documents is available at

<https://portal.etsi.org/TB/ETSIDeliverableStatus.aspx>

If you find errors in the present document, please send your comment to one of the following services:

<https://portal.etsi.org/People/CommitteeSupportStaff.aspx>

Notice of disclaimer & limitation of liability

The information provided in the present deliverable is directed solely to professionals who have the appropriate degree of experience to understand and interpret its content in accordance with generally accepted engineering or other professional standard and applicable regulations.

No recommendation as to products and services or vendors is made or should be implied.

No representation or warranty is made that this deliverable is technically accurate or sufficient or conforms to any law and/or governmental rule and/or regulation and further, no representation or warranty is made of merchantability or fitness for any particular purpose or against infringement of intellectual property rights.

In no event shall ETSI be held liable for loss of profits or any other incidental or consequential damages.

Any software contained in this deliverable is provided "AS IS" with no warranties, express or implied, including but not limited to, the warranties of merchantability, fitness for a particular purpose and non-infringement of intellectual property rights and ETSI shall not be held liable in any event for any damages whatsoever (including, without limitation, damages for loss of profits, business interruption, loss of information, or any other pecuniary loss) arising out of or related to the use of or inability to use the software.

Copyright Notification

No part may be reproduced or utilized in any form or by any means, electronic or mechanical, including photocopying and microfilm except as authorized by written permission of ETSI.

The content of the PDF version shall not be modified without the written authorization of ETSI.

The copyright and the foregoing restriction extend to reproduction in all media.

© ETSI 2021.

All rights reserved.

Contents

Intellectual Property Rights	5
Foreword.....	5
Modal verbs terminology.....	5
1 Scope	6
2 References	6
2.1 Normative references	6
2.2 Informative references.....	6
3 Definition of terms, symbols and abbreviations.....	8
3.1 Terms.....	8
3.2 Symbols.....	8
3.3 Abbreviations	9
4 Introduction and Background.....	11
5 Coexistence	11
5.0 Introduction	11
5.1 Bands.....	12
6 Measurements.....	12
6.1 Background & Motivation.....	12
6.2 Spectrum Occupancy Evaluations (SOEs)	13
6.3 Measurement Campaigns	15
6.3.0 Introduction.....	15
6.3.1 Measurement campaigns in Oulu, Finland	15
6.3.1.0 Introduction.....	15
6.3.1.1 Daily Surgery SOEs (Campaign 1)	15
6.3.1.2 Accident & Emergency Ward SOEs (Campaign 2)	25
6.3.1.3 X-Ray & Radiology Ward SOEs (Campaign 3).....	31
6.3.2 Analytical Stochastic Model for Spectrum Occupancy	33
6.3.3 Extracting Mathematical Interference model.....	36
6.3.4 Measurement Campaigns in Florence, Italy	39
6.3.4.0 Introduction.....	39
6.3.4.1 Occupancy.....	40
6.3.4.1.0 Introduction	40
6.3.4.1.1 Percentiles	41
6.3.4.2 PDF	42
6.3.4.3 Interference as a function of time and frequency	43
6.3.4.4 Parameters characterizing the distribution	44
6.3.4.5 Home and office environments	44
6.3.4.6 Extract the mathematical model.....	47
6.3.4.6.0 Introduction	47
6.3.4.6.1 First results of CNIT-UNIFI.....	47
6.4 Statistical model of the interference	55
6.4.0 Introduction.....	55
6.4.1 Cluster dimension	56
6.4.2 Inter-arrival time.....	57
6.4.3 Interfering cluster amplitude.....	60
6.4.4 Conclusions.....	62
6.5 Extracting the mathematical model of the interference	62
6.6 Further investigations: a more accurate statistical model of the interference.....	71
6.6.0 Introduction.....	71
6.6.1 Accurate statistical models of the interference	71
6.6.1.0 Introduction.....	71
6.6.1.1 Time-Frequency Statistical Model of the Interference	72
6.6.1.2 Cluster-Based Statistical Model of the Interference.....	74

7	SmartBAN communication system simulator	76
7.0	Introduction	76
7.1	Getting started	76
7.2	Simulator model	80
7.2.0	Introduction.....	80
7.2.1	Node.....	80
7.3	Hub.....	80
7.3.0	Introduction.....	80
7.3.1	Simulation parameters	81
7.4	PHY layer	82
7.4.0	Introduction.....	82
7.4.1	PHY transmitter	82
7.4.2	Channel, interference and noise	83
7.4.2.0	Introduction.....	83
7.4.2.1	Interference	83
7.4.3	PHY receiver	84
7.5	MAC - Frame retransmission	85
7.6	Verification results	87
8	Simulation results	87
8.0	Introduction	87
8.1	Simulation parameters	88
8.2	AWGN channel	88
8.3	Fading channel	90
8.4	Fading channel and interference.....	92
8.5	Discussion	94
Annex A:	Spatial Sample Clustering Algorithm	95
History		98

Intellectual Property Rights

Essential patents

IPRs essential or potentially essential to normative deliverables may have been declared to ETSI. The declarations pertaining to these essential IPRs, if any, are publicly available for **ETSI members and non-members**, and can be found in ETSI SR 000 314: "*Intellectual Property Rights (IPRs); Essential, or potentially Essential, IPRs notified to ETSI in respect of ETSI standards*", which is available from the ETSI Secretariat. Latest updates are available on the ETSI Web server (<https://ipr.etsi.org/>).

Pursuant to the ETSI Directives including the ETSI IPR Policy, no investigation regarding the essentiality of IPRs, including IPR searches, has been carried out by ETSI. No guarantee can be given as to the existence of other IPRs not referenced in ETSI SR 000 314 (or the updates on the ETSI Web server) which are, or may be, or may become, essential to the present document.

Trademarks

The present document may include trademarks and/or tradenames which are asserted and/or registered by their owners. ETSI claims no ownership of these except for any which are indicated as being the property of ETSI, and conveys no right to use or reproduce any trademark and/or tradename. Mention of those trademarks in the present document does not constitute an endorsement by ETSI of products, services or organizations associated with those trademarks.

DECT™, **PLUGTESTS™**, **UMTS™** and the ETSI logo are trademarks of ETSI registered for the benefit of its Members. **3GPP™** and **LTE™** are trademarks of ETSI registered for the benefit of its Members and of the 3GPP Organizational Partners. **oneM2M™** logo is a trademark of ETSI registered for the benefit of its Members and of the oneM2M Partners. **GSM®** and the GSM logo are trademarks registered and owned by the GSM Association.

BLUETOOTH® is trademark registered and owned by Bluetooth SIG, Inc.

Foreword

This Technical Report (TR) has been produced by ETSI Technical Committee Smart Body Area Network (SmartBAN).

Modal verbs terminology

In the present document "**should**", "**should not**", "**may**", "**need not**", "**will**", "**will not**", "**can**" and "**cannot**" are to be interpreted as described in clause 3.2 of the [ETSI Drafting Rules](#) (Verbal forms for the expression of provisions).

"**must**" and "**must not**" are **NOT** allowed in ETSI deliverables except when used in direct citation.

1 Scope

The present document specifies the state-of-the-art and the future investigations on coexistence for allowing Smart Body Area Network (SmartBAN) devices to properly work and co-operate in the Industrial, Scientific and Medical (ISM) band. Interference appears to be one of the major threats as well as coexistence with other existing systems radiating in the same portion of the frequency spectrum. The present document describes the coexistence measurements and analysis that need to be considered in order to specify the requirements for the SmartBAN compatible devices.

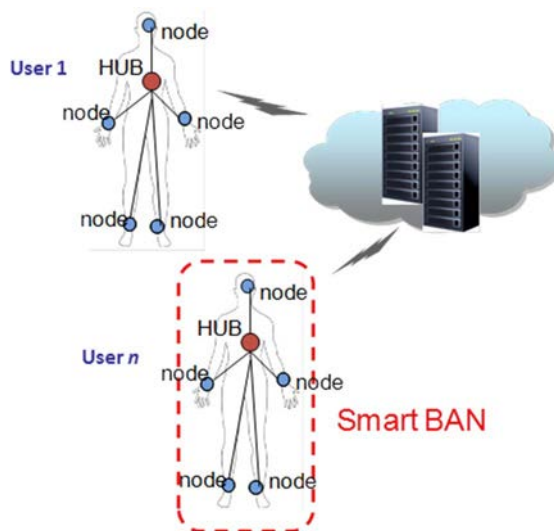


Figure 0: Scope of a SmartBAN

2 References

2.1 Normative references

Normative references are not applicable in the present document.

2.2 Informative references

References are either specific (identified by date of publication and/or edition number or version number) or non-specific. For specific references, only the cited version applies. For non-specific references, the latest version of the referenced document (including any amendments) applies.

NOTE: While any hyperlinks included in this clause were valid at the time of publication, ETSI cannot guarantee their long term validity.

The following referenced documents are not necessary for the application of the present document but they assist the user with regard to a particular subject area.

- [i.1] ETSI TS 103 326 (V1.1.1) (04-2015): "Smart Body Area Network (SmartBAN); Enhanced Ultra-Low Power Physical Layer".
- [i.2] Void.
- [i.3] IEEE 802.11™: "IEEE Standard for Information technology--Telecommunications and information exchange between systems Local and metropolitan area networks--Specific requirements Part 11: Wireless LAN Medium Access Control (MAC) and Physical Layer (PHY) Specifications".

- [i.4] Valenta, V. (2010): "Survey on spectrum utilization in Europe: Measurements, analyses and observations", 5th International Conference on Cognitive Radio Oriented Wireless Networks Communications.
- [i.5] ITU-R (2011): "ITU-R handbook for spectrum monitoring".
- [i.6] Recommendation ITU-R SM.2256: "Spectrum occupancy measurements and evaluation".
- [i.7] Recommendation ITU-R SM.2180 (2010): "Impact of ISM equipment on radio communication services".
- [i.8] Vuohtoniemi R., Virk M. H., Hämäläinen M., Iinatti J., & Mäkela J.-P. (2015): "Stochastic Spectral Occupancy Modeling: A Body Area Network Perspective in ISM Band", 9th International Symposium on Medical Information & Communication Technology (ISMICT). Kamakura, Japan.
- [i.9] J. J. Lehtomäki, e. a. (2012): "Energy detection based estimation of channel occupancy rate with adaptive noise estimation", IEICE Transactions on Communications.
- [i.10] Virk M. H., Vuohtoniemi R., Hämäläinen M., Iinatti J., & Mäkela J.-P. (2014): "Spectrum Occupancy Evaluations at 2.35-2.50 GHz ISM Band in a Hospital Environment", International Conference on Body Area Networks (BodyNets'14). London, UK.
- [i.11] ETSI TS 103 325 (2015): "Smart Body Area Network (SmartBAN); Low Complexity Medium Access Control (MAC) for SmartBAN".
- [i.12] MATLAB, Product help, R2011b.
- [i.13] Yazdandoost K.Y. and Sayrafian-Pour K.: "Channel Model for Body Area Network (BAN)" IEEE P802.15-08-0780-09-0006, 2009.
- [i.14] Proakis J.G.: "Digital Communications", McGraw-Hill, 2001.
- [i.15] Griffin A.: "Coding CPFSK for Differential Demodulation", University of Canterbury Christchurch, New Zealand, 2000.
- [i.16] IEEE 802.15.6™ (2012): "IEEE Standard for Local and metropolitan area networks -- Part 15.6: Wireless Body Area Networks".
- [i.17] Rahman M., Elbadry M. and Harjani R.: "An IEEE 802.15.6 Standard Compliant 2.5 nJ/Bit Multiband WBAN Transmitter Using Phase Multiplexing and Injection Locking" IEEE Journal of Solid-State Circuits, Vol. 50, No. 5, May 2015, pp. 1126 -1136.
- [i.18] L. Mucchi, R. Vuohtoniemi, H. Virk, A. Conti, Matti Hämäläinen, Jari Iinatti, and Moe Z. Win: "Spectrum Occupancy and Interference Model Based on Network Experimentation in Hospital", in IEEE Transactions on Wireless Communications, vol. 19, no. 9, pp. 5666-5675, September 2020, doi: 10.1109/TWC.2020.2995116.
- [i.19] P. C. Pinto and M. Z. Win, "Communication in a Poisson field of interferers-Part I: Interference distribution and error probability" in IEEE Transactions on Wireless Communications, vol. 9, no. 7, pp. 2176-2186, July 2010.
- [i.20] M. Z. Win and P. C. Pinto: "Communication in a Poisson field of interferers-Part II: Channel capacity and interference spectrum" in IEEE Transactions on Wireless Communications, vol. 9, no. 7, pp. 2187-2195, July 2010.
- [i.21] P. C. Pinto, A. Giorgetti, M. Z. Win, and M. Chiani: "A stochastic geometry approach to coexistence in heterogeneous wireless networks," IEEE Journal on Selected Areas in Communications, vol. 27, no. 7, pp. 1268-1282, September 2009.
- [i.22] A. Rabbachin, A. Conti, and M. Z. Win: "Wireless network intrinsic secrecy", IEEE/ACM Transactions on Networking, vol. 23, no. 1, pp. 56-69, February 2015.
- [i.23] M. Win, A. Rabbachin, J. Lee, and A. Conti: "Cognitive network secrecy with interference engineering", IEEE Network, vol. 28, no. 5, pp. 86-90, September 2014.

- [i.24] H. ElSawy, A. Sultan-Salem, M.-S. Alouini, and M. Z. Win: "Modeling and analysis of cellular networks using stochastic geometry: A tutorial", IEEE Communications Surveys and Tutorials, vol. 19, no. 1, pp. 167-203, 1st Quart., 2017.
- [i.25] G. E. P. Box, G. M. Jenkins, G. C. Reinsel, and G. M. Ljung, Time Series Analysis: "Forecasting and Control", 5th ed. Hoboken, NJ, USA: Wiley, 2015.
- [i.26] J. Lin: "Divergence measures based on the Shannon entropy", IEEE Transactions on Information Theory, vol. 37, no. 1, pp. 145-151, January 1991.
- [i.27] M. Sheppard. MIT Lincoln Laboratory. March 11, 2019.
- NOTE: Available at [FBD - "Find the Best Distribution" tool](#).
- [i.28] K. Krishnamoorthy, Handbook of Statistical Distributions With Applications, 2nd edition. Boca Raton, FL, USA: CRC, Press, 2016.
- [i.29] F. Zabini and A. Conti: "Inhomogeneous Poisson Sampling of Finite-Energy Signals With Uncertainties in Rd", IEEE Transaction on Signal Processing, vol. 64, iss. 18, pp. 4679-4694, 2016.
- [i.30] IEEE 802.11b™: "IEEE Standard for Information Technology -- Telecommunications and information exchange between systems - Local and Metropolitan networks -- Specific requirements -- Part 11: Wireless LAN Medium Access Control (MAC) and Physical Layer (PHY) specifications: Higher Speed Physical Layer (PHY) Extension in the 2.4 GHz band".
- [i.31] IEEE 802.11g™: "IEEE Standard for Information technology -- Local and metropolitan area networks -- Specific requirements -- Part 11: Wireless LAN Medium Access Control (MAC) and Physical Layer (PHY) Specifications: Further Higher Data Rate Extension in the 2.4 GHz Band".
- [i.32] IEEE 802.11n™: "IEEE Standard for Information technology -- Local and metropolitan area networks -- Specific requirements -- Part 11: Wireless LAN Medium Access Control (MAC) and Physical Layer (PHY) Specifications Amendment 5: Enhancements for Higher Throughput".

3 Definition of terms, symbols and abbreviations

3.1 Terms

Void.

3.2 Symbols

For the purposes of the present document, the following symbols apply:

C	Channel Number
$E_i, E(\cdot)$	Expected Value
f_c	Centre Frequency
H_0	Null hypothesis
H_1	Alternative Hypothesis
i	Channel Identifier
K	Number of Samples Collected from the Band in One Sweep
k	Shape Parameter
\hat{L}	Maximized Value Of Likelihood Function
n	Number of Samples Collected in the Channel
O_i	Observed Value
PFA_{DES}	Probability of False Alarm
$P(X_i(j))$	Sample Power j at Channel i
T	Number of Sweeps
T_{CME}	Threshold for Consecutive Mean Excision
t	Time

X	Sample Space
α	Significance Level
$\Gamma()$	Gamma Function
λ	Arrival Rate
μ	Location Parameter
σ	Scale Parameter
γ	Noise Threshold
ν	shape parameter
σ_k	The log-normal variance of the measured data between path loss and K-factor
σ_p	The log-normal variance in dB around the mean, representing the variations measured at different body and room locations.

NOTE: This parameter will depend on variations in the body curvature, tissue properties and antenna radiation properties at different body locations.

E_b/N_0	Energy per bit to noise power spectral density ratio
h	Modulation index
I_{dB}	Implementation losses in dB
K_0	The fit with measurement data for the K-factor for low path loss
K_{dB}	K factor of Ricean distribution in dB
L	Pulse length
L_{slot}	Length of slot
m	Numerator of modulation index
m_0	The average decay rate in dB/cm for the surface wave travelling around the perimeter of the body
m_k	The slope of the linear correlation between path loss and K-factor
M	M-ary number
NF_{dB}	Noise Figure in dB
n_k	Zero mean and unit variance Gaussian random variable
n_p	Zero mean and unit variance Gaussian random variable
p	Denominator of modulation index
P_0	The average loss close to the antenna
P_1	The average attenuation of components in an indoor environment radiated away from the body and reflected back towards the receiving antenna
P_b	Bit error probability
PL_{dB}	Path loss in dB
$PPDU_{rep}$	Times of PPDU repetition
$Q()$	Q function
R	Data rate
S_{dBm}	Receiver sensitivity
T_{min}	T_s/L_{slot}

3.3 Abbreviations

For the purposes of the present document, the following abbreviations apply:

ACK	ACKnowledgement
AIC	Akaike Information Criterion
ANL	Average Noise Level
ARA	Antenna Research Associate
AWGN	Additive White Gaussian Noise
BAN	Body Area Network
BCH	Bose, Chaudhuri, and Hocquenghem
BER	Bit Error Rate
BIC	Bayesian Information Criterion
BLE	Bluetooth® Low Energy
BPF	Bandpass Filter
BT	Bluetooth®
CCA	Clear Channel Assessment
CCA-ED	Clear Channel Assessment based on Energy Detection
CDF	Cumulative Distribution Function
CM	Channel Model
CO	Channel Occupancy

CSRR	Clean Sample Rejection Rate
DSSS	Direct Sequence Spread Spectrum
ED	Energy Detection
EGC	Equal Gain Combining
FBO	Frequency Band Occupancy
FCME	Forward Consecutive Mean Excision
FER	Frame Error Rate
FH	Frequency Hopping
GEV	Generalized Extreme Value
GEVD	Generalized Extreme Value Distribution
GFSK	Gaussian Frequency Shift Keying
HI	High Interference
ICT	Information and Communication Technology
ISM	Industrial, Scientific and Medical
ITU-R	International Telecommunication Union - Radio communication sector
JPG	Joint Photographic experts Group
JSD	Jensen-Shannon Divergence
KS	Kolmogorov-Smirnov
LI	Low Interference
LNA	Low Noise Amplifier
LTE	Long Term Evolution
MAC	Medium Access Control
MATLAB	Matrix Laboratory

NOTE: A multi-paradigm numerical computing environment and fourth-generation programming language. A proprietary programming language developed by MathWorks™.

MC	Measurement Campaign
Med-FCME	Median Forward Consecutive Mean Excision
ML	Maximum Likelihood
MLE	Maximum Likelihood Estimate
MLSD	Maximum-Likelihood Sequence Detector
MPDU	MAC Protocol Data Unit
MRI	Magnetic Resonance Imaging
OBW	Occupied BandWidth
OFDM	Orthogonal Frequency Division Multiplexing
OYS	Oulun Yliopistollinen Sairaala (Oulu University Hospital)
PDF	Probability Distribution Function
PHY	PHYSical layer
PLCP	Physical Layer Convergence Procedure
PMF	Probability Mass Function
PPDU	Physical-layer Protocol Data Unit
PSDU	Physical-layer Service Data Unit
RBW	Resolution BandWidth
RF	Radio Frequency
RV	Random Variable
SA	Spectrum Analyser
SNR	Signal-to-Noise Ratio
SOE	Spectrum Occupancy Evaluation
SRO	Spectrum Resource Occupancy
SSC	Spatial Sample Clustering
TC	Technical Committee
TCME	Threshold for Consecutive Mean Excision
TLSD	t Location-Scale Distribution
TS	Technical Specification
UHF	Ultra High Frequency
UWB	Ultra WideBand
WBAN	Wireless Body Area Network
WLAN	Wireless Local Area Network
WPAN	Wireless Personal Area Networks

4 Introduction and Background

Modern medical and health monitoring equipment is moving towards the trend of wireless connectivity between the data collection or control centre and the medical devices or sensors. Therefore, the need for standardized communication interfaces and protocols between the actors is required. This network of actors performing some medical monitoring or functions in this context is called a Smart Body Area Network (SmartBAN).

Most emerging radio technologies for Wireless Personal Area Networks (WPAN) are designed to operate around the 2,4 GHz ISM band. Since both standardized (such as Bluetooth® and IEEE 802.11 [i.3]) and non-standardized (proprietary) devices use the same frequency band, interference may lead to significant performance degradation of medical (and other) devices operating in the band. The main goal of the present document is to describe the interference problem and to highlight a coexistence framework for the medical Information and Communication Technology (ICT) to operate in a proximal environment. In the present document, a synthesis of the problem of interference and coexistence around the 2,4 GHz ISM band is given. Measurements carried out in hospital and campus will be described in order to have a better insight on the problem. Then, the measurement campaigns exhaustively accumulated data in order to formulate a mathematical model of the interference at the channel in the 2,36 to 2,5 GHz band will be described.

5 Coexistence

5.0 Introduction

A number of use cases have been identified as potential scenarios for SmartBAN. These use cases serve as scenarios where real channel occupancy measurements are needed. The environments to be considered for investigating the coexistence issues are such as:

- Hospital
- Home
- Office
- Outdoor

These cases include the typical environments where a patient wearing a SmartBAN system lives and stays. However, the present document is focusing on indoor environments only.

Moreover, existing interferers are classified into two classes based on their usage of the spectrum. Devices implementing the Direct Sequence Spread Spectrum (DSSS) technique constitute one class of interferers that utilize a fixed channel in the band. Typically this channel is 22 MHz wide, although the width of the signal depends on the transmitter's implementation. The second class of interferers is represented by devices implementing a type of Frequency Hopping (FH) mechanism. Note that the IEEE 802.11 [i.3] specifications include a frequency hopping technique that uses a deterministic frequency pattern. On the other hand, the Bluetooth® specifications define a pseudo-random frequency sequence based on the Bluetooth device's address and its internal clock. While interference among systems from the same type, such as Bluetooth on Bluetooth, or IEEE 802.11 [i.3] on IEEE 802.11 [i.3], interference can be significant, it is usually considered early on in the design stages of the protocol (phenomena is called as multiuser interference). A third class can be included, which comprehend the devices using the Orthogonal Frequency Division Multiplexing (OFDM) technique. Therefore, the worst realistic interference scenario consists of a mix of heterogeneous devices, i.e. devices belonging to different classes.

In evaluating the performance with respect to coexistence issues, variations in the operational environment need to be considered, including both the characteristics of the interfering wireless services and the Radio Frequency (RF) propagation characteristics. This ensures that the evaluation takes into account the uncertainty in an installation's location and in the interfering traffic. Evaluating the performance requirements in terms of coexistence issues provides a method for quantifying the applications interference susceptibility and assists in establishing usage policies.

The analytical model for evaluating the coexistence in terms of the operational environment is developed based on the following process:

- Characterize the interference under static conditions, i.e. when both interfering and desired signals remain stationary. Empirical test results are used to estimate model parameters and to substantiate the model.
- Extract a mathematical model of the aggregate interference in all operational environments.

5.1 Bands

For coexistence purposes the typical interference levels are evaluated in the following bands:

- ISM band
- 30 MHz before the ISM band
- 30 MHz after the ISM band
- Option for UWB lower band

6 Measurements

6.1 Background & Motivation

Radio frequency is a finite resource coordinated by regulatory bodies all over the globe. For medical usage, varying regulations are imposed in different countries involving the allocation of various chunks of both licensed and unlicensed frequency resource [i.4]. Some of the license-free solutions include e.g. sub-gigahertz ISM band, 2,4 GHz ISM band and 3 GHz to 10 GHz ultrawide band, etc. [i.4]. 2,4 GHz ISM band is an unregulated, license-free frequency band where many communication technologies share the frequency resources, e.g. Wireless Local Area Networks (WLANs), Bluetooth® (BT), wireless sensor networks, cordless phones, etc. In a hospital environment, if a Wireless Body Area Network (WBAN) is planned to be deployed in the 2,4 GHz ISM band, it will require certain measures in order to co-exist with other wireless communication technologies.

ETSI SmartBAN Physical Layer (PHY) defines 40 channels in the 2,4 GHz ISM band, including 37 data channels and 3 control channels. Each channel is 2 MHz wide and no guard bands between two adjacent channels are defined [i.1]. There had been other considerations as well for PHY solutions, e.g. channels in 2,36 GHz to 2,40 GHz band, which has already been allocated for medical use in USA. However, in Europe, this particular band has been allocated for LTE special purpose use.

Increasing deployments of wireless technologies inside hospital premises will significantly increase the electromagnetic clutter in hospital environments and hence interference will be the limiting factor. Spectrum Occupancy Evaluations (SOEs) provide statistical quantification of spectrum utilization patterns and highlight temporal characteristics of the band under consideration. In essence, SOEs can also be used as a probe to reflect upon the degree to which a victim network would suffer under the influence of an aggressor. In other words, SOE can provide an insight regarding the opportunities a wireless network will have, causing presumably no interference to already existing networks. Yet another way to look at SOE is to study the suitability of a particular frequency band for the deployment of a new kind of network. In a nut-shell, it is highly motivating to perform SOEs in 2,36 GHz to 2,4 GHz band and 2,4 GHz ISM band in order to characterize aggregate interference which would potentially be harmful to ETSI SmartBAN compliant devices.

6.2 Spectrum Occupancy Evaluations (SOEs)

Generally, spectrum occupancy measurements involve the collection of measurement data, processing the measured data for occupancy assessment and development of models to characterize the spectrum utilization. The key factors influencing the measurements are measurement bandwidth span, channel bandwidths, number of channels, observation time per channel, revisit time to a specific channel, total duration of monitoring and statistical integration time if monitoring is sufficiently long. The International Telecommunication Union - Radio communication sector (ITU-R) guidelines for spectrum occupancy measurements are elaborated in a special handbook [i.5] and also in two short reports [i.7] and [i.6]. Stochastic parameters regarding spectrum occupancy evaluations include Channel Occupancy (CO), Frequency Band Occupancy (FBO) and Spectrum Resource Occupancy (SRO). Spectrum occupancy measurements usually involve:

- Spectrum sensing, utilizing an antenna coupled with a band pass filter and a spectrum analyser.
- Sample collection and saving the records in a hard disk drive.
- Processing and analysis of recorded data in order to calculate occupancies of interest.

Spectrum occupancy measurement handbook published by ITU-R [i.5] suggests to divide the sample space, i.e. one full record of the band (one sweep) into channels of the expected system, which is utilizing the spectrum resource. Then, each channel is searched for a number of samples above a predefined noise threshold. If more than 50 % of the samples in the channel are above a noise threshold, the channel is marked as occupied. In this way, individual Channel Occupancies (COs) are calculated for all the channels.

There are two more metrics which can also be calculated, Frequency Band Occupancy and Spectrum Resource Occupancy. FBO provides statistical information about how much the whole frequency band is used, independently of a particular system. SRO is a system-specific metric, which gives information about the utilization of resources available to a specific system [i.5]. After an intensive review of literature, it was found that there were propositions which lacked objectivity in relation to the fully unregulated band, like ISM, with so diverse access technologies. Even those studies which were performed especially for the ISM band could not grasp the whole picture.

For example:

- i) Many of the studies considered revisit time of more than a second for a span of more or less 100 MHz, which is impractical for bursty transmissions, and a large portion of the band might appear empty during observation. If a too fast revisit time is used, one might not get enough samples above the noise threshold in a certain channel to declare it occupied with enough confidence.
- ii) Another example of ambiguity is the channelization of the band under observation. A number of studies talked about ISM band but end up finding occupancies for WLAN only. Although ITU-R suggests a method which involved at the first division of the sample space into channels of the wideband system, calculation of occupancies and then modifying the sample space by deleting the samples identified inside a wideband channel. Secondly, the modified sample space was supposed to be divided in channels of the narrowband system (or next wideband system with narrower bandwidth as compared to the previous one) and then following the same procedure as before. But in real scenarios, sometimes it can lead to misclassification or even no detection, depending on the quality of samples acquired, which in turn depends on the radio channel conditions.
- iii) Overestimation or underestimation of occupancies due to less careful noise threshold setting, an insufficient number of samples in order to obtain statistical confidence, and inability to dig the signal out in case of a very low Signal-to-Noise Ratio (SNR). 50 % premise, used by ITU-R handbook [i.5], results in underestimation of true occupancies because channel nulls or under-sampling can vanquish a formidable part of the channel, which would then appear to be as noise.
- iv) A comprehensive study of occupancies in the ISM band considering possible coexisting systems had been lacking.
- v) Efficient and robust bandwidth and centre frequency estimation algorithms are missing.

In order to dig legitimate signals very close to noise levels, especially in the case of low Signal-to-Noise Ratio (SNR) or spread spectrum scenarios, one cannot rely upon static noise thresholds. From previous research works, a dynamic noise thresholding algorithm known as median Forward Consecutive Mean Excision (Med-FCME) [i.9] is adopted. Contrary to previous implementations, the algorithm is applied per each sweep. The idea was to establish a noise threshold for every sweep because, after a single sweep, a blind period is encountered, when measurement equipment was saving the sweep data, and supposedly the noise floor is also fluctuating. Clean Sample Rejection Rate (CSRR) is a measure to quantify the number of noise-only samples wrongly classified as outliers having signal components by FCME. The concept of CSRR is presented in [i.9]. CSRR can be preset as a probabilistic limit so that only a given amount of misclassification is tolerated, i.e. a false alarm. This metric is termed as the desired probability of false alarm, PFA_{DES} . The desired probability of false alarm value is given as a parameter to the FCME algorithm which calculates a threshold for consecutive mean excision T_{CME} as:

$$T_{CME} = -\ln(PFA_{DES}), \quad (1)$$

and then performs the iterative algorithm to find out the noise thresholds. In the measurement campaign, a target CSRR is set to be 5 %, i.e. $PFA_{DES} = 0,05$. Hence, $T_{CME} = 2,99$.

The most important goals achieved through this undertaking can be listed as:

- a) CO, FBO and SRO evaluation for the 2,35 to 2,50 GHz band in a hospital environment to characterize potential interferers in two different countries (Finland and Italy).
- b) A novel centre frequency and bandwidth estimation algorithm named Spatial Sample Clustering (SSC).
- c) An overhauled, robust and much more objective mechanism for SOE evaluations with a sufficiently low desired probability of false alarm.
- d) Mathematical models for quantification of interference.

For various equations including CO, FBO, SRO calculation and the complete analytical approach towards the problem, please refer to [i.8].

The spectrum sensing approach used was Energy Detection (ED) because of its simplicity of implementation. Other methods like cyclostationarity or wavelet decomposition cannot be used as any information about the signals being encountered is known. This makes the process blind, i.e. any electromagnetic energy being radiated into the channel has to be taken into account and no decisions about the nature or any feature of the already existing systems is taken. This is exactly the same as Clear Channel Assessment (CCA) based on ED as defined in the recently accepted ETSI SmartBAN PHY document [i.1].

A Neyman-Pearson type of energy detector chain is used and a statistic decision based on the dynamically calculated noise threshold is formulated. This problem can be written mathematically as a hypothesis test, i.e. a null hypothesis that a channel contains only noise, and an alternative hypothesis that a channel contains noise along with a legitimate signal.

H_0 : The channel contains only noise (Null Hypothesis)

H_1 : The channel contains noise and signal (Alternative Hypothesis)

$$D(X_i) = \frac{1}{n} \sum_{j=1}^n P(X_i(j)) \underset{H_1}{\overset{H_0}{\leq}} \gamma. \quad (2)$$

where i is the channel identifier, n is the number of samples collected from the channel, $P(X_i(j))$ is the sample power j at the channel i , and γ is the noise threshold. So, if the average power in the channel exceeds a certain threshold, there is a signal plus noise in a channel (alternative hypothesis), otherwise, the null hypothesis stands.

6.3 Measurement Campaigns

6.3.0 Introduction

Various measurement campaigns were undertaken in Oulu (Finland) and Florence (Italy) to analyse the channel usage patterns essentially at the 2,35 GHz to 2,50 GHz band. Different analysis techniques have been applied in order to dig out maximum information regarding varying spectrum usage mainly in modern hospital environments. Office and home environments were studied in Florence only. The process had been evolutionary and the campaigns differ slightly in parameter settings as well as in implementation perspective. More light will be shed on it in the following clauses. After evaluations of spectrum occupancy, mathematical models for channel occupancy description were extracted.

The measurement results, in both Finland and Italy, had been in accord in general. However, there had been slight variations due to the differing radio environments, different measurement equipment and different analysis strategies. The measurement campaigns carried out in Oulu University Hospital, Oulu, Finland is first presented. Later the corresponding measurement campaigns carried out in San Giuseppe Hospital in Empoli, Florence, Italy is described.

6.3.1 Measurement campaigns in Oulu, Finland

6.3.1.0 Introduction

Oulun Yliopistollinen Sairaala or Oulu University Hospital (OYS), situated in the city of Oulu is the north most of the five university hospitals in Finland. The hospital is affiliated with the University of Oulu, Faculty of Medicine and operates with more than 1 000 beds. The hospital is also equipped with state-of-the-art medical equipment, several ambulatory bays and a helipad.

Three measurement campaigns were carried out in OYS premises between December 2013 to June 2014. The following list describes the locations used in the campaigns:

- Daily Surgery (10th - 16th December 2013)
- Accident & Emergency Ward (10th - 17th June 2014)
- X-ray & Radiology (18th - 25th June 2014)

6.3.1.1 Daily Surgery SOEs (Campaign 1)

Figure 1 shows the map of the ground floor of the Daily surgery ward where the measurements were carried out. A red dot shows the location where the measurement equipment was placed. Green circles show the locations of the active Wi-Fi[®] access points installed on the premises. Such channel occupancy measurements are always highly dependent upon the location or placement of the equipment because the measurement equipment itself does not emit any probing signal in the air and the measurements rely only on the energy detection perceived from the radio channel. It should be noted here that in this kind of measurement no assumptions on radio signal propagation characteristics (i.e. channel model) are needed, as only electromagnetic radiations' level in the air is of interest. In other words, no signal decoding is done here, it is just simple old school blind energy detection that was done.

However, sometimes it becomes important to identify the interfering radiation or signal. That is why in the data analysis phase a blind detect and identify method (SSC) is implemented in order to characterize the specific systems occupying the frequency band of interest. For more details about SSC, please refer to [i.8].

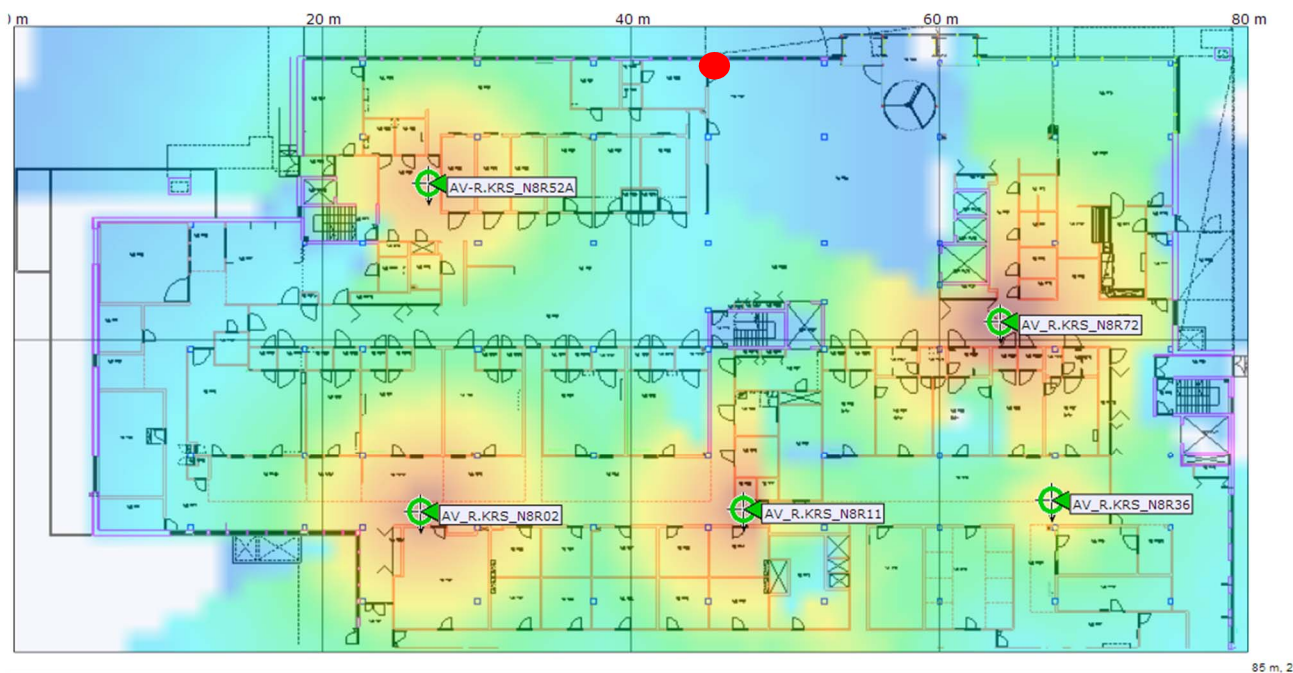


Figure 1: Map of ground floor (Daily Surgery Ward)

Measurements were carried out using high-performance Spectrum Analyser (SA) Agilent™ E4446A connected to a computer. Instrument Control Toolbox was used to connect MATLAB [i.12] directly to the spectrum analyser enabling control over SA and direct measurement results' analysis. The spectrum analyser was connected with a 1 m length cable to an omnidirectional, wideband antenna ARA CMA-118/A. Measurement setup is displayed in Figures 3 and 4. Before the measurement campaign signal levels were measured and the dynamic range of the spectrum analyser was optimized for the specific environment. Measurement campaigns are affected by certain key parameters which are set before the start of the campaign. Such parameters set for the campaign in Daily Surgery are listed in Table 1.

NOTE: SA Agilent™ E4446A is (are) an example(s) of a suitable product(s) available commercially. This information is given for the convenience of users of the present document and does not constitute an endorsement by ETSI of this (these) product(s).

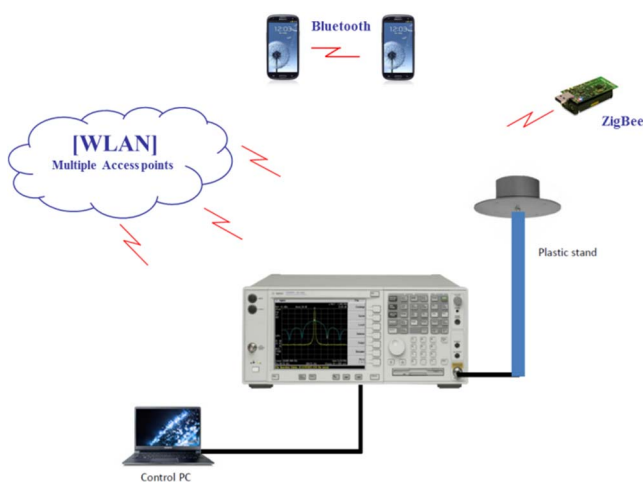


Figure 2: Logical Measurement Setup

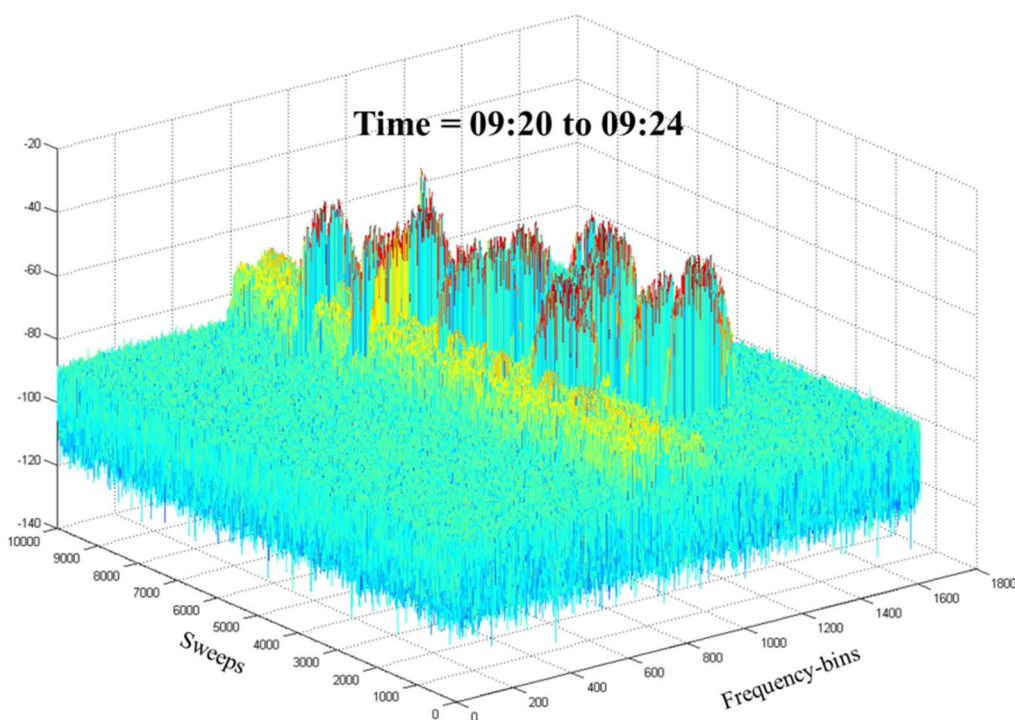


Figure 3: Actual cabinet keeping the SA, omnidirectional antenna and control PC

Table 1: Parameter setting for Daily Surgery Campaign

Parameter Name	Value
Frequency band	2,35 to 2,50 GHz
Bandwidth	150 MHz
Number of recorded frequency bins	1 601
Resolution bandwidth	300 kHz
Bin-width	93,7 kHz
No. of sweeps	10 000
Sweep time	2 ms approximately
Processing time	22 ms
Integration time	4 minutes
Measurement duration	7 days (6 × 24 hrs + 1 × 10 hrs)

The campaign in the Daily Surgery section of Oulu University Hospital lasted for a week, and 564 GigaBytes (GB) of data divided into 4 minute long blocks were collected. Figure 4 shows a plot regarding one such block. This is unprocessed raw data plot displaying all the detected signal energy (traffic) in the band of interest. Also, the corresponding noise floor can be seen. In order to be processed, in the analysis phase data was passed through dynamic noise thresholding, SSC and occupancy evaluation blocks.

**Figure 4: Raw Interference Plot**

Some of the interesting plots and figures from the week-long campaign are presented next. Figures 5 to 8 show occupancy evaluations for a single day, Friday 13th of December, 2013 and then few plots shed light upon one week-long SOE. The processed data plots reveal the systems working in the band of interest.

It should be noted that the colour schemes used in temperature plots, i.e. Figures 5 to 7 are locally significant. For example, the red colour in Figure 5 marks near about 10 % occupancy whereas in Figure 6, it marks about 0,6 % occupancy. The band from 2,35 GHz to 2,40 GHz is found to be completely empty, which means that the newly allocated band 2 360 MHz to 2 400 MHz for medical purposes in US seems to be open for exploitation in OYS. However, in Europe, this particular band is allocated for LTE, which might cause interference for the Medical BANs in the future if it is taken into use. SSC was unable to distinguish among different narrowband systems. There had been 2 MHz wide signals as well as 1 MHz wide signals. Bluetooth Smart or Bluetooth Low Energy (BLE) use 2 MHz wide signals with frequency hopping and some proprietary protocols, like the one used in Logitech Mouse/Keyboards, utilize 2 MHz bandwidth with time-division multiplexing. SSC cannot infer a hopping pattern so it was not possible to discriminate with confidence among 2 MHz wide signals. Enough doubt is left to distinguish a ZigBee[®] system from a 2 MHz wide Bluetooth system, as both use the same channel allocation scheme and bandwidths. That is why all narrowband systems are shown in one single plot without any further processing in Figure 7. It also means that SRO for narrowband systems cannot be calculated as distinguishing among different systems is not possible.

Interesting finding is that the system independent metric FBO seems almost to follow the pattern of a system-dependent metric, which is the highest, i.e. the most significant SRO of a system as shown in Figure 8. In the proposed case, IEEE 802.11b [i.30] and IEEE 802.11g [i.31] had been the most impactful systems with the highest SRO among all, and FBO nearly follows its distribution. Of course, it is quite legit and logical, as occupancies for IEEE 802.11n [i.32] were found to be very close to zero.

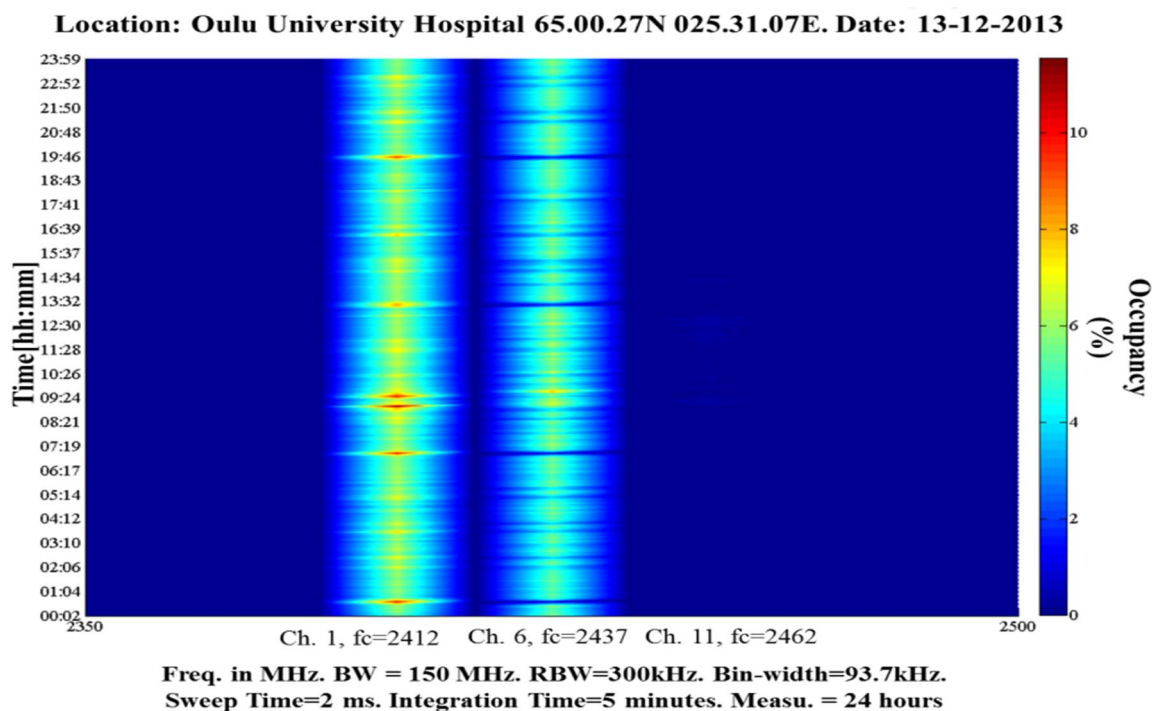


Figure 5: CO, IEEE 802.11b/g [i.30] and [i.31] (13-12-2013)

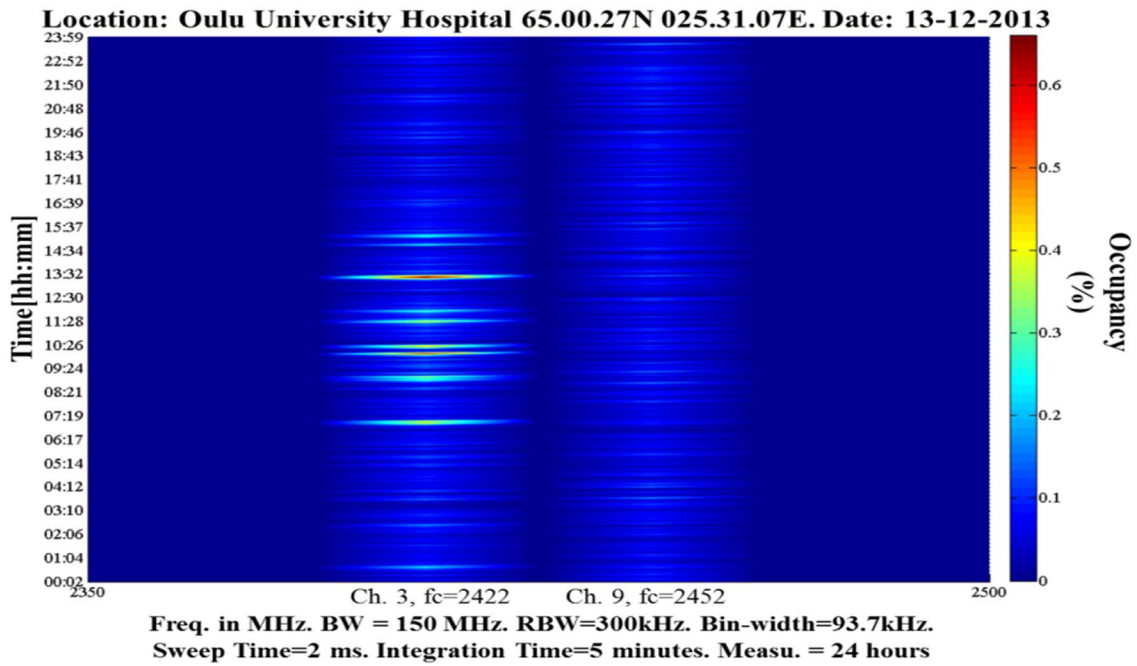


Figure 6: CO, IEEE 802.11n [i.32] (13-12-2013)

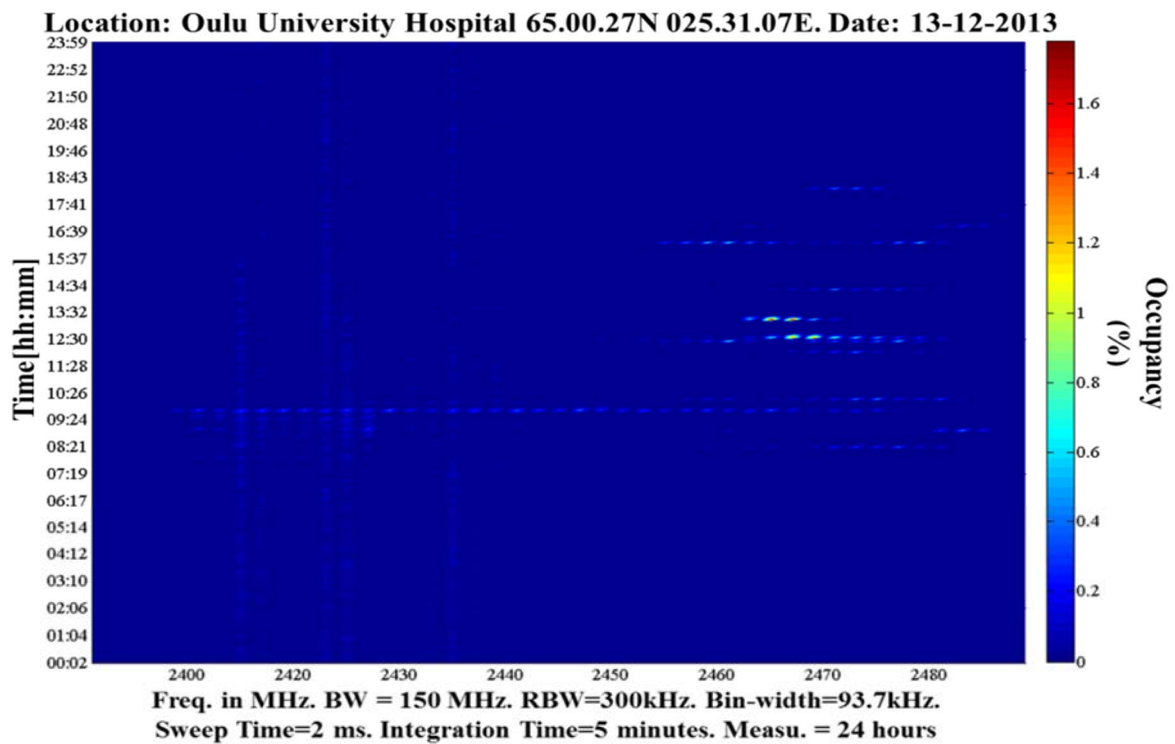


Figure 7: Occupancy of Narrowband systems (13-12-2013)

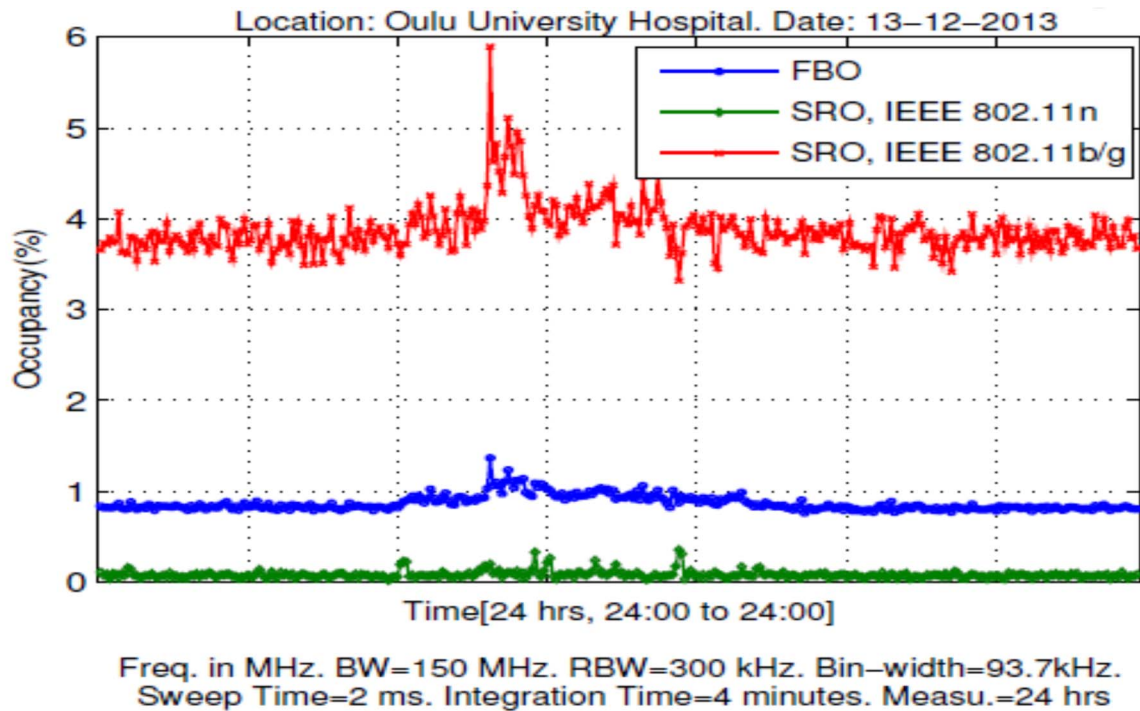


Figure 8: FBO and SRO for the identified systems (13-12-2013)

Figure 9 shows variations of FBO and Figure 10 shows variations of SRO for IEEE 802.11 [i.3] type systems over a period of a week.

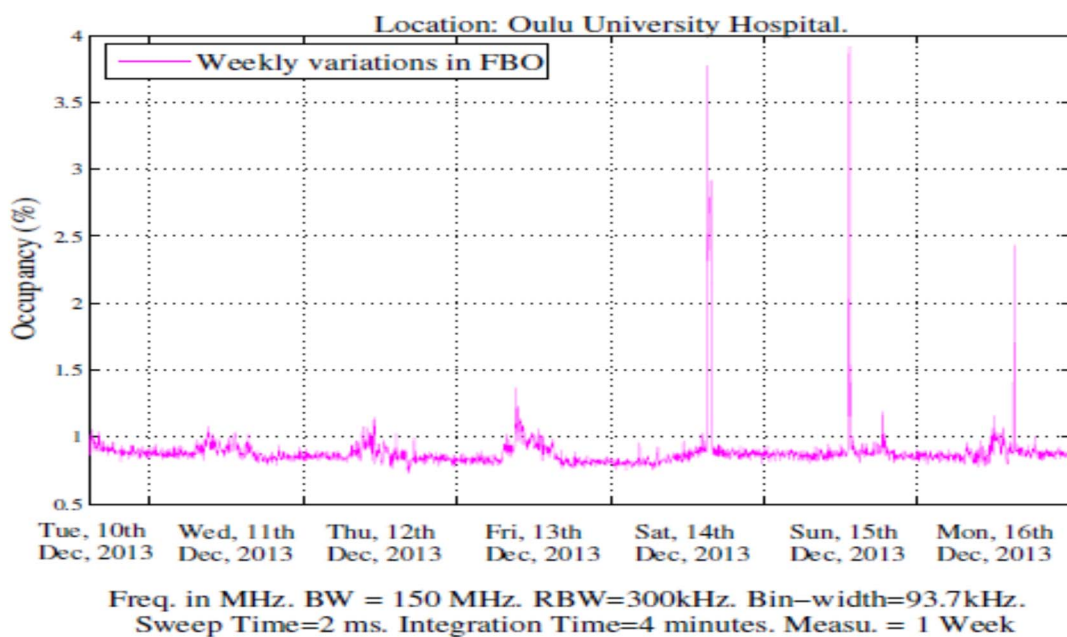


Figure 9: FBO weekly variations

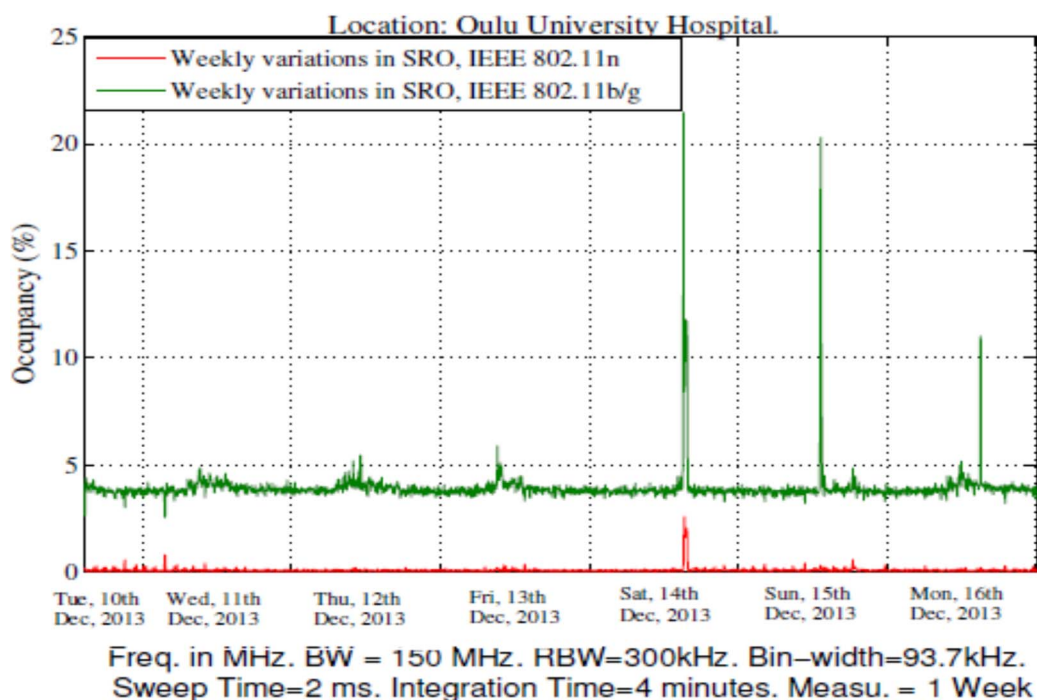


Figure 10: Weekly variations of SRO for two IEEE 802.11 [i.3] systems

Previous literature had shown that channel occupancies had been between 10 to 15 % even at some of the busiest hotspots. Literature often views it as a problem inherent to measurement equipment, which underestimates the true, legitimate occupancy values in comparison to measured ones. The proposed method has been robust enough to fight against channel nulls, variable noise floor and to identify various systems working in parallel.

Figures 9 and 10 depict whole week FBO and SRO analyses starting from 10th of December and ending on 16th of December. During the measurements campaign, on Saturday and Sunday, some maintenance and updates were scheduled at the hospital premises. There had been a significant amount of wireless traffic being generated. The proposed system detected 50 % to 60 % occupancies in the time window of 2 hours. Plots of Saturday are presented here only as an example, i.e. from Figure 11 to Figure 14. During maintenance, all channels were occupied, as shown in Figure 11, even the channel no. 11, which had shown the least activity during the other days. There had been no narrowband activity in the whole day except when maintenance and update processes were going on, and the plot in Figure 13 seems to suggest the existence of a Bluetooth based device as a frequency hopping pattern can be seen. Figure 14 shows that while the SRO metric for IEEE 802.11b [i.30] and IEEE 802.11g [i.31] was touching the 22 % mark, FBO was still at 4 %. This is a very interesting result: there are still 96 % of the band resources free when there was a certain channel occupied more than 50 % of the time. The region from 2,35 GHz to 2,4 GHz had always been found empty and can be utilized for medical applications. Figures 15 and 16 show comparisons among channel occupancies of the IEEE 802.11b [i.30] and IEEE 802.11g [i.31] and IEEE 802.11n [i.32] systems over a period of one week.

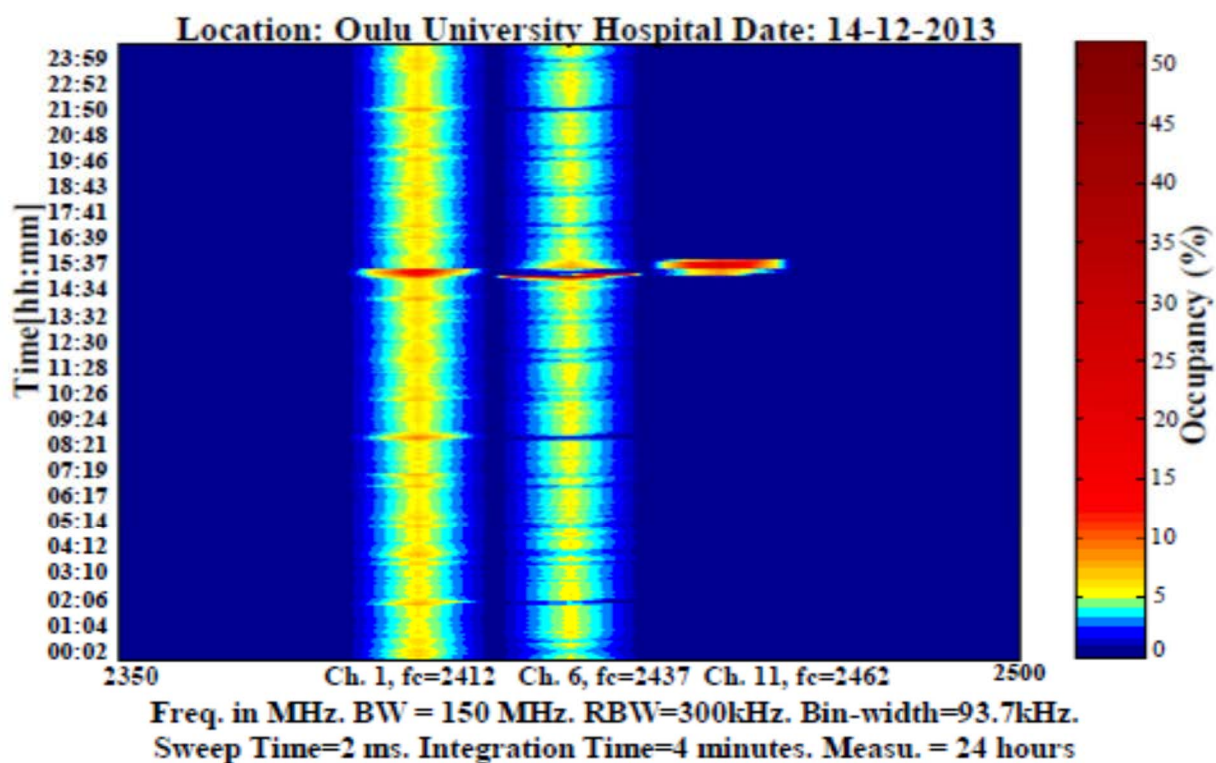


Figure 11: CO, IEEE 802.11b/g [i.30] and [i.31] (14-12-2013)

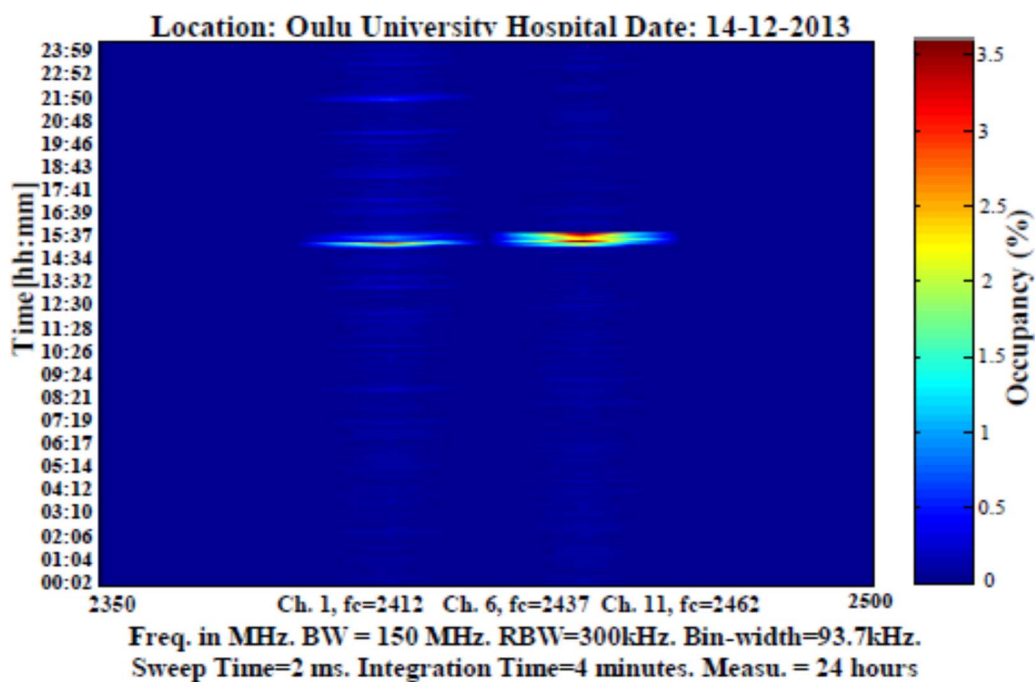


Figure 12: CO, IEEE 802.11n [i.3] (14-12-2013)

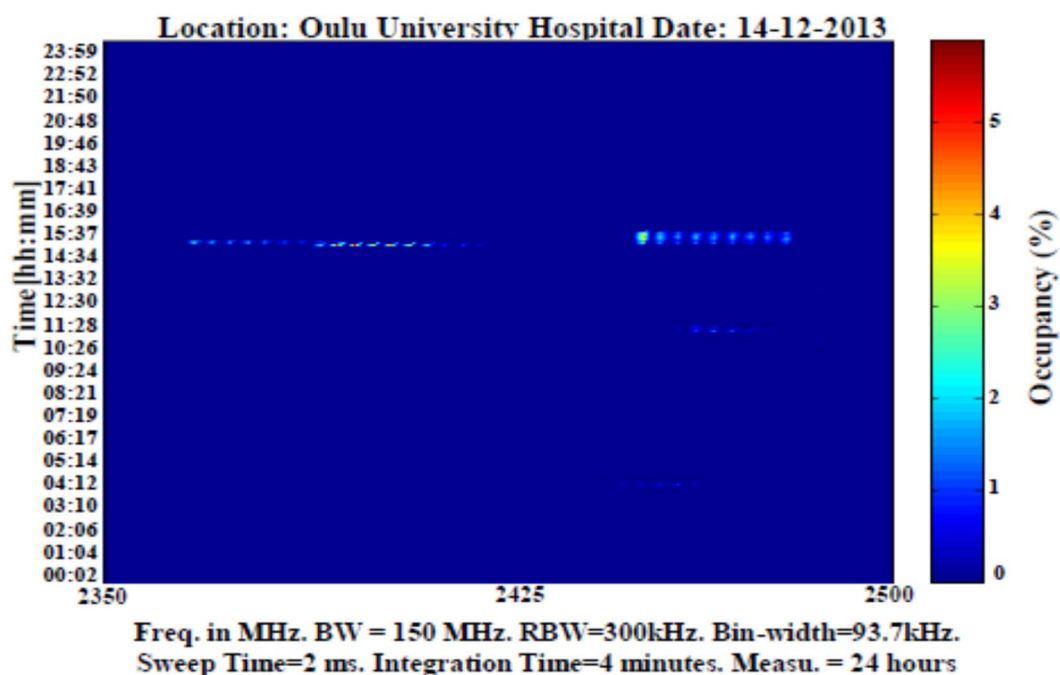


Figure 13: Occupancy, Narrowband Systems (14-12-2013)

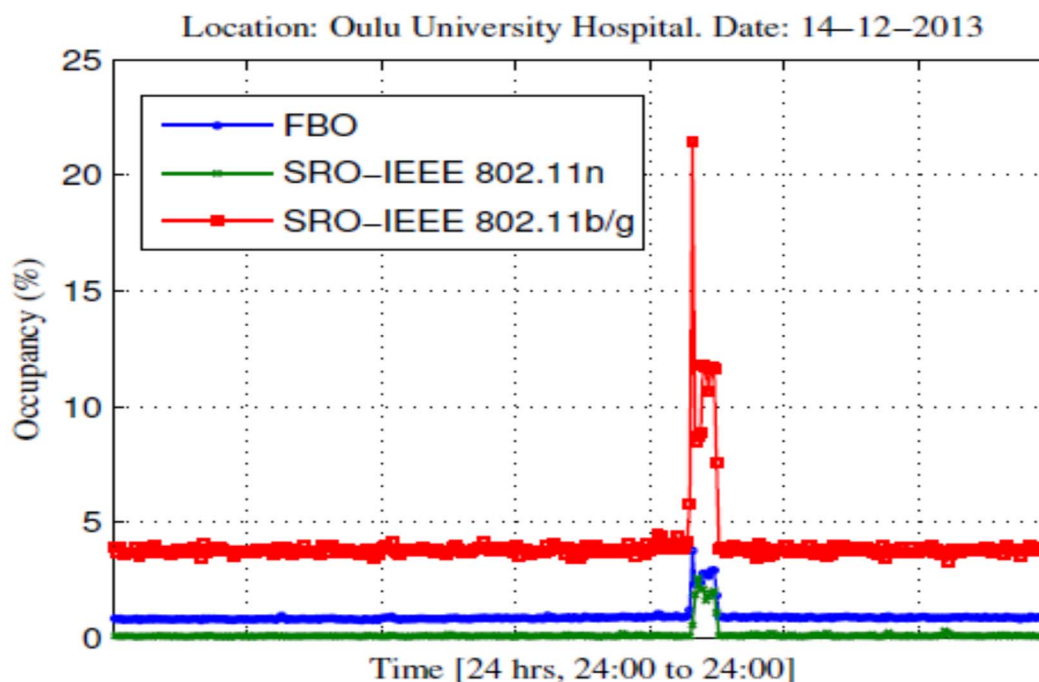


Figure 14: FBO, SRO for the identified systems (14-12-2013)

Figure 15 presents channel occupancy comparison among 20 MHz wide IEEE 802.11b [i.30] and IEEE 802.11g [i.31] channels throughout the week-long campaign. Out of the 14 legitimate channels of this system, three channels (1, 6 and 11) were found to be occupied, which is the, so called, safest configuration of the system, i.e. three non-overlapping channels are operating in the same environment. One strange observation was that whenever Channel 1 was highly occupied, the occupancy level of Channel 6 fell down. This behaviour had been consistent throughout the whole span of measurement.

However, there exists an explanation for such behaviour. IEEE 802.11b [i.30] and IEEE 802.11g [i.31] only specifies centre frequencies and a spectral mask. IEEE 802.11b [i.30] spectral mask requires that the signal power should be at least 30 dB less than its peak power at ± 11 MHz and at least 50 dB less at ± 22 MHz from the centre frequency. If there is a very powerful transmitter, the signal can be quite strong even beyond ± 22 MHz point, which means all channels will actually overlap, even the non-overlapping ones. This phenomenon gives rise to a problem known as the near-far problem where two communication systems encounter interference when a foreign station that transmits on an adjacent channel is in much closer proximity than the intended one. Figure 15 shows actually the near-far problem, where the access point which is assigned Channel 11 is much closer to our measurement equipment as compared to the access point which is assigned Channel 6. In the case of IEEE 802.11n [i.32] systems, the comparison of channel occupancies in Figure 16 clearly shows that the near-far problem is non-evident.

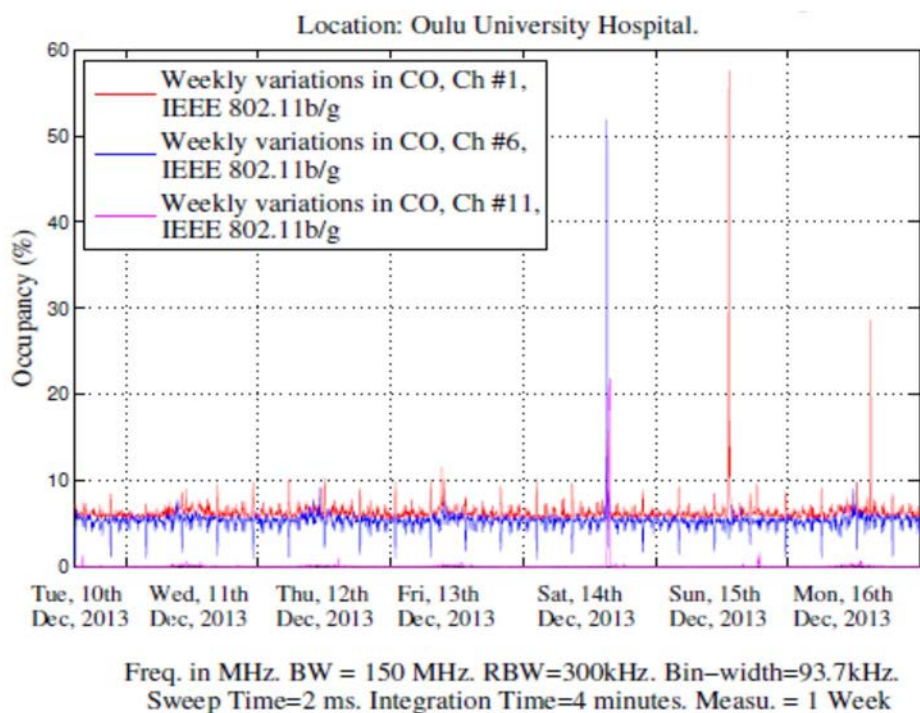


Figure 15: CO comparison among IEEE 802.11b/g [i.30] and [i.31] channels over the period of a week

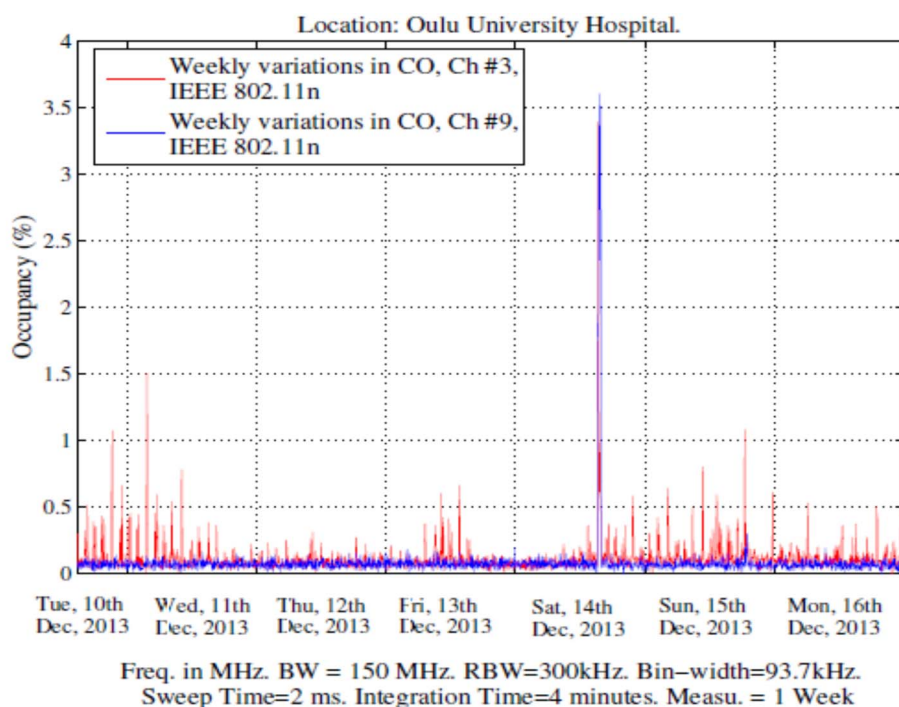


Figure 16: CO comparison among IEEE 802.11n [i.32] channels over the period of a week

The analysis suggests that 2,4 GHz ISM band still provides enough opportunities to be considered for medical BANs. Even in the case of high occupancies, there were free resources, and especially, there were white spaces available in between the bursty transmissions, which suggests that the cognitive solution might save the day. Also radio network planning in hospitals should be done with due care. Inappropriate network planning can lead to intra-network interference. However, it is always a question of the required Quality-of-Service (QoS) level, what occupancy level is acceptable in the case of medical-related communication.

6.3.1.2 Accident & Emergency Ward SOEs (Campaign 2)

In the second measurement campaign, which was carried out at the accident & emergency ward at OYS, the measurement strategy was updated. Due to the location of the SA and the connected antenna, an extended ISM band Low Noise Amplifier (LNA) had to be added, as well as a specially designed Bandpass Filter (BPF) to increase the level of received energy. LNA had almost 20 dB gain in the extended ISM band and a significantly low noise figure. A logical representation of a measurement equipment after the addition of LNA is shown in Figure 17.

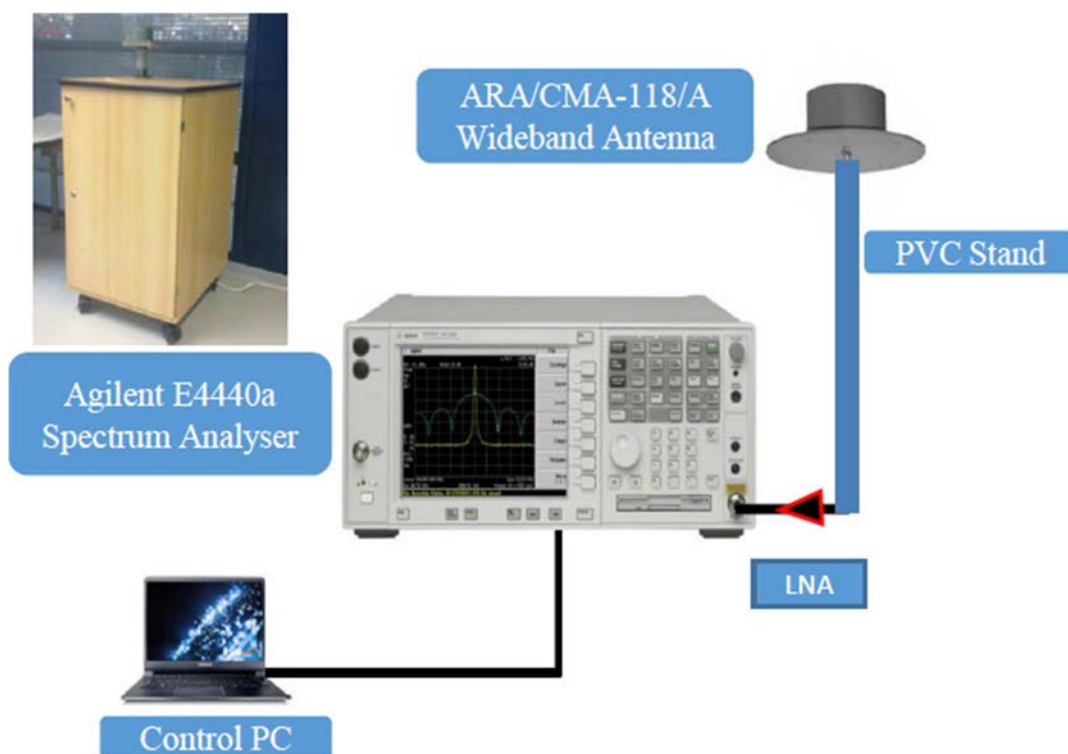


Figure 17: Measurement Equipment with extended ISM band LNA

The frequency band of interest is based again on the requirements given by the ETSI TC SmartBAN [i.1]. During the data post-processing phase, the frequency band was divided into 150 hypothetical WBAN channels, each with 1 MHz bandwidth. SOE metrics evaluated include Channel Occupancy (CO) and Spectrum Resource Occupancy (SRO). Channel statistics were obtained using a Neyman-Pearson type of detector along with a dynamic noise threshold algorithm (Med-FCME) at a false alarm probability of 0,05. The measurement parameters used in this particular campaign are given in Table 2.

Table 2: Measurement Parameters for Accident & Emergency Ward

Parameter Name	Value
Frequency band	2,35 GHz to 2,50 GHz
Bandwidth	150 MHz
Frequency bins	1 200
Resolution bandwidth	250 kHz
Bin-width	125 kHz
No. of sweeps	1 250 per minute
Sweep time	3 ms approximately
Processing time	45 ms
Integration time	1 minute
Measurement duration	1 week

$T \times K$ data samples were collected from the band into one minute long blocks. $T = 1\,250$ represents the number of sweeps, i.e. sensing iterations over the band per minute, whereas K represents the number of samples collected from the band in one sweep. Bin-separation, i.e. the distance between any two adjacent samples was 125 kHz. In this way, $K = 1\,200$ frequency bins (or frequency points) represent 150 MHz wide frequency band. The Resolution Bandwidth (RBW) for the SA was chosen to be 250 kHz, which is exactly $\frac{1}{4}$ of the minimum channel bandwidth (1 MHz) of ISM band users, as proposed by ITU-R in [i.5].

To give the analysis a proper perspective, a hypothetical scenario is considered. The band 2,35 GHz to 2,50 GHz is divided into 150 channels, where each channel is 1 MHz wide. If a WBAN device would work in any of these channels, it might perform a clear channel assessment before transmission and back-off if the channel is sensed busy. The main idea here is to get statistics, which would describe how many times or how long the channel was found to be occupied or idle over a period of time. In order to establish that in a certain sweep a channel X_i ; $i = 1, 2, 3, \dots, 150$ was occupied or not, a hypothesis test is performed. The problem is formulated as either observing only noise N or observing a signal with noise. Mathematically:

$$\begin{aligned}
 &H_0 : X_i = N, i = 1, 2, 3, \dots, 150 \\
 &\text{and} \\
 &H_1 : X_i = S|N, i = 1, 2, 3, \dots, 150
 \end{aligned} \tag{3}$$

where H_0 is the null hypothesis that there is only noise in the channel and H_1 is the alternative hypothesis that there is signal plus noise in the channel. A detection decision problem takes the form given by:

$$D(X_i) = \frac{1}{n} \sum_{j=1}^n P(X_i(j)) \underset{H_1}{\overset{H_0}{\leq}} \gamma \tag{4}$$

where $\sum P(X_i(j))$ is the sum of $j = 1, 2, 3, \dots, n$ sample powers in linear units for a channel X_i , $D(X_i)$ is the decision statistic and γ is the decision threshold.

Mean power in the channel X_i is then compared to the threshold, which is obtained using a dynamic noise threshold algorithm called median forward consecutive mean excision. If the power is found to be less than the threshold, the channel is defined as not to be occupied, and vice versa. The method is pretty similar to the real implementations of Clear Channel Assessment based on Energy Detection (CCA-ED). In other words, if the signal energy in the channel crosses a certain threshold set for CCA, the channel is marked busy until the medium energy is below the threshold. The decision statistic for a specific channel X_i can simply be marked either 0 if unoccupied or 1 if occupied. Hence, a binary $T \times K$ matrix, which provides an occupancy matrix over the period of 1 minute, was produced. Using this strategy, 183 GB of data recorded during the measurement campaign was processed into a minute-long binary block. For example, a binary matrix O_{MAT} with elements $O_{MAT}(T, C)$ is produced by calculating mean powers for every channel X_i using decision statistic as:

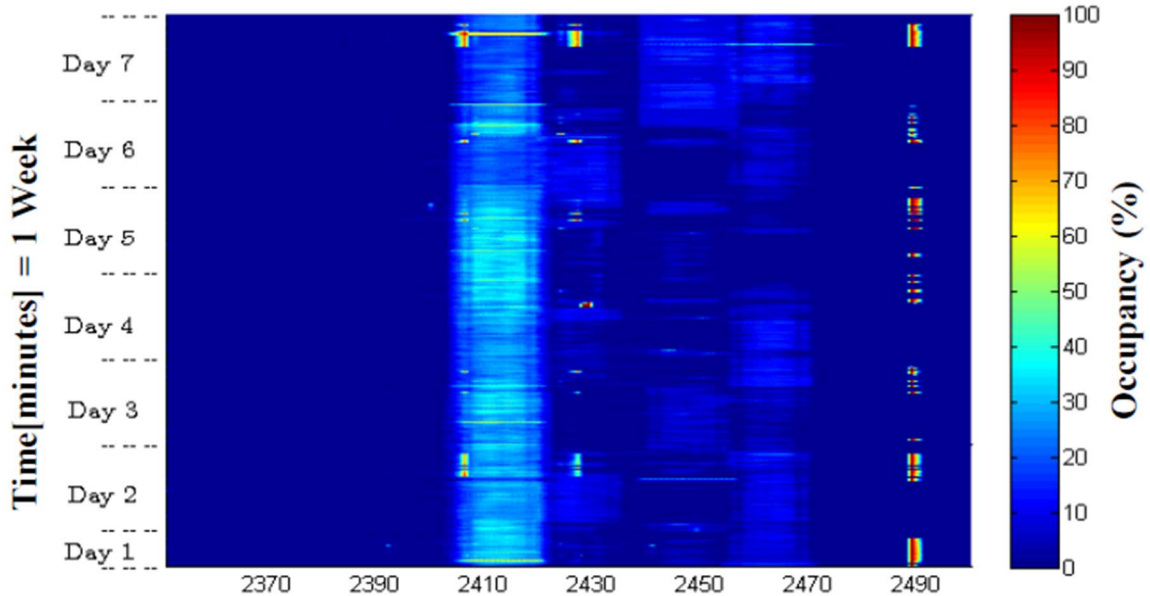
$$O_{MAT}(T, C) = \begin{cases} 1, & \text{if } \frac{1}{n} \sum_{j=1}^n P(X_i(j)) > \gamma \\ 0, & \text{if } \frac{1}{n} \sum_{j=1}^n P(X_i(j)) < \gamma, \end{cases} \tag{5}$$

where $T = 1, 2, 3, \dots, 1250$ is the sweep number and $C = 1, 2, 3, \dots, 150$ is the channel number.

Spectrum occupancy evaluations were then performed just as in the previous campaign. Figure 18 shows a plot regarding channel occupancies for all 150 channels over a period of 1 week. Similarly, a channel occupancy plot can be presented for each day as shown in Figure 19. Maximum and mean occupancies over a period of the whole week are shown in Figure 20. Maximum curve points show the maximum level of occupancy observed in a specific channel, and the mean points represent the average occupancy observed in that particular channel over the week. Moreover, mean occupancies provide an interesting insight that occupancy levels fluctuate greatly but, on average, a large part of the studied frequency band is free. It can be observed in the plots that there are WLAN users within a band from 2 400 MHz to 2 470 MHz. Some low-powered narrowband signals with Occupied BandWidth (OBW) varying from 2 to 3 MHz, which might belong to some system utilizing audio/video wireless transceivers, were also observed. Most of the narrowband activity was observed around the centre frequencies $f_c = 2\ 406$ MHz, $2\ 427$ MHz and $2\ 490$ MHz. The frequency band from 2 350 MHz to 2 400 MHz was used the least. However, occasionally some very low power signals were found with OBW close to 10 MHz. Those signals may belong to 13 cm Ultra-High Frequency (UHF) amateur radio users who can use the frequency band from 2 300 MHz to 2 400 MHz on a secondary basis internationally. Evidence of such stray signals can be seen in Figure 21. However, because of their seldom appearing during longer analyses, they were averaged out from the final results.

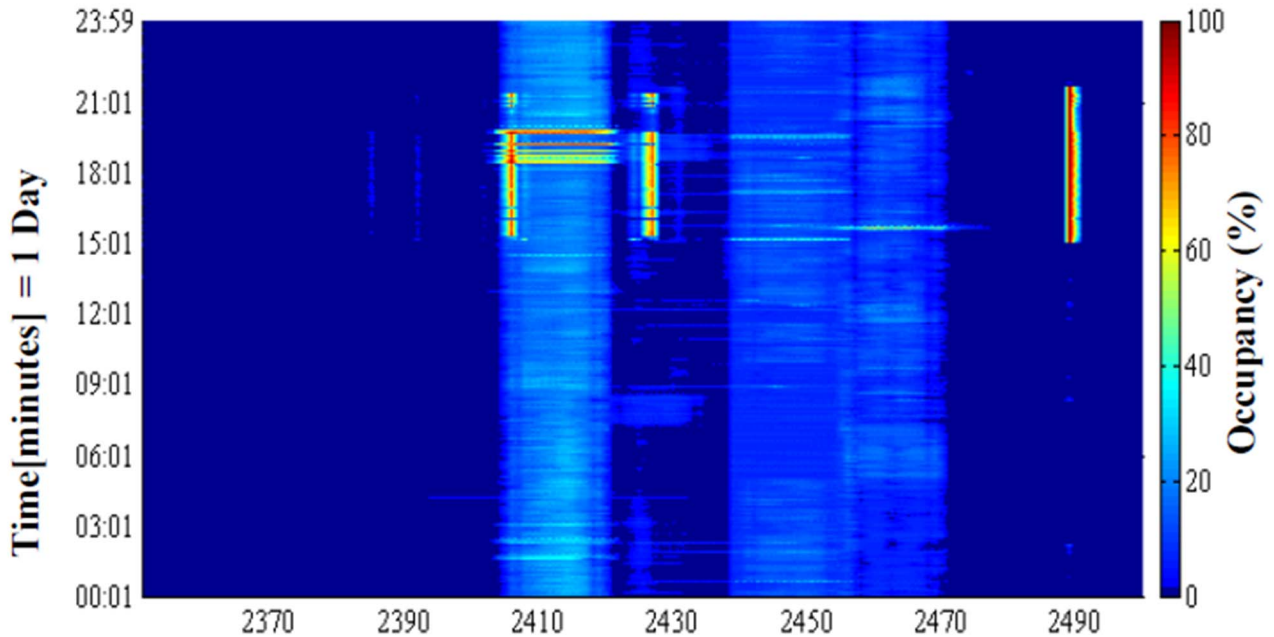
SRO is a measure reflecting how much of the band resources are being utilized simultaneously at a given time. Figure 22 shows the SRO observed over the whole week for the full band under observation, i.e. 2 350 MHz to 2 500 MHz. Maximum SRO was observed on day 6, when it reached about 16 %. The mean SRO calculated was about 4,5 %, which implies that 95,5 % of the channel resources out of 150 were unoccupied, on average, over the whole campaign.

However, Figure 22 might be taken as a little biased, because the band from 2 350 MHz to 2 400 MHz is mostly empty. That is why the SRO for 2 360 MHz to 2 400 MHz band and 2 401 MHz to 2 480 MHz band were calculated separately, as shown in Figure 23. It can be observed that the 40 channels from 2 360 MHz to 2 400 MHz are scarcely occupied. Maximum SRO, 6,49 % was observed on day 6 and the mean SRO was observed to be 0,1 %. Whereas, while observing 80 channels from 2 401 MHz to 2 480 MHz, which is actually the 2,4 GHz ISM band, the maximum SRO was observed to be 26,38 % and the mean SRO was 8,01 %. Hence, still 91,99 % of the channel resources are available in the 2,4 GHz ISM band.



**Freq. in MHz. BW = 150 MHz. RBW=250 kHz. Bin-width=125 kHz.
Sweep Time=3 ms. Integration Time=1 minute. Measu. = 1 Week**

Figure 18: Weekly Occupancy in Accident & Emergency Ward



**Freq. in MHz. BW = 150 MHz. RBW=250 kHz. Bin-width=125 kHz.
Sweep Time=3 ms. Integration Time=1 minute. Measu. = 1 Day**

Figure 19: A Single day occupancy for Accident & Emergency Ward

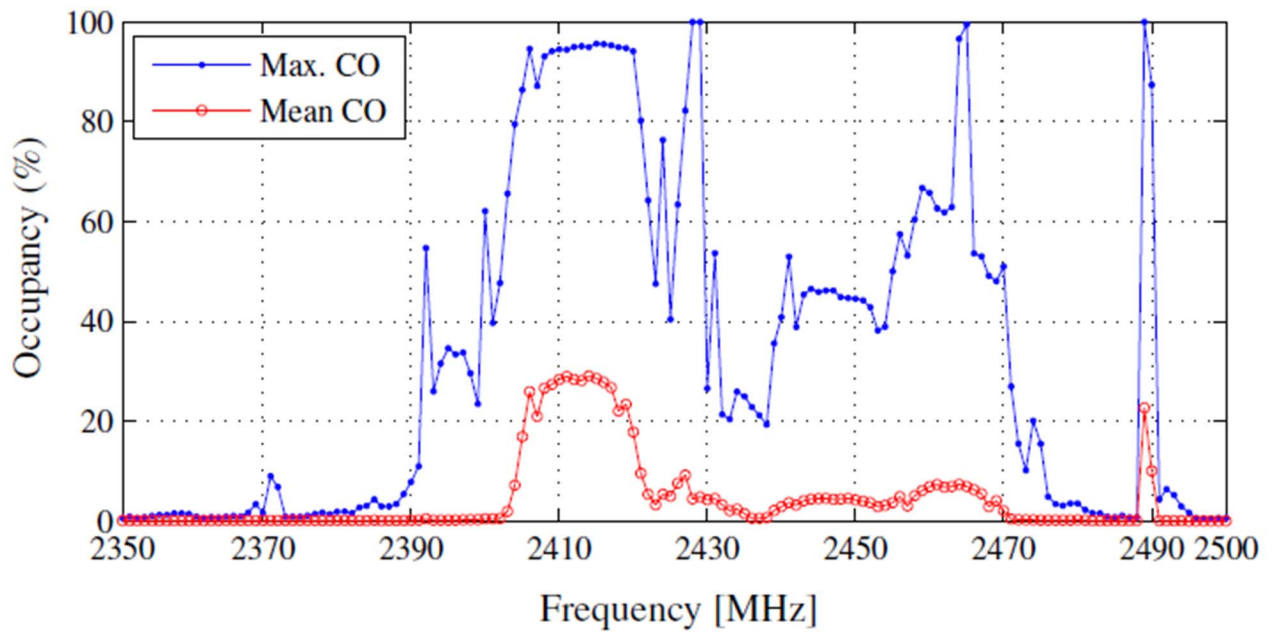


Figure 20: CO, Mean and Maximum curves at Accident & Emergency Ward

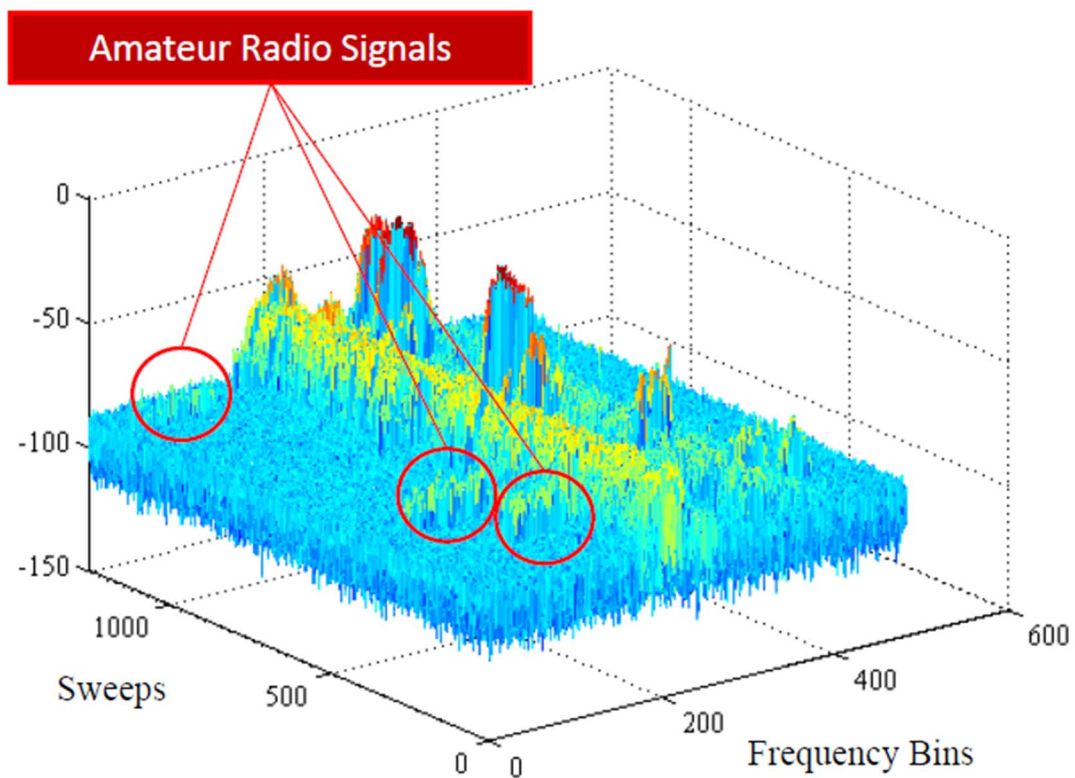


Figure 21: Existence of possible Amateur Radio Signals

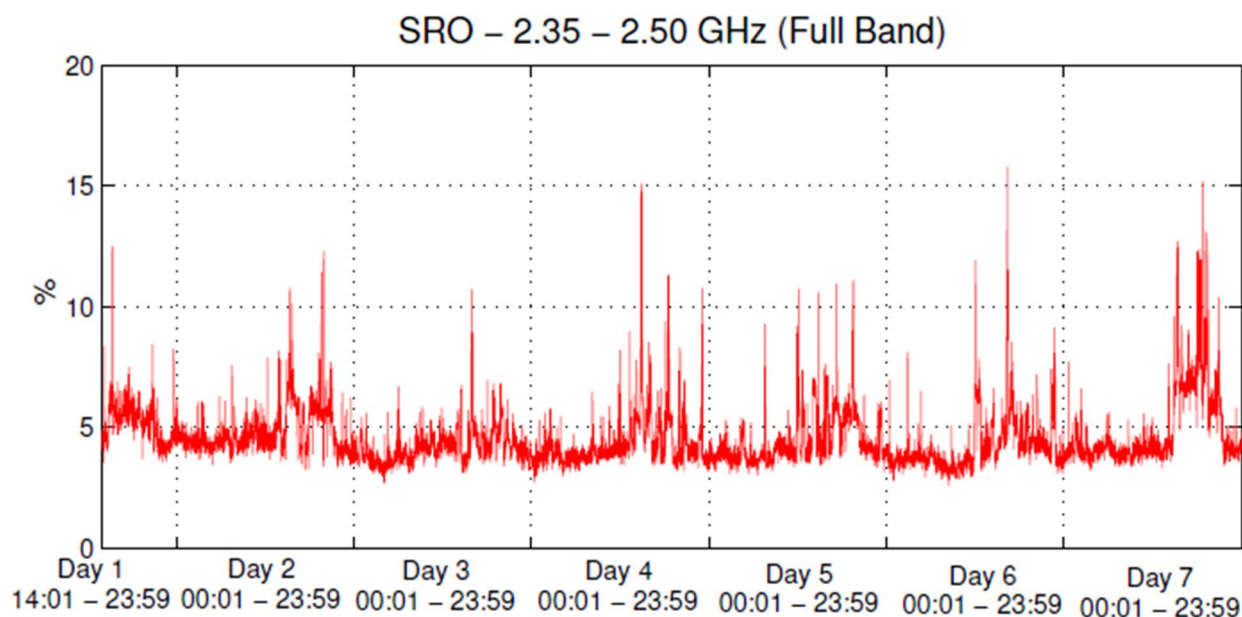


Figure 22: SRO (Full Band) at Accident & Emergency Ward

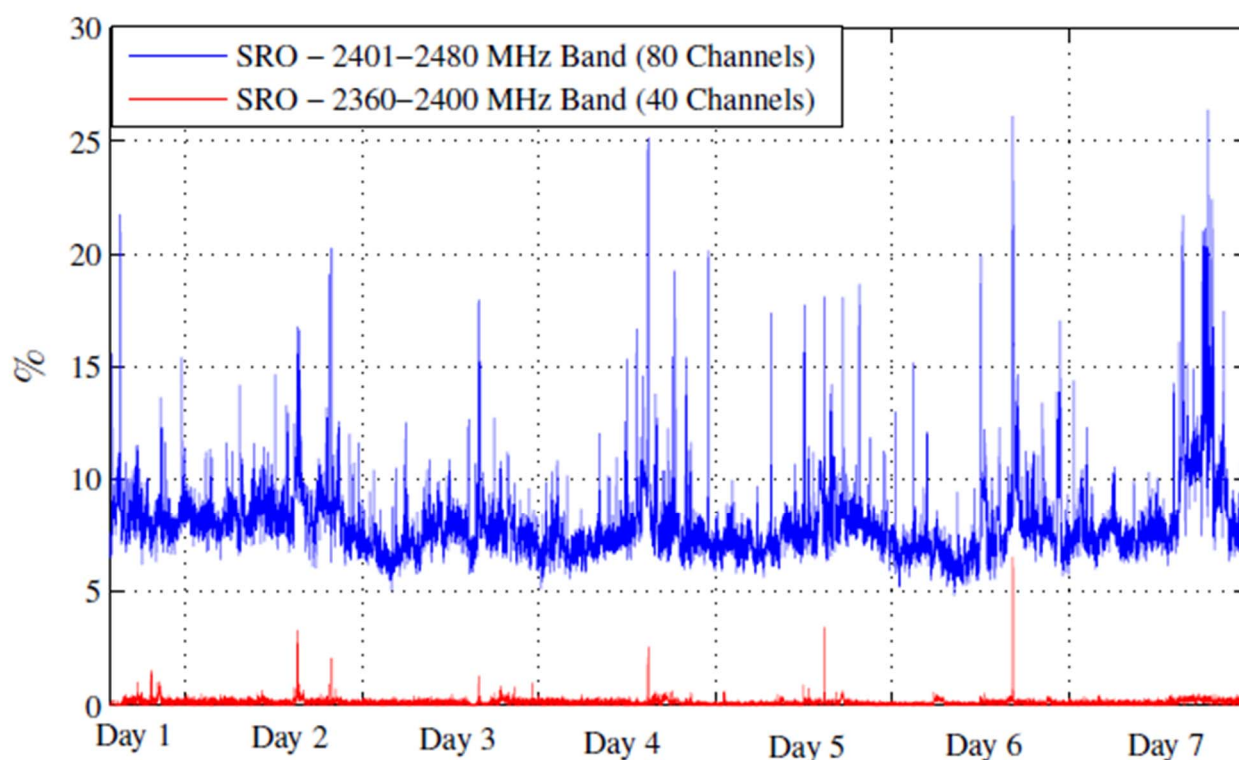


Figure 23: SRO for 2 360 MHz to 2 400 MHz and 2 401 MHz to 2 480 MHz bands

Various channels in the band were observed to be highly occupied, i.e. CO reached 90 % to 100 %. On the other hand, some channels were not occupied at all. However, mean occupancies over the week in channels ranging from 2 401 MHz to 2 426 MHz reached 30 %. SRO for the whole band from 2 350 MHz to 2 500 MHz band was observed to be 4,5 %, on average, and the maximum was seen to be 16 %. SRO for the band from 2 360 MHz to 2 400 MHz was observed to be 0,1 % on average, which implies that this portion of the band is open for further exploitation. Finally, SRO for 2 401 MHz to 2 480 MHz was calculated, and it showed that there were 91,99 % channel resources free, on average.

6.3.1.3 X-Ray & Radiology Ward SOEs (Campaign 3)

A similar campaign as described in the previous clause was undertaken at the X-ray & radiology ward of Oulu University Hospital. The campaign lasted for a week and the measurements were analysed exactly in the same way as in the accident & emergency ward's case. The X-ray & radiology ward contained state-of-the-art computer-aided tomography machines, X-ray machines, microwave and radio ablation & diathermy machines. Some sweeping radiations have been witnessed throughout the band that might have arisen due to the use of microwave and radio ablation & diathermy devices because the radiation leakage of other devices does not fall in the ISM band or pre-ISM band. The detected radiation powers have usually been close to -85 dBm and occasionally stronger powers were detected. The first six days of the campaign showed this kind of behaviour. An example of such behaviour is shown in Figure 24. However, on the 7th day, there had been a narrowband emission near 2 390 MHz which was present in the last campaign as well. Figure 25 displays the occupancy on the last day of the campaign, 25th June 2014. Figure 26 shows the occupancy for the whole week.

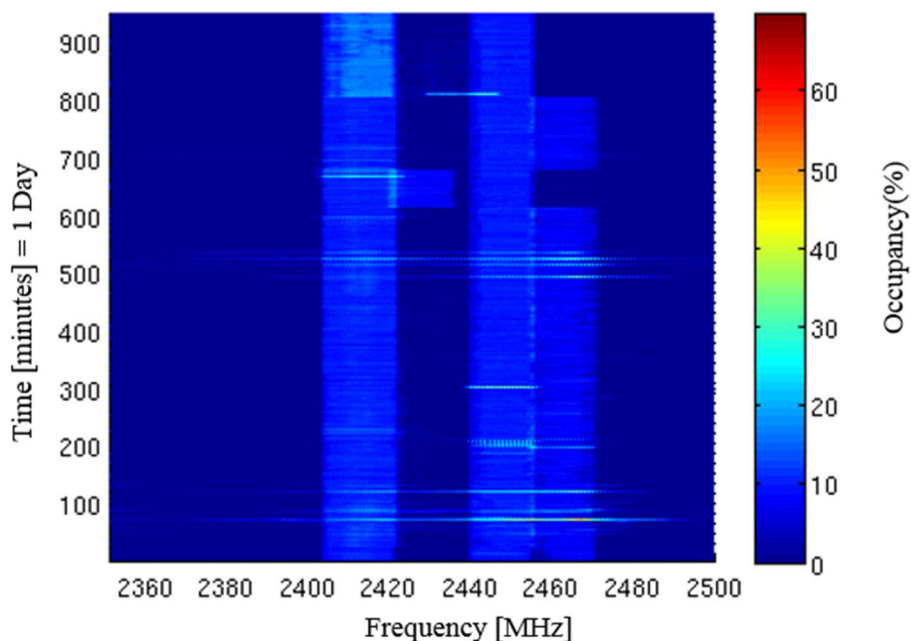


Figure 24: Occupancy for the first day (18th June 2014) at X-Ray & Radiology Ward

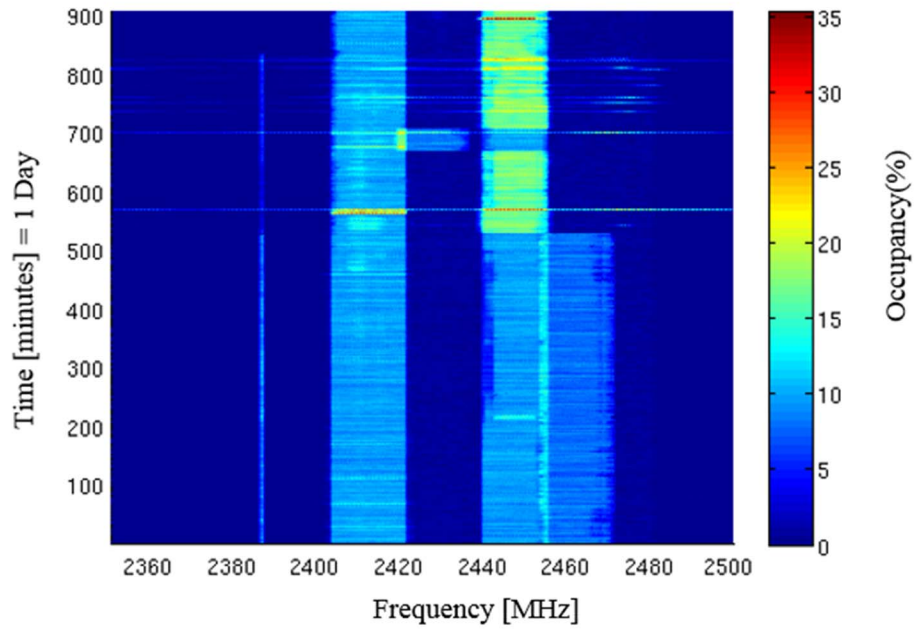


Figure 25: Occupancy on the last day (25th June 2014) at X-Ray & Radiology Ward

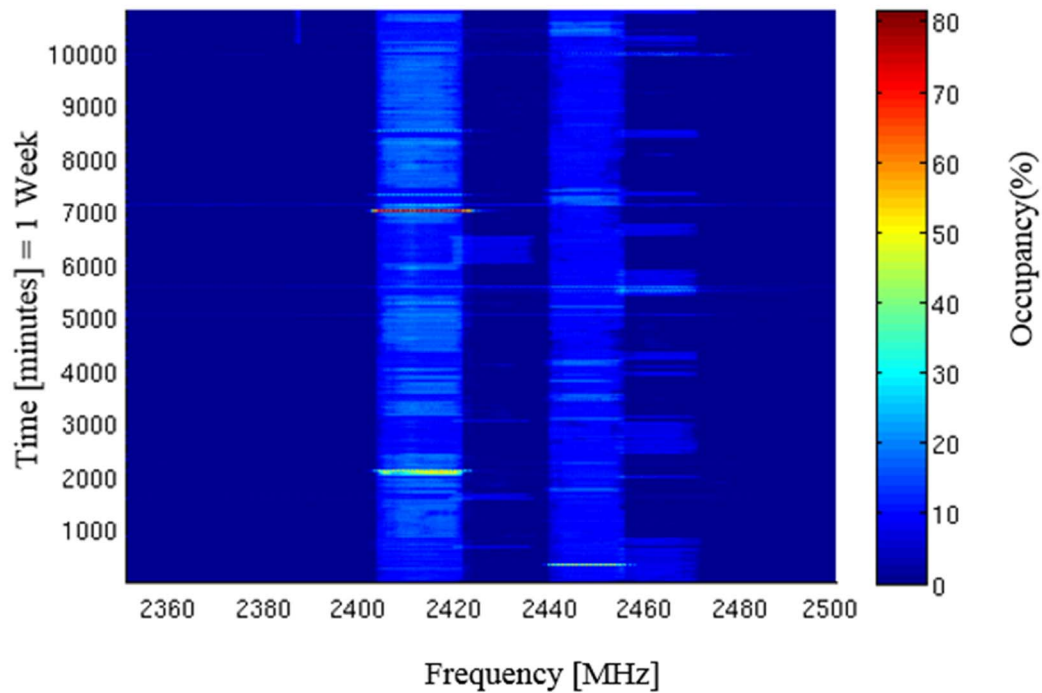


Figure 26: Weekly occupancy at X-Ray & Emergency Ward

6.3.2 Analytical Stochastic Model for Spectrum Occupancy

In order to mathematically characterize the potential interference to WBANs in a hospital environment, stochastic mathematical models for channel and spectrum resource occupancy in 2,35 GHz to 2,50 GHz band are proposed. The models present a spectrum occupancy framework from the viewpoint of WBANs. The probability density functions proposed by the model are then validated by statistical hypothesis tests utilizing real measurement data. Measurement data from Oulu University Hospital was used to validate the models. The idea behind this work was to formulate a statistical perspective regarding frequency resource utilization in a hospital environment, which would provide industry and academia with tools to regenerate similar utilization patterns in the laboratory and simulation environment. The model can be used in simulations for WBANs considering interference management, network design, and testing coexistence scenarios, etc. Detection and channel decision statistics were calculated just as mentioned in the previous clauses.

Without going into the details regarding the formulation of the models, here the most important results obtained are presented. For more details about the model formulation and theory behind the idea, please refer to [i.10]. The stochastic modelling process for an individual channel can be viewed logically as a coin-flip experiment with two possible outcomes. Relating to the fact that a binary matrix representing occupied (1) and unoccupied (0) channels is created, the previous presumption makes sense. A binomial process models the signal arrival times within a 1-minute long block. A Poisson process models the arrival times of signals in an arbitrarily long train of 1 minute long blocks. Markovian chains are defined for the models, and then the Chi-square test statistic is used to validate the model against the real measured data. Arrival rates were estimated using the Maximum Likelihood Estimate (MLE) from the data acquired from the hospital.

1 440 minutes (24 hours) long data are considered as a statistical population for a single channel. Random samples with replacement worth of 432 minutes are recorded, which accounts for 35 % of the actual population. Arrival rates were estimated from the data, so one degree of freedom is lost. A Monte-Carlo type of simulation was done for 10 000 iterations and Chi-square test statistic χ^2 was evaluated as:

$$\chi^2 = \frac{\sum_{i=1}^n (O_i - E_i)^2}{E_i}, \quad (6)$$

where O_i is the observed value and E_i is the expected value. Degree of freedom is calculated as $n-1-1$ because the arrival rate λ was estimated, whereas n is the cumulative frequency of the observation set $\{O\}$. After obtaining Chi-square statistics, the p-value (probability) can be evaluated by calculating the Cumulative Distribution Function (CDF) of the Chi-square distribution. P-value is then compared against a significance level $\alpha=0,05$, i.e. 95 % certain about the results is wanted. Figure 27 shows the results for Channel no. 62, which was one of the most occupied channels.

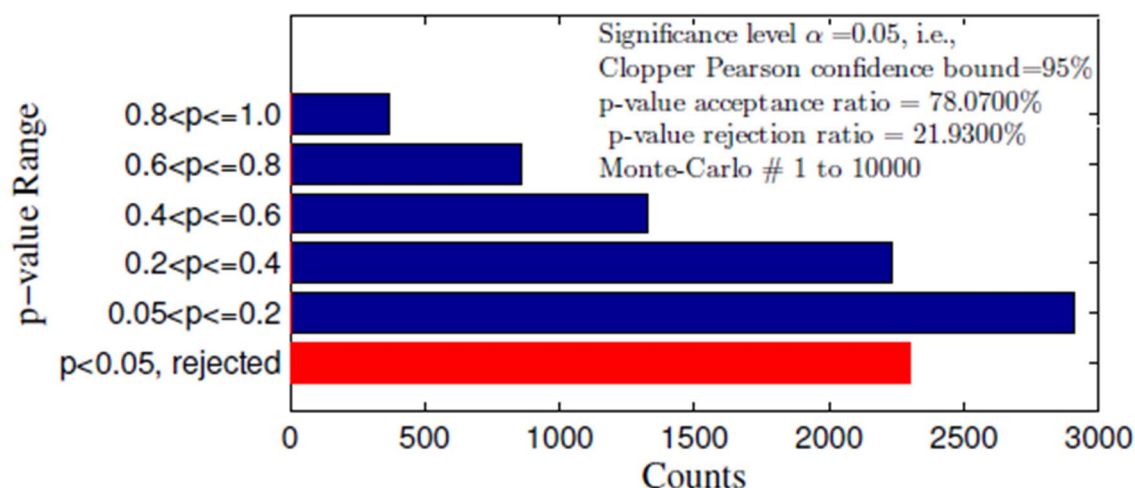


Figure 27: P-value ranges against Monte-Carlo iterations

The results show that 78 % of the time the null hypothesis was accepted, i.e. the model was consistent with the actual data. After analysing all the channels, an interesting phenomenon was observed. Channels with low occupancy levels were fitted to the model better as compared to the highly occupied ones. For example, the same hypothesis testing for channel no. 50, $f_c = 2\,400$ MHz results in 94,79 % acceptance ratio. The reason for deviation is the fact that the highly occupied channels result in very large mean arrival rate λt of the order of hundreds, e.g. λt for Ch. 62 = 393,32. An example, mean arrival rate for a low occupancy channel Ch. 50 is $\lambda t = 4,76$. Rate λt can be thought of as an average rate over t in the whole day, for all local arrival rates λ per minute. This makes the process doubly Poisson, i.e. arrival rates themselves are random variables. Theory suggests that the Poisson process with very large λ tends towards Normal distribution and the process can be approximated by applying Yate's continuity correction and undergoing Normal approximation to Poisson. By applying Normal approximation to the highly occupied channels, the null hypothesis acceptance ratio was found out deteriorated further to approximately 71 %. As an example, Probability Distribution Function (PDF) and CDF fitting plots for Channel 62 are presented in Figures 28 and 29.

For SRO, when the spectrum is divided into 150 channels, an analogy of 150 coins being flipped simultaneously can be conceived. If the outcomes of all coin flips are independent, the process can be defined as a discrete multi-state Markov process with Poisson distribution depending upon the number of trials n , just as explained in the previous clause. The only difference here is that the model can choose any state from 0 to 150. At least one state has to be chosen. For example, if 10 channels out of 150 are found occupied simultaneously, then the state selected is 10. If none is occupied, state is 0, representing SRO = 0 %. Every state can be reached from any other state. Complete transition matrix for such a model is of course quite complicated to calculate. However, thanks to the Markov property, the last state has to be known and the probabilities can be calculated directly from the probability distribution functions. Hypothesis testing was performed with the null hypothesis that the SRO at any sweep n follows a Poisson distribution. A Monte-Carlo type of simulation was performed for 10 000 iterations and χ^2 statistic was evaluated. In every iteration, a single sweep data was randomly selected from the pool of the whole day, i.e. 150 points were selected. Every point represented a channel and a number K was counted, which represented the number of total channels being occupied at that particular time. The hypothesis acceptance ratio was found to be 99,96 %. PDF and CDF fitting plots are shown in Figures 30 and 31. Table 3 provides a short summary of acceptance ratios for both CO and SRO models. Poisson process converges to normality in case of higher occupancies but hypothesis tests' results become more deteriorated. This suggests that the channel should be characterized by a continuous distribution other than Normal or Gaussian. In the case of spectrum resource occupancy model, the results showed remarkable consistency.

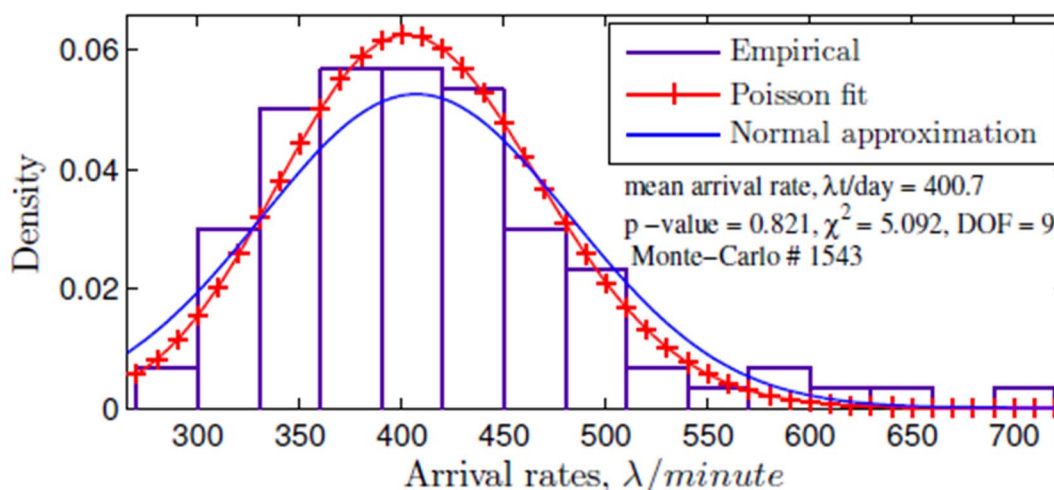


Figure 28: PDF Fitting to Channel 6, $f_c=2412$

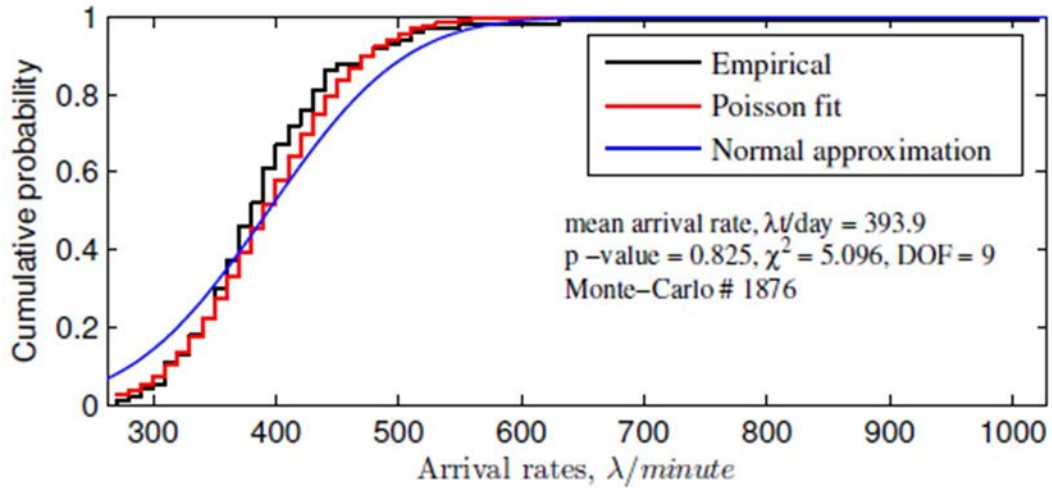


Figure 29: CDF fitting to Channel 62, $f_c=2412$

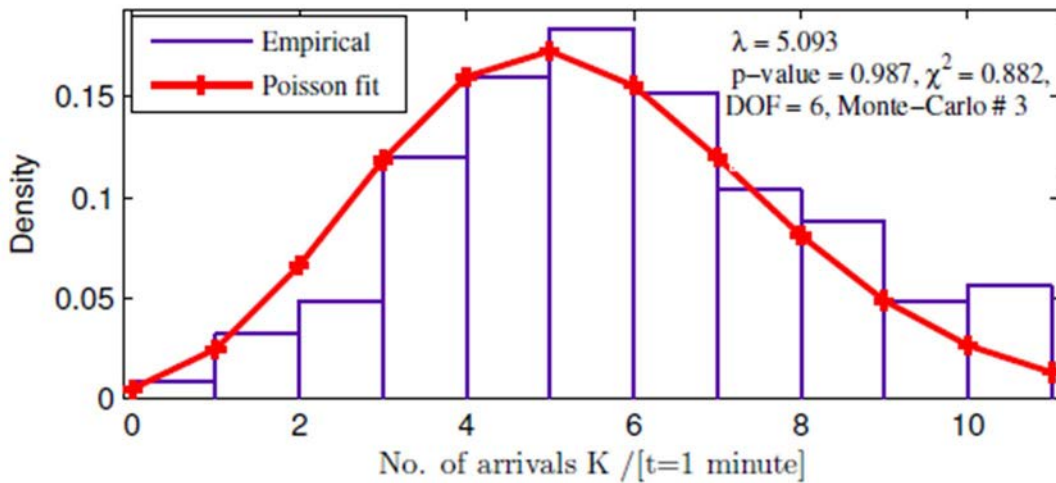


Figure 30: PDF fit for SRO an arbitrary sweep

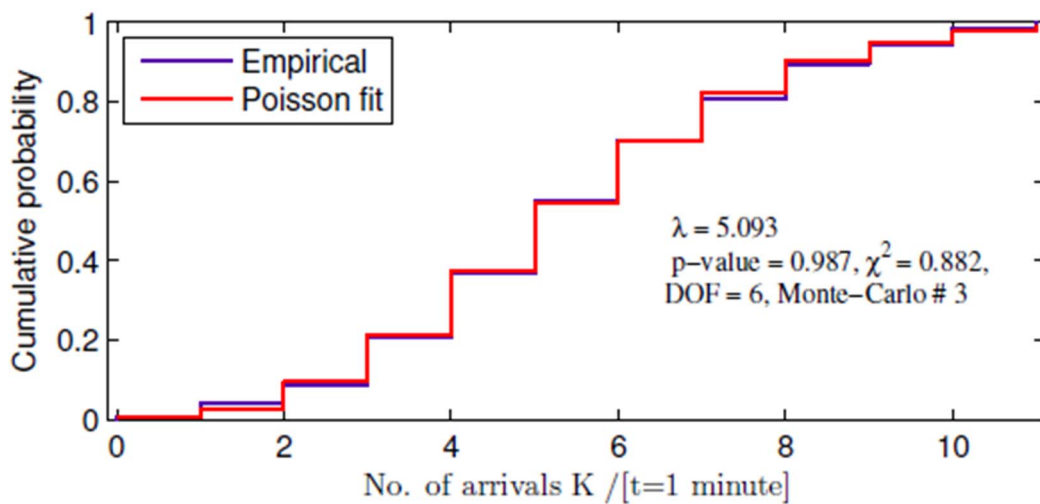


Figure 31: CDF fit for SRO at an arbitrary sweep

Table 3: Summary of Acceptance ratios

	Binary, 1 minute long Binomial Process Statistic = Binomial Exact	Concatenated, N minutes long Poisson Process Statistic = χ^2
CO Model	100%	78.07%
SRO Model	100%	99.96%

6.3.3 Extracting Mathematical Interference model

The analytical models were not very efficient in describing the behaviour of highly occupied channels and the original data. The Normal approximation to Poisson resulted in deteriorated model acceptance ratios. This observation poses the insight that a better model would be continuous, perhaps long-tailed and heavily skewed. For the extraction of mathematical model, the largest data set which was acquired from the daily surgery ward is selected. The total amount of recorded data was 564 GB. Mathematical distribution modelling for the data of such a large scale is a tough nut to crack for a single machine. A distributed computer architecture could have been an option, but it is opted, for simplicity, optimality based on an observation that most of the elements in the sample space were the noise-only samples. So, if those noise-only samples were declared to be zero, a sparse matrix of 4 minutes long data block is got. Then nonzero elements from the sparse were collected and queued. At the end, when all the data blocks and their corresponding vectors were processed, they can be concatenated to make a single large vector. Finally, this vector is passed through a script which applies various distributions to it and decides the best fit. The decision is based on Bayesian information criterion, as:

$$BIC = -2 \cdot \ln \hat{L} + k \cdot \ln(n), \quad (7)$$

where n is the number of data points in the vector, i.e. number of observations, \hat{L} is the maximized value of likelihood function for the model as:

$$\hat{L} = p(x|\hat{\theta}, M). \quad (8)$$

Here x is the vector, $\hat{\theta}$ are the values of parameters that maximize the likelihood function and M is the corresponding model under evaluation. In the case of whole day spectrum variations, Normal, Extreme-value, Generalized Extreme-value, Generalized Pareto, Logistic and t-location scale distributions were applied and evaluated, as it was decided to use the vector samples in logarithmic units rather than linear. To model the variations in the spectrum over the time period of a week and a day individually as well, the best fitting mathematical distribution models were evaluated. It was observed that spectrum was varying in a fashion that could be best described by Generalized Extreme Value (GEV) and the next most likely model was the t-location scale. Interestingly, week-long variations and all individual day-long variations were following the same distribution. Probability distribution function for GEV can be written as:

$$y = f(x|k, \mu, \sigma) = \left(\frac{1}{\sigma}\right) \exp \left[- \left[1 + k \frac{(x-\mu)}{\sigma} \right]^{\frac{1}{k}} \right] \left[1 + k \frac{(x-\mu)}{\sigma} \right]^{-1-\frac{1}{k}}, \quad (9)$$

for $1 + k \frac{(x-\mu)}{\sigma} > 0$. Here k is the shape parameter, μ is the location parameter, and σ is the scale parameter. The distribution was Type II Frechet distribution as k was greater than zero in every case. Hence, the expected value of x from a sample space X can be given as:

$$E(X) = \mu - \frac{\sigma}{k} + \frac{\sigma}{k} g_1, \quad (10)$$

where $g_n = \Gamma(1 - nk) \forall n \in N = \{1,2,3,4, \dots\}$ and $\Gamma(t)$ is the gamma function.

In addition to that, models for week-long variations in FBO, SRO and certain channel occupancies were evaluated. The models under deeper study, in this case, were Beta, Birnbaum-Saunders, Burr, Exponential, Extreme-value, Gamma, Generalized extreme-value, Generalized Pareto, Inverse Gaussian, Logistic, Log-Logistic, Lognormal, Nakagami, Normal, Rayleigh, Rician, t location-scale and Weibull.

Weekly variations in IEEE 802.11b [i.30] and IEEE 802.11g [i.31], Channel 1 occupancies were observed to follow Burr Type XII distribution whereas the next most likely model was GEV. The PDF for Burr is given as:

$$Y = \frac{kc}{\alpha} \left(\frac{x}{\alpha}\right)^{c-1} \quad (11)$$

and

$$\Phi = \left(1 + \left(\frac{x}{\alpha}\right)^c\right)^{k+1} \quad (12)$$

then

$$y = f(x|\alpha, c, k) = \frac{Y}{\Phi} \quad \forall x, \alpha, c, k > 0. \quad (13)$$

The distribution has been observed to be heavily skewed and long-tailed, which suggests a large number of unique higher occupancy values that essentially make up the tail far away from the distribution head or mean. Long-tailed behaviour was seen from 8 % to 60 % of occupancies with low probability density, whereas higher density values comprising the head were seen from 4 % to 7 %.

Week-long variations in IEEE 802.11b [i.30] and IEEE 802.11g [i.31], Channel 6 occupancies are following the t location-scale model. The PDF for t-location scale is given as:

$$f(x|\mu, \sigma, v) = \frac{\Gamma\left(\frac{v+1}{2}\right)}{\sigma\sqrt{\pi v}\Gamma\left(\frac{v}{2}\right)} \left(\frac{v + \frac{(x-\mu)^2}{\sigma^2}}{v}\right)^{-\frac{v+1}{2}}, \quad (14)$$

where μ is a location parameter, σ is a scale parameter and v is a shape parameter. If all the distribution parameters for x are greater than zero, just as in the proposed case, then $\frac{x-\mu}{\sigma}$ have a Student's t distribution with v degrees of freedom. It was observed that the degree of freedom $v = 1,99 \cong 2$, which implies a special case and the distribution is reduced to fairly simple form as:

$$f(x) = \frac{1}{2} + \frac{x}{2\sqrt{2+x^2}}. \quad (15)$$

It is a heavy two-tailed distribution, and in the proposed case, it was made up of one left short tail and another right long tail. Left tail was comprised of occupancy values ranging from 0,6 % to 3 % with very low probability density, head ranged from 4 % to 7 % with sufficiently higher probability density values, and the right tail wagged from 8 % to 53 %, again with very low density.

Variations in IEEE 802.11b [i.30] and IEEE 802.11g [i.31], Channel 11 had been observed to follow the Logistic model. PDF of the Logistic distribution is given as:

$$f(x|\mu, \sigma) = \frac{\exp\left(-\frac{x-\mu}{\sigma}\right)}{\sigma\left(1 + \exp\left(-\frac{x-\mu}{\sigma}\right)\right)^2}, \quad (16)$$

where μ is the location parameter and $\sigma > 0$ is the scale parameter. This model also belongs to the family of heavy-tailed distributions, and in the proposed case, it was lacking shoulder with large kurtosis. The reason was that the channel was found to be completely unoccupied on some occasion. It should be noted that the occupancies are a measure of average usage over the integration time of 4 minutes. It means that on certain occasions Channel 11 was unoccupied for equal to or more than 4 minutes. The tail was observed to be wagged from 1 % to 21 % with very low density, and the head was comprised of 0,01 % to 0,9 % with higher probability density. IEEE 802.11n [i.32] Channel 3 and Channel 9 were also observed to be following the Logistic model. Both of these channels had low occupancy levels ranging from 0 % to 4 %, approximately. Moreover, weekly variations in FBO and SRO (for WLAN systems) were following t-location scale distribution. Table 4 provides a summary of best fit models and Table 5 provides the parameters for the models. Following assumptions can be inferred from the results:

- 1) Extremely low occupancies, model is Logistic.
- 2) Moderately low occupancies, model is t-location scale or GEV.
- 3) Higher occupancies, model is Burr Type XII.

Table 4: Summary of Models with BIC values

Observation	Best fit model with BIC value	Next best fit model & BIC value
Day 1 spectrum variations	GEV, 1.7017e+06	t-location scale, 1.8271e+06
Day 2 spectrum variations	GEV, 1.5874e+06	t-location scale, 1.6852e+06
Day 3 spectrum variations	GEV, 1.5854e+06	t-location scale, 1.6940e+06
Day 4 spectrum variations	GEV, 1.5681e+06	t-location scale, 1.6946e+06
Day 5 spectrum variations	GEV, 1.6713e+06	t-location scale, 1.7990e+06
Day 6 spectrum variations	GEV, 1.7507e+06	t-location scale, 1.8707e+06
Day 7 spectrum variations	GEV, 1.6795e+06	t-location scale, 1.7988e+06
Whole week spectrum variations	GEV 1.7843e+06	t-location scale, 1.8975e+06
Whole week IEEE 802.11b/g Ch.1	Burr Type XII, 3.4712e+03	GEV 3.4808+03
Whole week IEEE 802.11b/g Ch.6	t-location scale, 4.2516e+03	Logistic, 4.8131e+03
Whole week IEEE 802.11b/g Ch.11	Logistic, -1.7821e+04	Generalized Pareto, -8.6108e+03
Whole week IEEE 802.11n Ch.3	GEV, -6.7644e+03	t-location scale, -6.3864+03
Whole week IEEE 802.11n Ch.9	Logistic, -9.4174e+03	t-location scale, -9.2838e+03
Whole week FBO variations	t-location scale, -6.5017e+03	GEV, -6.4239e+03
Whole week SRO (IEEE 802.11b/g)	GEV, -1.8972e+04	t-location scale, -1.8916e+04
Whole week SRO (IEEE 802.11n)	t-location scale, -387.73	Log-logistic, 264.27

Table 5: Models with parameter description

Observation	Distribution Model	Parameter Description
Day 1 spectrum variations	GEV	$k = 0.6676, \sigma = 2.9557, \mu = -85.9427$
Day 2 spectrum variations	GEV	$k = 0.6370, \sigma = 2.8504, \mu = -85.5746$
Day 3 spectrum variations	GEV	$k = 0.7941, \sigma = 2.8023, \mu = -85.7233$
Day 4 spectrum variations	GEV	$k = 0.8568, \sigma = 2.6080, \mu = -85.9357$
Day 5 spectrum variations	GEV	$k = 0.7900, \sigma = 2.7385, \mu = -85.8011$
Day 6 spectrum variations	GEV	$k = 0.8520, \sigma = 3.0775, \mu = -85.6074$
Day 7 spectrum variations	GEV	$k = 0.7739, \sigma = 2.9172, \mu = -85.6607$
Whole week spectrum variations	GEV	$k = 0.7812, \sigma = 2.8348, \mu = -85.9843$
Whole week IEEE 802.11b/g Ch.1	Burr Type XII	$\alpha = 5.7691, c = 43.5808, k = 0.2567$
Whole week IEEE 802.11b/g Ch.6	t-location scale	$\mu = 5.3937, \sigma = 0.3650, \nu = 1.9946$
Whole week IEEE 802.11b/g Ch.11	Logistic	$\mu = -0.0094, \sigma = 0.0290$
Whole week IEEE 802.11n Ch.3	GEV	$k = 0.2759, \sigma = 0.0380, \mu = 0.0711$
Whole week IEEE 802.11n Ch.9	Logistic	$\mu = 0.0563, \sigma = 0.0047$
Whole week FBO variations	t-location scale	$\mu = 0.8664, \sigma = 0.0360, \nu = 2.4698$
Whole week SRO (IEEE 802.11b/g)	GEV	$k = 0.4101, \sigma = 0.0022, \mu = 0.0055$
Whole week SRO (IEEE 802.11n)	t-location scale	$\mu = 3.8262, \sigma = 0.1370, \nu = 2.2628$

- Percentage of occupancy of each band, i.e. the amount of time that the received amplitude keeps over the noise level plus 20 dB.
- Probability distribution function of the received samples.
- The best PDF that approximates the real samples' distribution.
- The waterfall graph of the interference levels as a function of both the time and frequencies.

6.3.4.1 Occupancy

6.3.4.1.0 Introduction

The occupancies for several points are reported in the following figures.

The occupancy of the frequencies of the ISM band over time is the percentage of time that the received amplitude keeps 20 dB over the noise level. Figures 33 and 34 show how different the traffic, and thus, the mutual interference, can be in different locations of a ward.

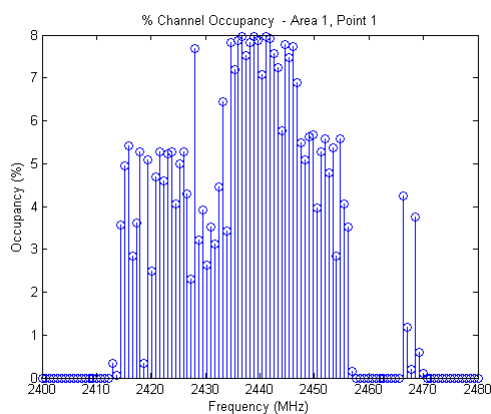


Figure 33: % occupancy for the blue point n. 1

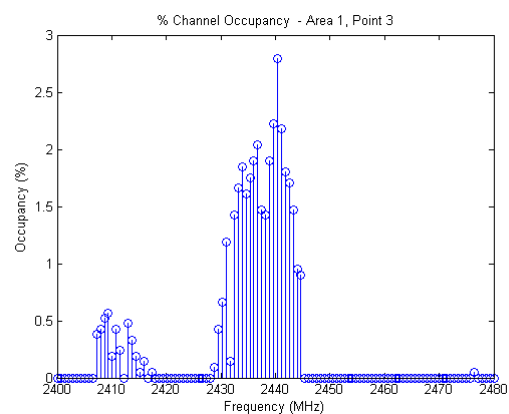


Figure 34: % occupancy for the blue point n. 3

6.3.4.1.1 Percentiles

Figures 35 and 36 show the percentiles of the interference plus noise power in the measured ISM band over time for two locations at zone 1. A percentile is a measure used in statistics indicating the value below which a given percentage of observations in a group of observations fall. For example, the 20th percentile is the value below which 20 % of the observations are found. Focusing on Figure 36, it is evident that the 90 % of the interference plus noise power samples (over the entire samples collected for 5 hours) fall below -87 dBm. Consequently, only 10 % of the total interference samples were higher than -87 dBm. The Average Noise Level (ANL) was measured to be -100 dBm.

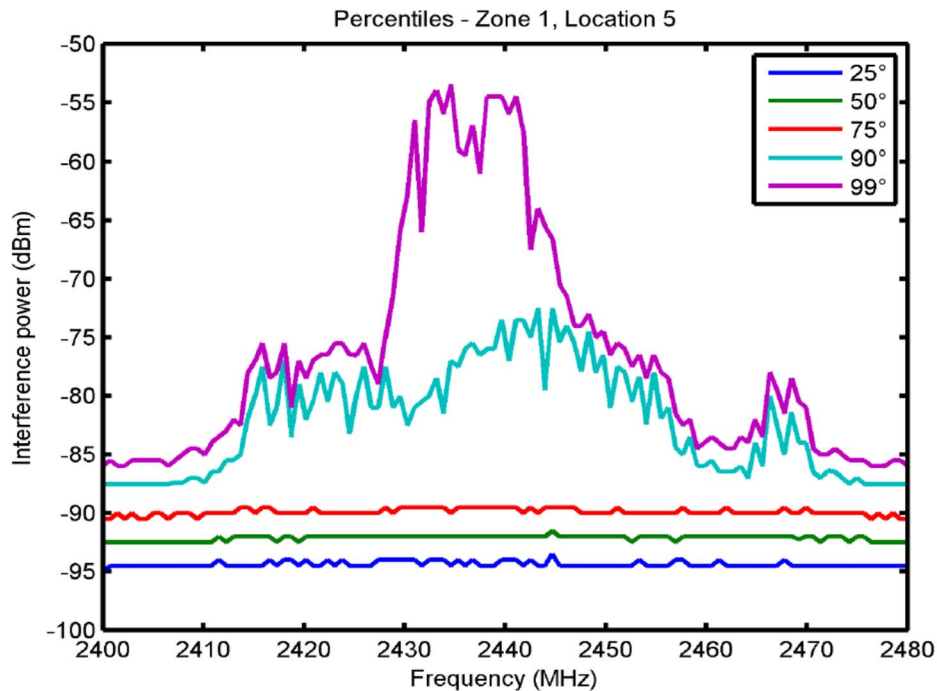


Figure 35: Percentiles - Corridor 1, Point 1

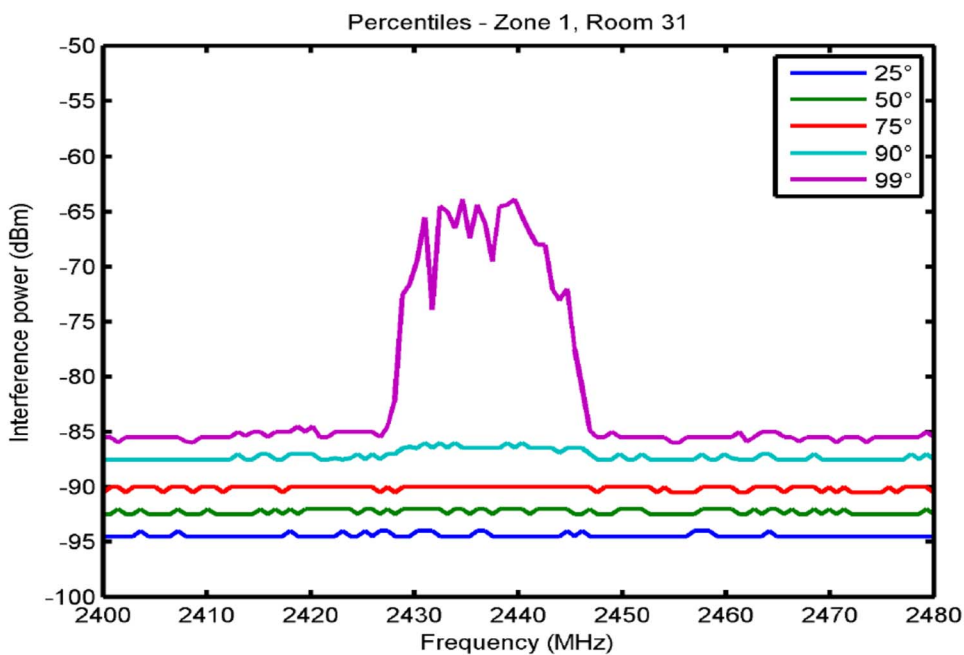


Figure 36: Percentiles - Corridor 1, Point 3

6.3.4.2 PDF

For the same locations, the fitting PDF for each frequency in the ISM band has been calculated.

How to read the following figures: the numbers on the y-axis of the graphics indicate the index associated with the best fitting PDF for the specific frequency observed. The PDFs considered have been enumerated from 1 to 16 and they are listed in Table 6.

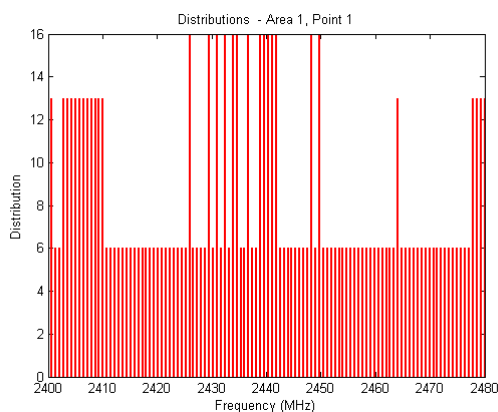


Figure 37: Best fitting PDF for each frequency; location: blue point n. 1

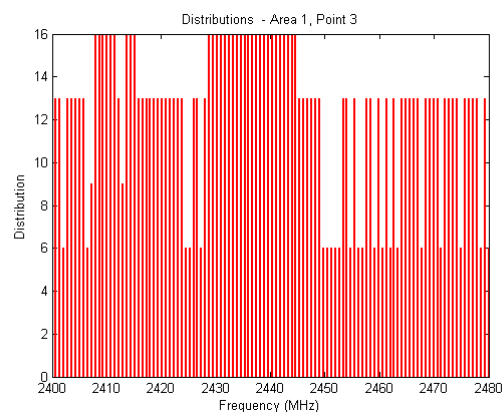


Figure 38: Best fitting PDF for each frequency; location: blue point n. 3

Table 6: Index of the probability distribution functions considered for finding the best fitting ones for each scanned frequency

Distribution	Index
Beta	1
Birnbaum-Saunders	2
Exponential	3
Extreme value	4
Gamma	5
Generalized extreme value	6
Generalized Pareto	7
Inverse Gaussian	8
Logistic	9
Log-logistic	10
Lognormal	11
Nakagami	12
Normal	13
Rayleigh	14
Rician	15
t location-scale	16
Weibull	17

As seen from Figures 37 and 38, if there is enough interference in a frequency, the distribution of the received samples is t location-scale, while if in a frequency there is only noise, then the distribution changes to the generalized extreme value. Also, the Normal distribution is frequent, but not as often as the GEVD.

The t Location-Scale Distribution (TLSD) has the density function:

$$f(x|\mu, \sigma, \nu) = \frac{\Gamma(\frac{\nu+1}{2})}{\sigma\sqrt{\pi\nu}\Gamma(\nu/2)} \cdot \left(\frac{\nu + \frac{(x-\mu)^2}{\sigma^2}}{\nu} \right)^{-\frac{\nu+1}{2}} \quad (17)$$

with location parameter μ , scale parameter $\sigma > 0$, and shape parameter $\nu > 0$. If x has a t location-scale distribution, with parameters μ , σ , and ν , then:

$$f(x|\mu, \sigma) = \frac{x-\mu}{\sigma} \quad (18)$$

has a Student's t distribution with ν degrees of freedom.

The t location-scale distribution is useful for modelling data distributions with heavier tails (more prone to outliers) than the normal distribution. It approaches the normal distribution as ν approaches infinity, and smaller values of ν yield heavier tails.

The probability density function for the **Generalized Extreme Value Distribution (GEVD)** with location parameter μ , scale parameter σ , and shape parameter $k \neq 0$ is:

$$y = f(x | k, \mu, \sigma) = \left(\frac{1}{\sigma}\right) \exp\left[-\left(1 + k \frac{(x-\mu)}{\sigma}\right)^{-\frac{1}{k}}\right] \left(1 + k \frac{(x-\mu)}{\sigma}\right)^{-1-\frac{1}{k}} \quad (19)$$

for

$$1 + k \frac{(x-\mu)}{\sigma} > 0, \quad (20)$$

$k > 0$ corresponds to the Type II case, while $k < 0$ corresponds to the Type III case. For $k = 0$, corresponding to the Type I case, the density is:

$$y = f(x | 0, \mu, \sigma) = \left(\frac{1}{\sigma}\right) \exp\left(-\exp\left(-\frac{(x-\mu)}{\sigma}\right) - \frac{(x-\mu)}{\sigma}\right) \quad (21)$$

Like the extreme value distribution, the generalized extreme value distribution is often used to model the smallest or largest value among a large set of independent, identically distributed random values representing measurements or observations. The generalized extreme value combines three simpler distributions into a single form, allowing a continuous range of possible shapes that includes all three of the simpler distributions. Any one of those distributions can be used to model a particular dataset of block maxima. The generalized extreme value distribution allows to "let the data decide" which distribution is appropriate. The three cases covered by the generalized extreme value distribution are often referred to as Types I, II, and III. Each type corresponds to the limiting distribution of block maxima from a different class of underlying distributions. Distributions whose tails decrease exponentially, such as the normal, lead to Type I. Distributions whose tails decrease as a polynomial, such as Student's t , lead to Type II. Distributions whose tails are finite, such as the beta, lead to Type III.

6.3.4.3 Interference as a function of time and frequency

In this clause, waterfall graphs are shown, i.e. the received amplitude levels as a function of time and frequency. As an example, Figures 37 and 38 show the waterfall graphs for the measurement points 1 and 3 at Corridor 1.

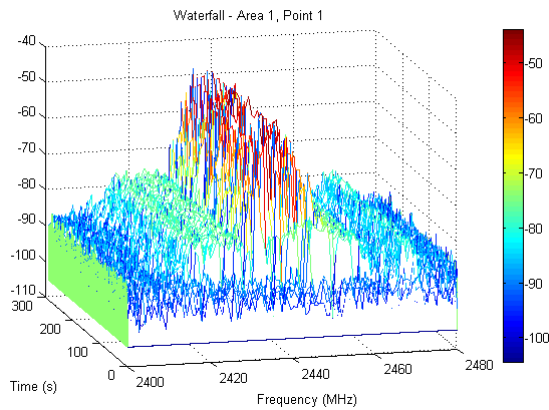


Figure 37a: Interference plus noise as a function of time and frequency; location: blue point n. 1

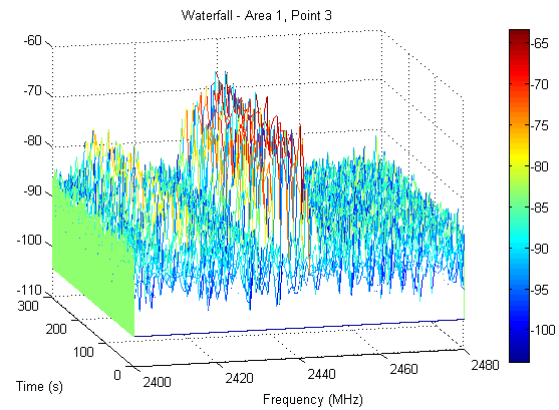


Figure 38a: Interference plus noise as a function of time and frequency; location: blue point n. 3

6.3.4.4 Parameters characterizing the distribution

The parameters of the distribution that best fit the received samples in each location of the hospital ward are reported. An example for location blue point n. 1 (corridor 1) is presented in Table 7.

Table 7: Parameters defining the distribution of the received samples for the location 1 of corridor 1

Frequency	Distribution	Parameters								
		Name	Description	Value	Name	Description	Value	Name	Description	Value
2412	generalized extreme value	k	(shape)	-0.205	sigma	(scale)	3.197	mu	(location)	-93.297
2417	generalized extreme value	k	(shape)	-0.050	sigma	(scale)	3.359	mu	(location)	-93.310
2422	generalized extreme value	k	(shape)	0.006	sigma	(scale)	3.371	mu	(location)	-93.472
2427	generalized extreme value	k	(shape)	-0.033	sigma	(scale)	3.405	mu	(location)	-93.507
2432	generalized extreme value	k	(shape)	0.071	sigma	(scale)	3.515	mu	(location)	-93.478
2437	tllocationscale	mu	(location)	-92.302	sigma	(scale)	2.600	nu	(degrees of freedom)	1.796
2442	tllocationscale	mu	(location)	-92.303	sigma	(scale)	2.501	nu	(degrees of freedom)	1.727
2447	generalized extreme value	k	(shape)	0.071	sigma	(scale)	3.590	mu	(location)	-93.484
2452	generalized extreme value	k	(shape)	0.018	sigma	(scale)	3.398	mu	(location)	-93.474
2457	generalized extreme value	k	(shape)	-0.110	sigma	(scale)	3.226	mu	(location)	-93.403
2462	generalized extreme value	k	(shape)	-0.241	sigma	(scale)	3.229	mu	(location)	-93.138
2467	generalized extreme value	k	(shape)	-0.078	sigma	(scale)	3.405	mu	(location)	-93.458
2472	generalized extreme value	k	(shape)	-0.256	sigma	(scale)	3.264	mu	(location)	-93.321

The values shown in Table 7 are the main parameters of the best PDF for the scanned frequencies. Frequencies are shown in the first left column. The second column indicates which is the best fitting PDF, and the remaining columns represent the derived main values of the associated PDF, as in Equations (17) and (19).

6.3.4.5 Home and office environments

The measurements in the home (Figures 39 and 40) and office environments (Figures 41 and 42) have been carried out for **one week** with the same device and settings as the ones described in the previous clause. The office environment, as well as the home, is a typical modern city office, with several internal Wi-Fi® access points and surrounded by other offices and houses. The city has also a free Wi-Fi® access network for public use and its signal is received also in the office. The home environment has a similar characterization, apart from the public Wi-Fi®, which is not present there.

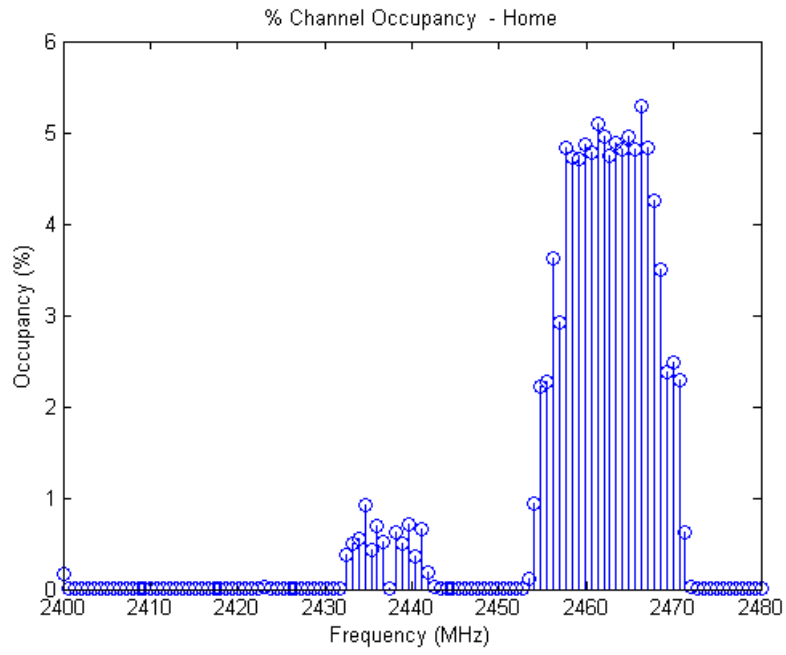


Figure 39: Occupancy @ HOME

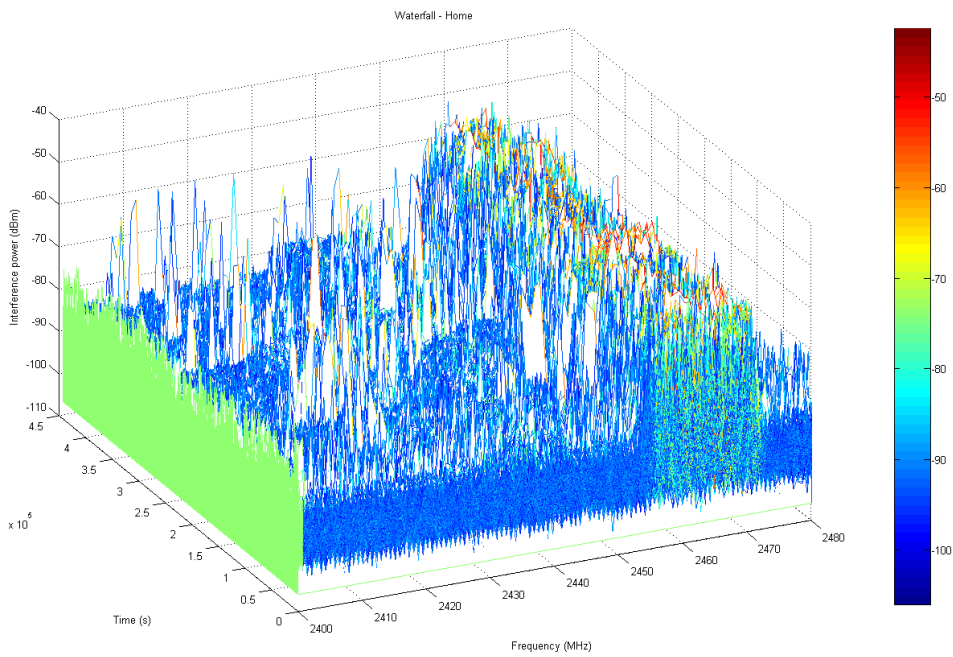


Figure 40: Waterfall @ HOME

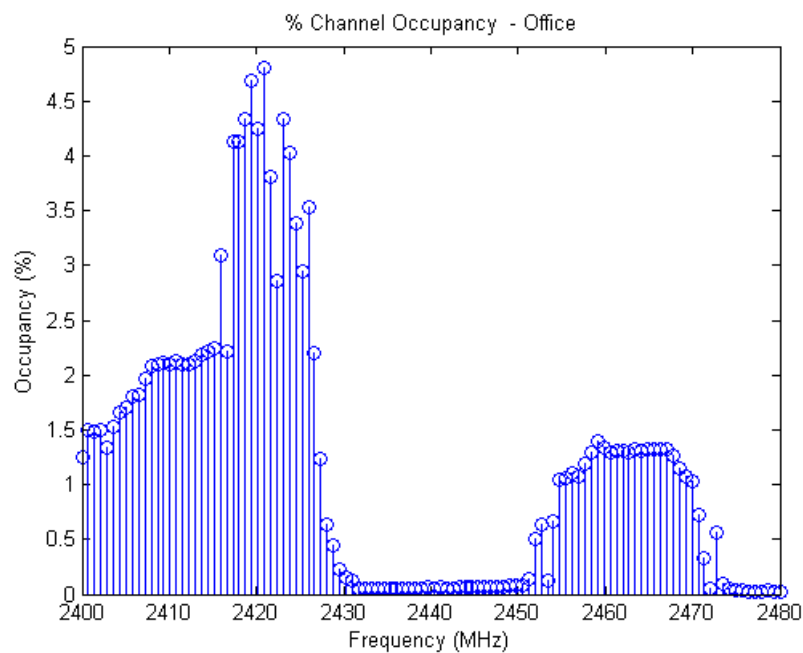


Figure 41: Occupancy @ OFFICE

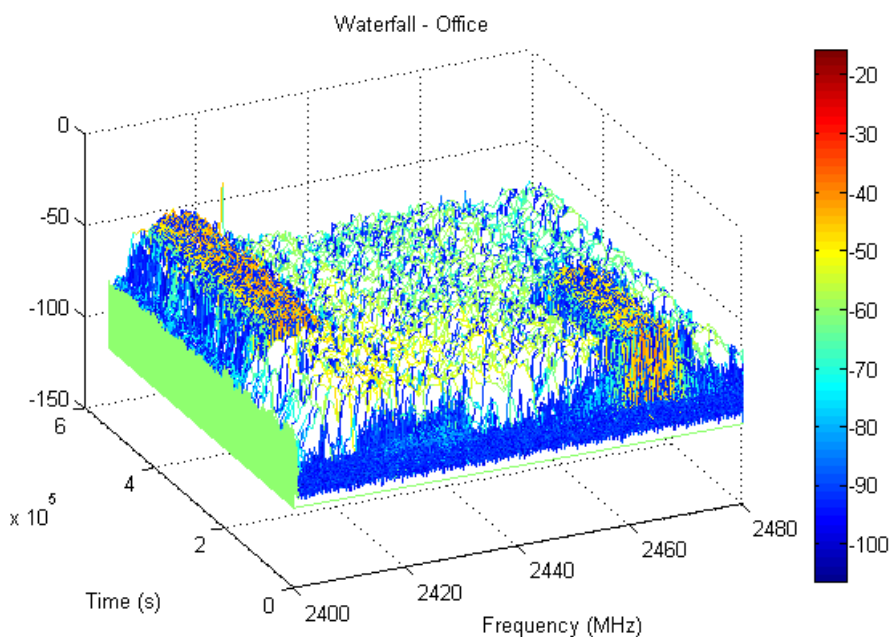


Figure 42: Waterfall @ OFFICE

Analysing the results, there is a correlation between the occupancy and the estimated distribution of the channel. In fact:

- for frequencies that are poorly utilized, the best fitting PDF of the interference samples over time is a normal or a generalized extreme value distribution;
- for frequencies with a high percentage of occupancy, the best fitting PDF of the interference samples is a t location-scale distribution.

6.3.4.6 Extract the mathematical model

6.3.4.6.0 Introduction

The above experiments and parameters extraction can be used to characterize the aggregate interference.

6.3.4.6.1 First results of CNIT-UNIFI

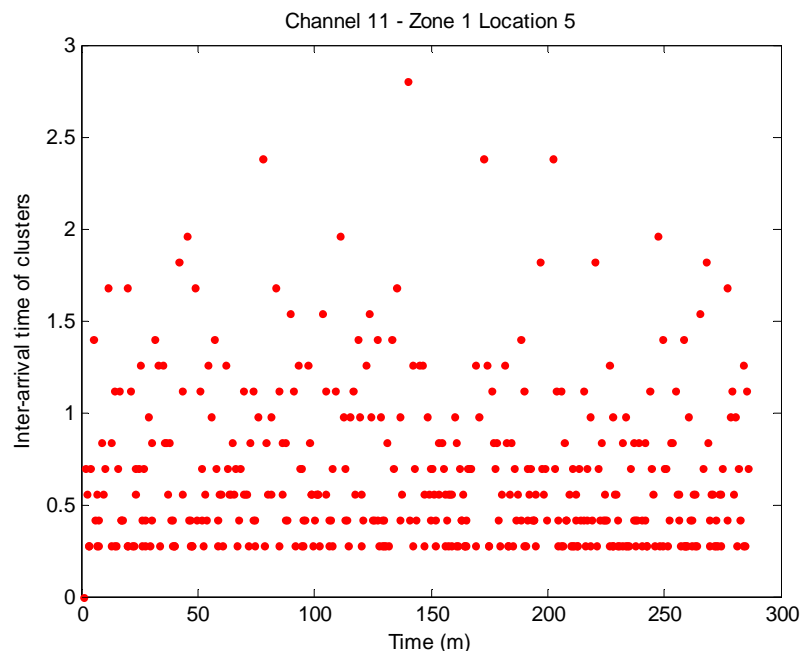
$T_c = 1,25$ ms

Centre Frequency: 2,462 GHz (Channel 11)

Zone 1 - Location 5

Inter-arrival time of interference clusters

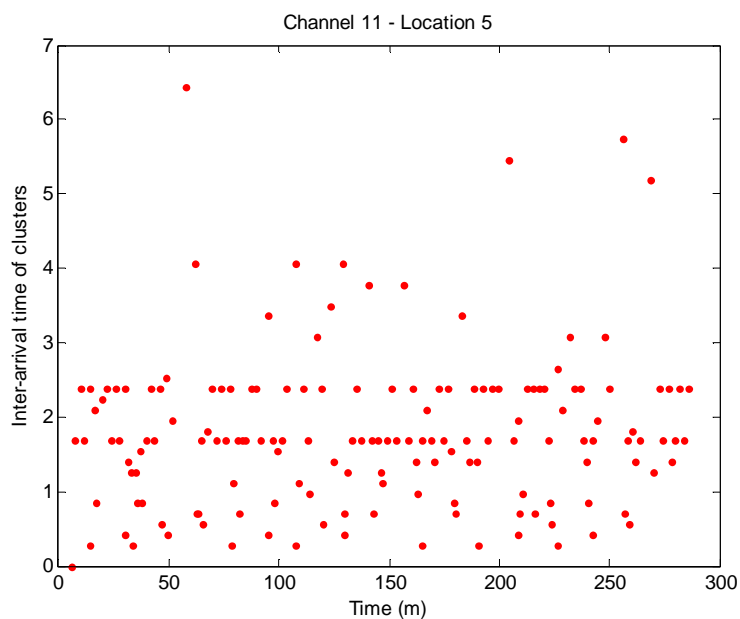
Figure 43 shows how the inter-arrival time between the interfering clusters is distributed over time. Figures 43 and 44 report in the x-axis the time measured in minutes, while in the y-axis the unit is microseconds.



NOTE: Inter-arrival time of interference clusters. The threshold is set at -90 dBm.

Figure 43: Inter-arrival time of interference clusters

- DistName: 'generalized extreme value'
 - NLogL: 1,2199e+03
 - BIC: 2,4588e+03
 - AIC: 2,4459e+03
 - AICc: 2,4459e+03
- ParamNames: {'k' 'sigma' 'mu'}
- ParamDescription: {'shape' 'scale' 'location'}
- Params: [0,5052 1,3957 1,9574]



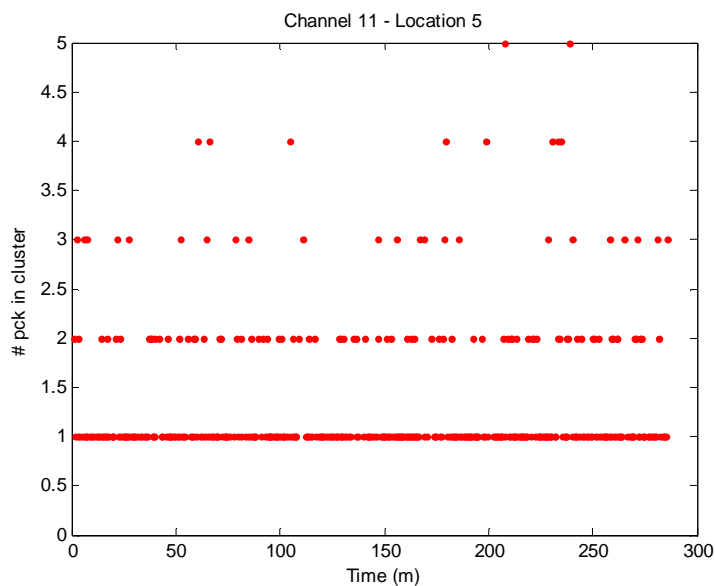
NOTE: Inter-arrival time of interference clusters. The threshold is set at -80 dBm.

Figure 44: Inter-arrival time of interference clusters

- DistName: 'generalized extreme value'
 - NLogL: 525,6960
 - BIC: 1,0666e+03
 - AIC: 1,0574e+03
 - AICc: 1,0575e+03
- ParamNames: {'k' 'sigma' 'mu'}
- ParamDescription: {'shape' 'scale' 'location'}
- Params: [-0,0066 5,9304 9,3913]

Dimension of clusters

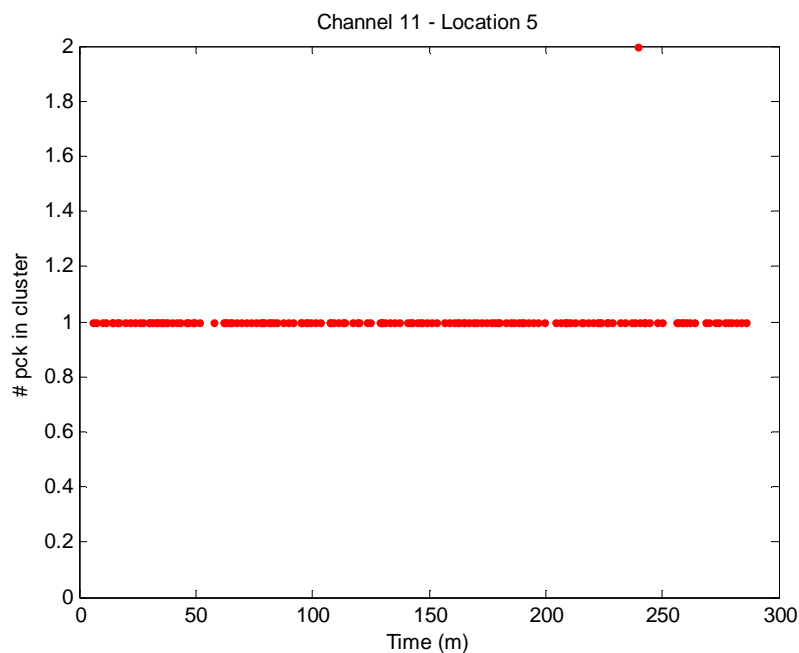
The following graphs show how the dimension of the interfering clusters is distributed over time. Figures 45 and 46 report in the x-axis the time measured in minutes, while in the y-axis the unit is the number of samples per cluster.



NOTE: Inter-arrival time of interference clusters. The threshold is set at -90 dBm.

Figure 45: Dimension of interfering clusters

- DistName: 'generalized pareto'
 - NLogL: -1,1562e+04
 - BIC: -2,3106e+04
 - AIC: -2,3119e+04
 - AICc: -2,3119e+04
- ParamNames: {'k' 'sigma' 'theta'}
- ParamDescription: {'shape' 'scale' 'threshold'}
- Params: [11,5876 3,1761e-15 1,0000]



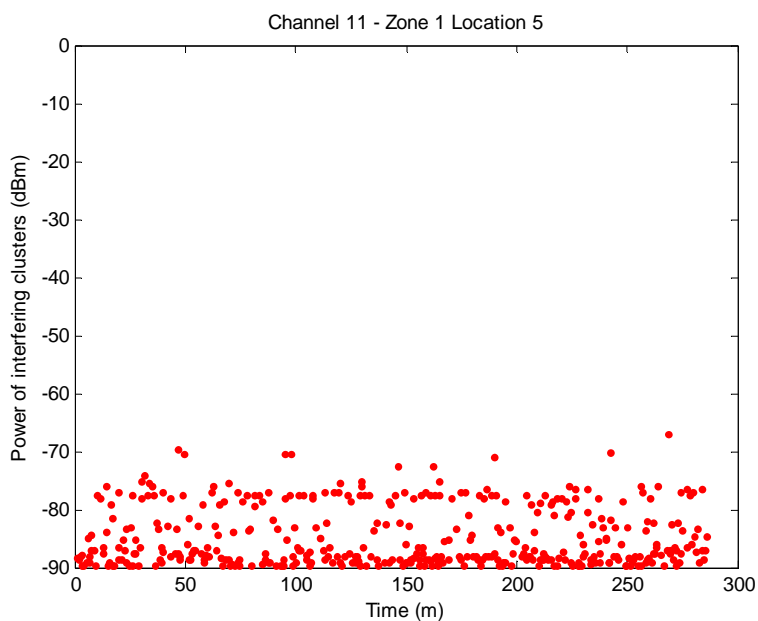
NOTE: Inter-arrival time of interference clusters. The threshold is set at -80 dBm.

Figure 46: Dimension of interfering clusters

- DistName: 'generalized extreme value'
 - NLogL: -1,1002e+05
 - BIC: -2,2002e+05
 - AIC: -2,2003e+05
 - AICc: -2,2003e+05
- ParamNames: {'k' 'sigma' 'mu'}
- ParamDescription: {'shape' 'scale' 'location'}
- Params: [28,9517 1,6105e-307 1]

Power of clusters

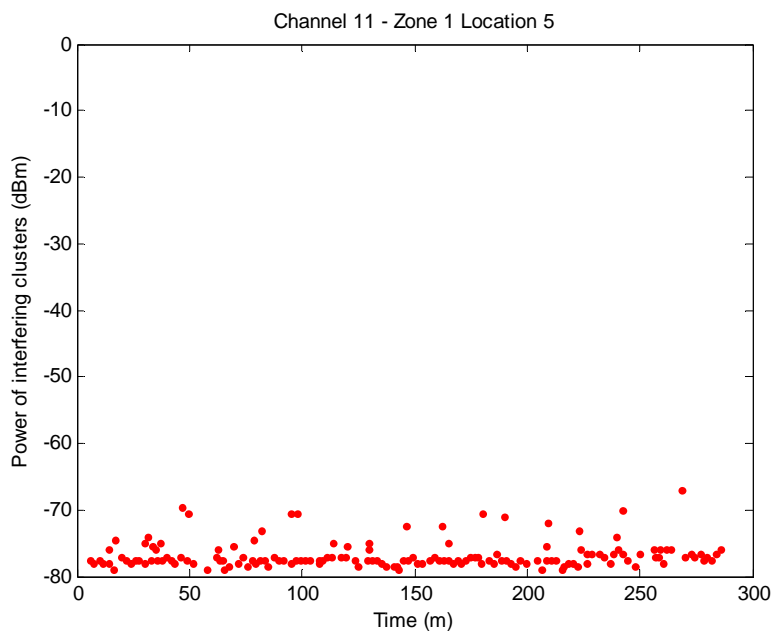
Figures 47 and 48 show how the amplitude of the interfering clusters is distributed over time. The figures report in the x-axis the time measured in minutes, while in the y-axis the unit is dBm.



NOTE: Inter-arrival time of interference clusters. The threshold is set at -90 dBm.

Figure 47: Power of the interference clusters

- DistName: 'generalized extreme value'
 - NLogL: 1,4321e+03
 - BIC: 2,8832e+03
 - AIC: 2,8702e+03
 - AICc: 2,8703e+03
- ParamNames: {'k' 'sigma' 'mu'}
- ParamDescription: {'shape' 'scale' 'location'}
- Params: [1,2060 1,4499 -88,6043]



NOTE: Inter-arrival time of interference clusters. The threshold is set at -80 dBm.

Figure 48: Power of interference clusters

- DistName: 'generalized extreme value'
 - NLogL: 274,2105
 - BIC: 563,5897
 - AIC: 554,4209
 - AICc: 554,5778
- ParamNames: {'k' 'sigma' 'mu'}
- ParamDescription: {'shape' 'scale' 'location'}
- Params: [0,2444 1,0261 -77,6274]

Zone 1 - Room 31

Inter-arrival time of clusters

Figures 49 and 50 show how the inter-arrival time between the interfering clusters is distributed over time. The figures report, in the x-axis, the time measured as the number of samples, while, in the y-axis, the unit as samples.

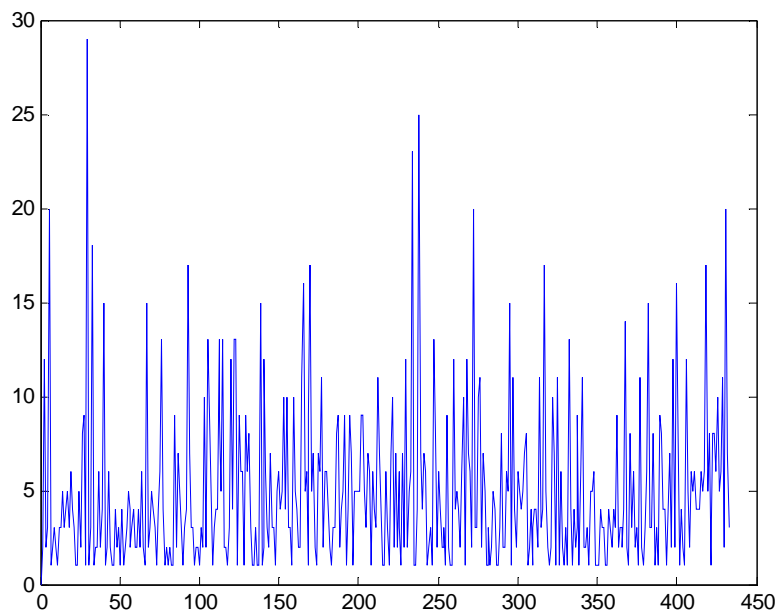


Figure 49: Inter-arrival discrete time of the interference clusters

- DistName: 'generalized extreme value'
 - NLogL: 1,0920e+03
 - BIC: 2,2022e+03
 - AIC: 2,1900e+03
 - AICc: 2,1900e+03
- ParamNames: {'k' 'sigma' 'mu'}
- ParamDescription: {'shape' 'scale' 'location'}
- Params: [0,4614 1,9890 2,5822]

Dimension of clusters

Figures 50 and 51 show how the dimension of the interfering clusters is distributed over time. The figures report, in the x-axis, the time measured as the number of samples, while, in the y-axis, the unit as samples.

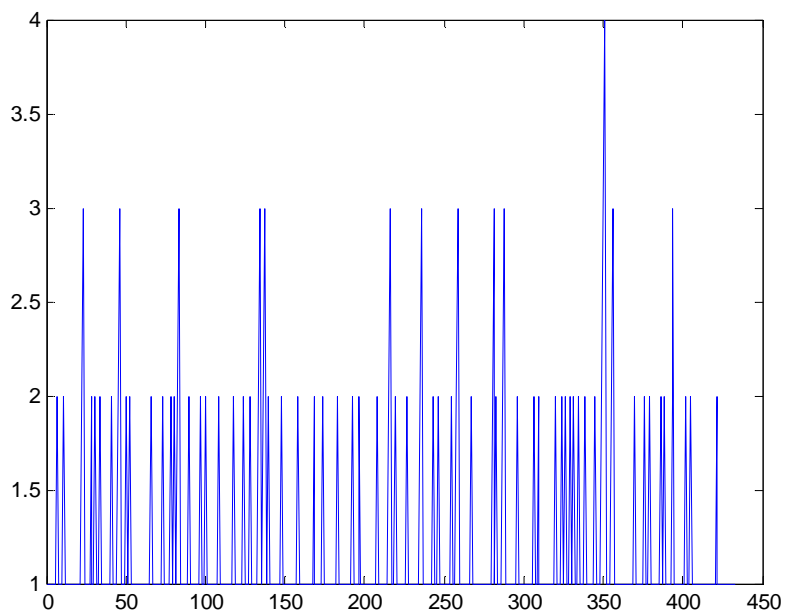


Figure 50: Interference cluster (discrete) dimension

- DistName: 'generalized pareto'
 - NLogL: -1,0466e+04
 - BIC: -2,0913e+04
 - AIC: -2,0926e+04
 - AICc: -2,0926e+04
- ParamNames: {'k' 'sigma' 'theta'}
- ParamDescription: {'shape' 'scale' 'threshold'}
- Params: [8,3355 2,8089e-15 1,0000]

Mean power of clusters

Figure 51 shows how the power of the interfering clusters is distributed over time. The figures report, in the x-axis the time measured as the number of samples, while, in the y-axis, the unit as dBm.

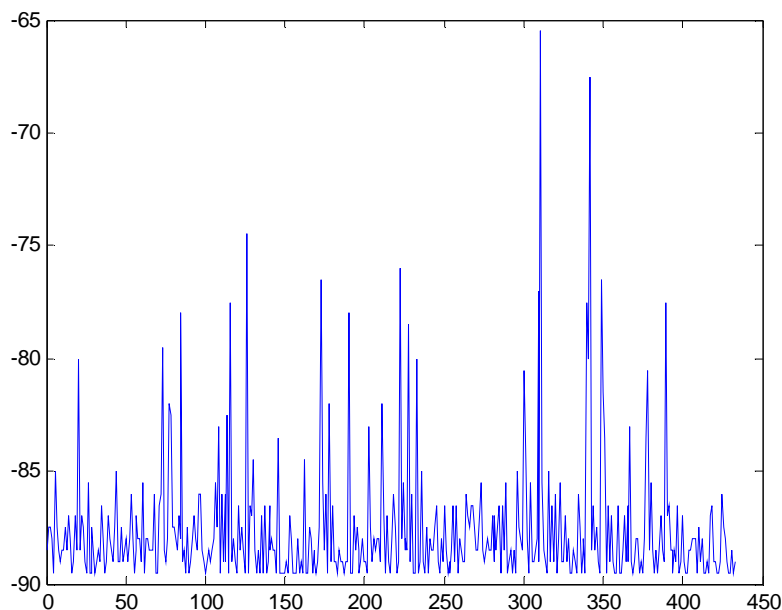


Figure 51: Mean power of the interference clusters

- DistName: 'generalized extreme value':
 - NLogL: 739,8401
 - BIC: 1,4979e+03
 - AIC: 1,4857e+03
 - AICc: 1,4857e+03
- ParamNames: {'k' 'sigma' 'mu'}
- ParamDescription: {'shape' 'scale' 'location'}
- Params: [0,7747 0,7522 -88,9698]

6.4 Statistical model of the interference

6.4.0 Introduction

The statistical model of the interference in the ISM band has been developed using only data from the two measurement campaigns (December 2013 and June 2014) carried out at Oulu University Hospital, since the measurements in Florence's hospital did not have a sufficient amount of samples per sweep.

In particular, two channels have been evaluated: the best and the worst one. Channel #6 (2 437 MHz) of December 2013 measurements is the best one and Channel #1 (2 412 MHz) of June 2014 measurements is the worst one.

The statistical model of the interference starts modelling three characteristics of the interference: clusters dimension, interarrival time and cluster amplitude.

6.4.1 Cluster dimension

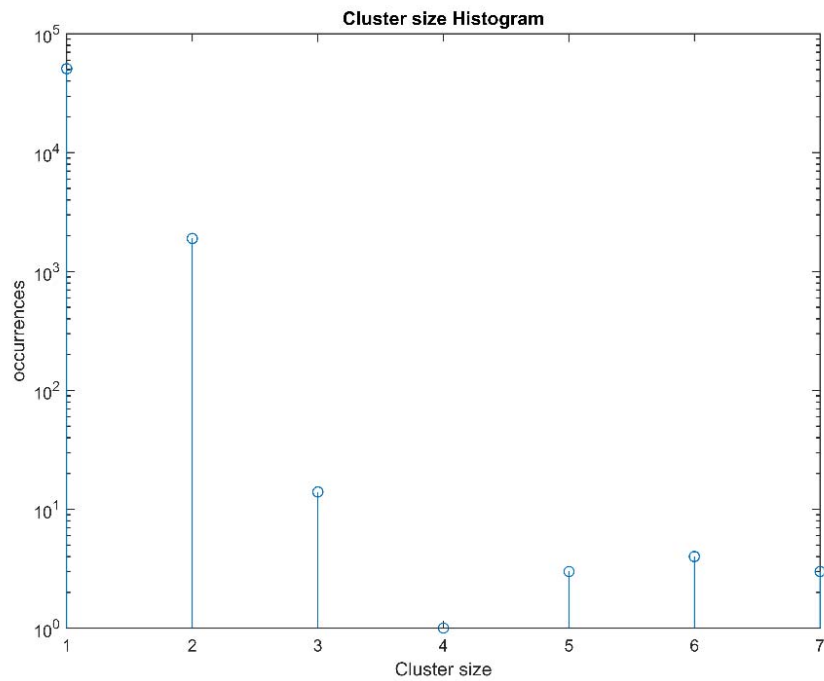


Figure 51a: Channel 6 (December 2013) - Cluster dimension

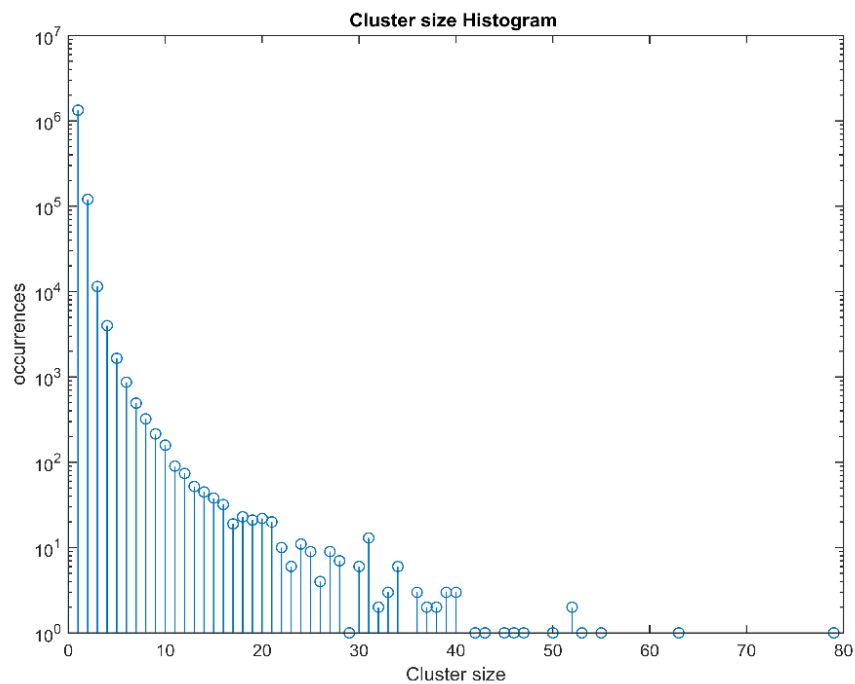


Figure 52: Channel 1 (June 2014) - Cluster dimension

The maximum dimension of cluster in December 2013 is only 7, while in June 2014 is 80 consecutive samples as shown in Figures 51a and 52, respectively.

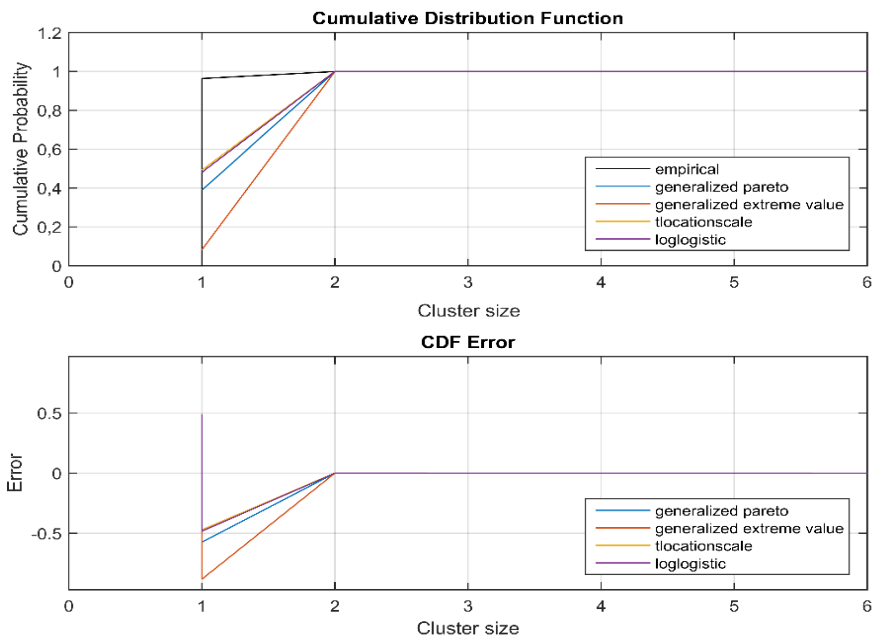


Figure 53: Cluster dimension CDF - Ch #6

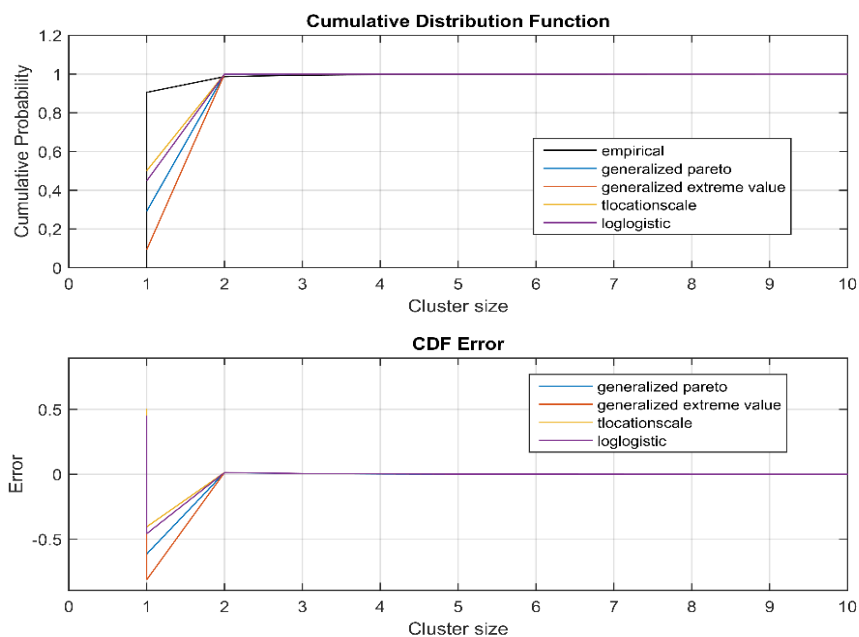


Figure 54: Cluster dimension CDF - Ch #1

The best fitting distribution for cluster dimension is Pareto for both Channel # (worst)1 and #6 (best). The error between the different CDFs to the original data set are presented in Figures 53 and 54 for Channels #6 and #1, respectively.

6.4.2 Inter-arrival time

In channel #6 (December 2013) the interarrival time is much larger, i.e. interference clusters occur sporadically. This means intermittent interference in the band (2 437 MHz). The results are shown in Figure 53.

In channel #1 (June 2014) the interarrival time is very low, i.e. interference clusters occur very frequently. This means almost continuous interference in the band (2 412 MHz). The results are shown in Figure 54.

Corresponding CDF curves are shown in Figures 55 and 56 for Channel #6 and Channel #1, respectively.

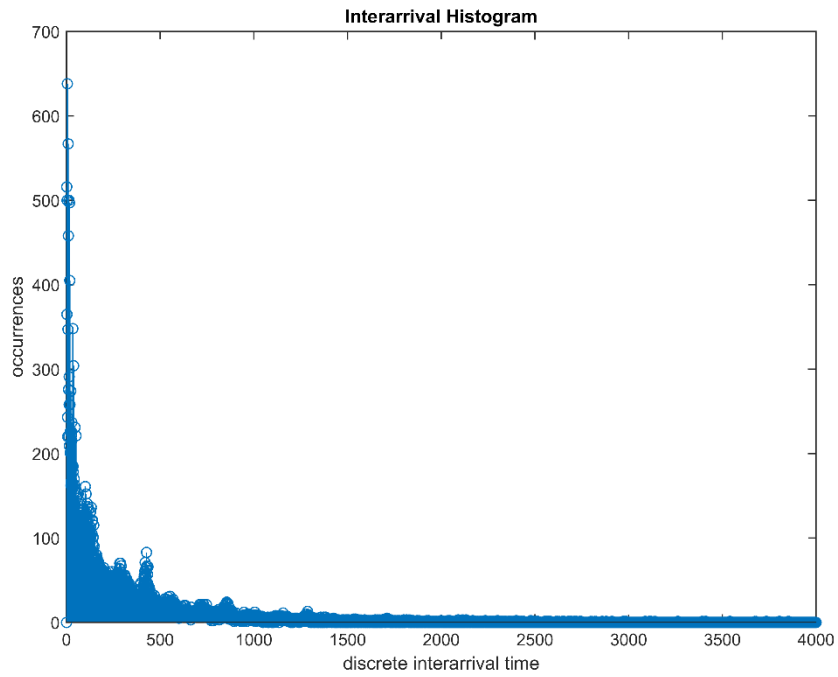


Figure 55: Inter-arrival time, Channel 6 (December 2013)

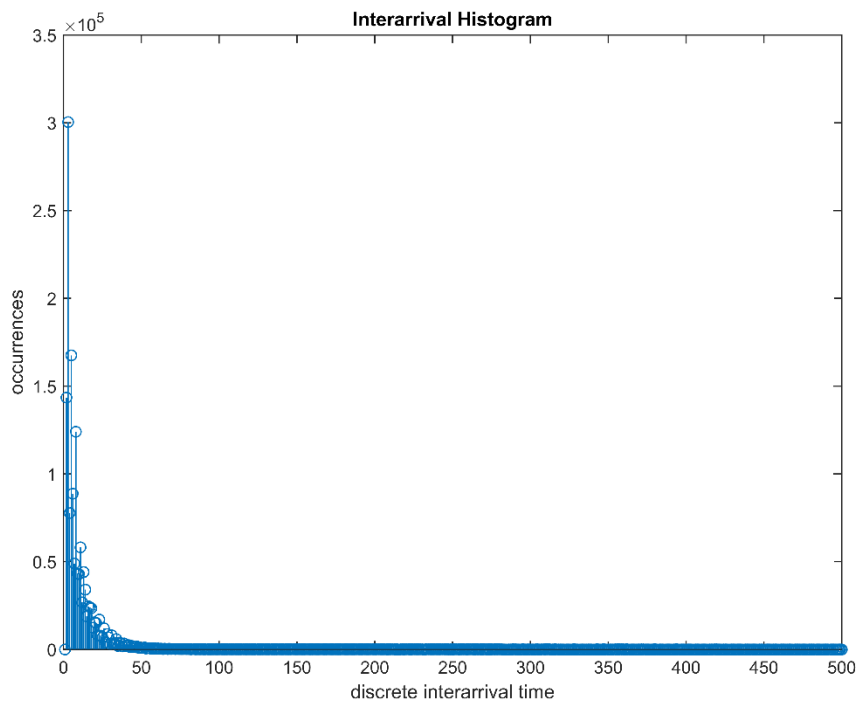


Figure 56: Inter-arrival time, Channel (June 2014)

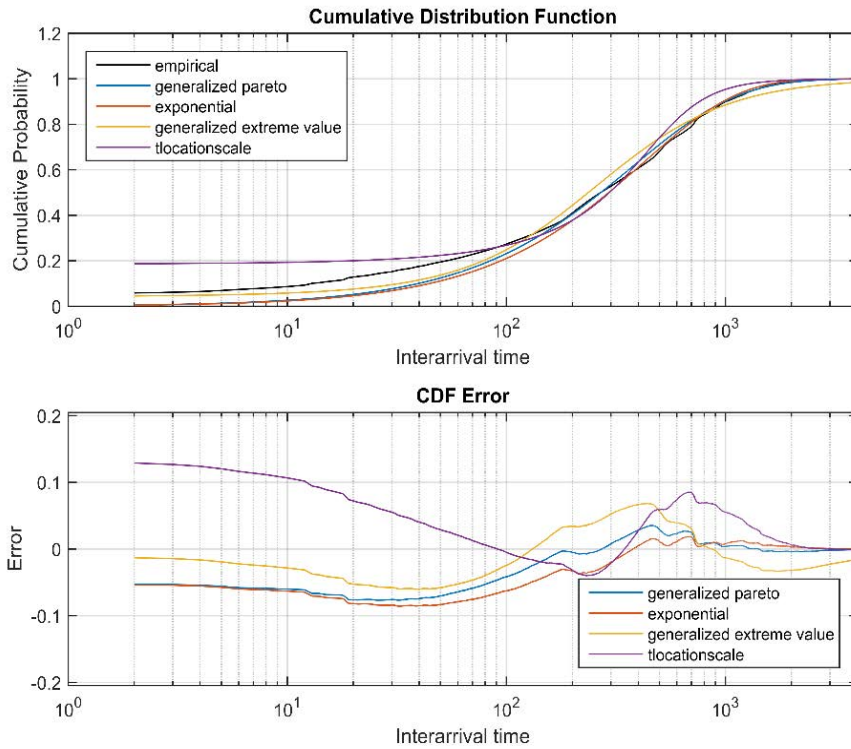


Figure 57: Inter-arrival time CDF - Ch #6

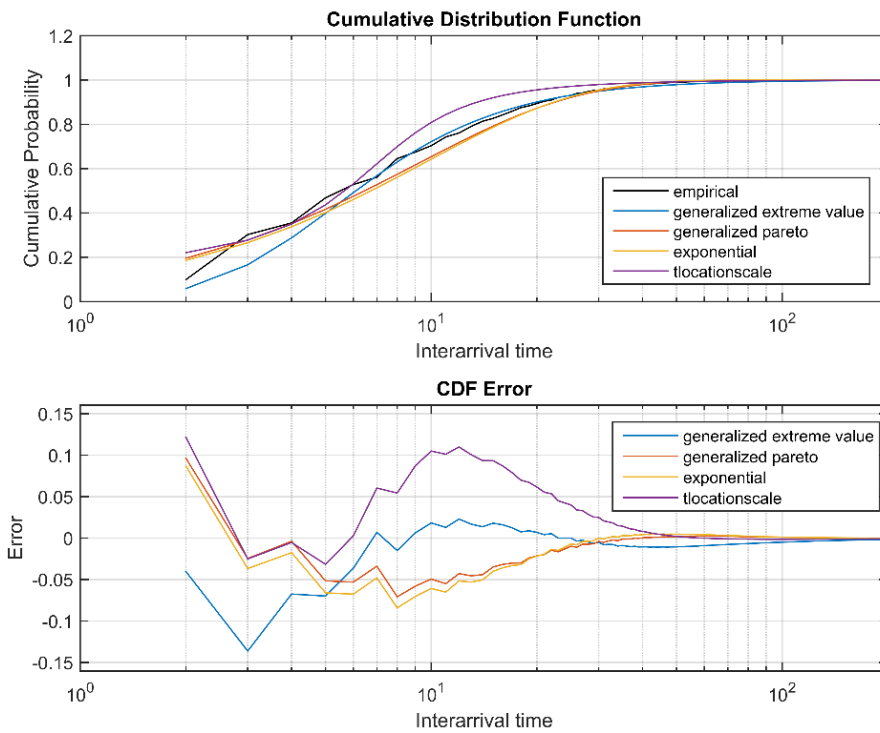


Figure 58: Inter-arrival time - Ch #1

The best fitting distribution for inter-arrival time of clusters is Pareto for both Channel #1 (worst) and Channel #6 (best).

6.4.3 Interfering cluster amplitude

In Channel #6 (December 2013) the amplitude of the clusters ranged between -87 and -85 dBm (Figure 59), while in Channel #1 (June 14) ranged between -84 and -62 dBm (Figure 60). The best fitting CDF for the cluster amplitude is the GEV for both Channel #6 (best) and Channel #1 (worst) as shown in Figures 61 and 62, respectively.

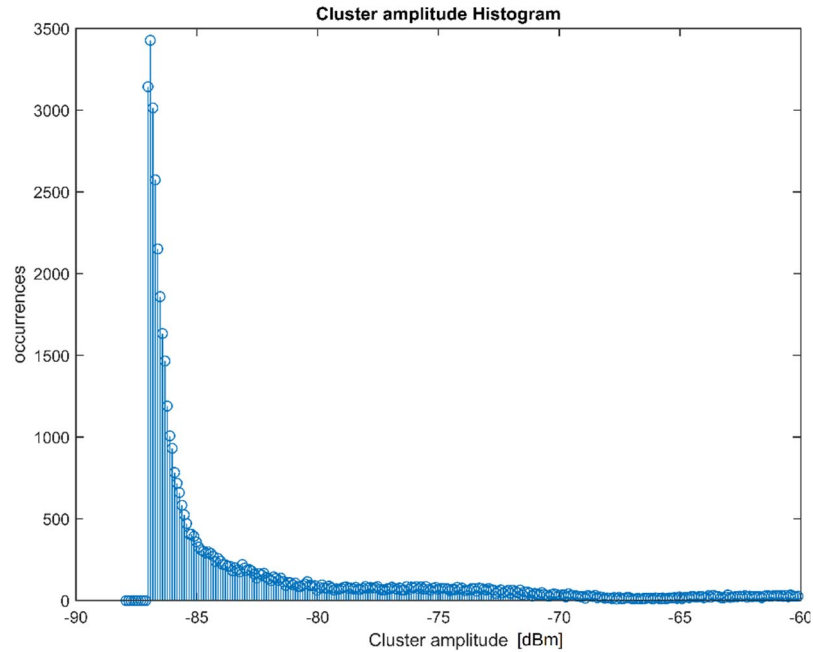


Figure 59: Cluster amplitude, Channel 6 (December 13)

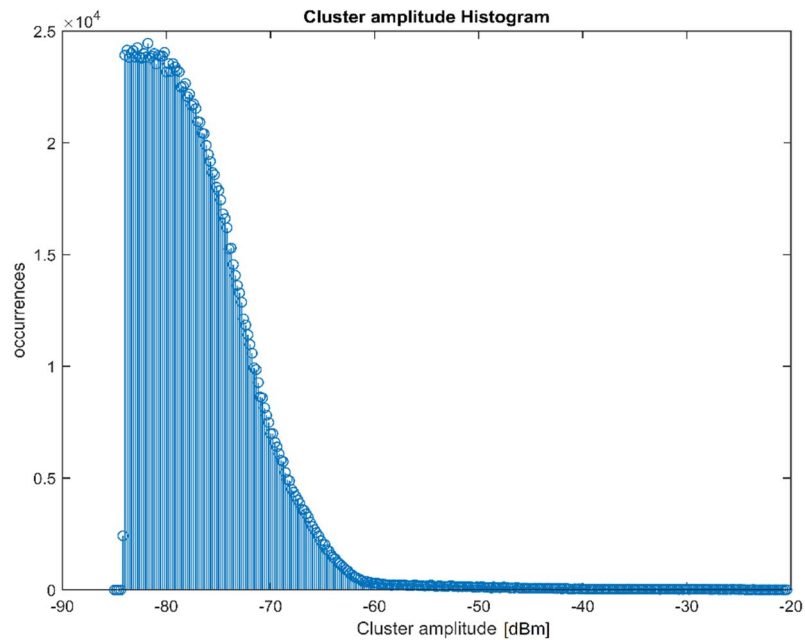


Figure 60: Cluster amplitude, Channel 1 (June 2014)

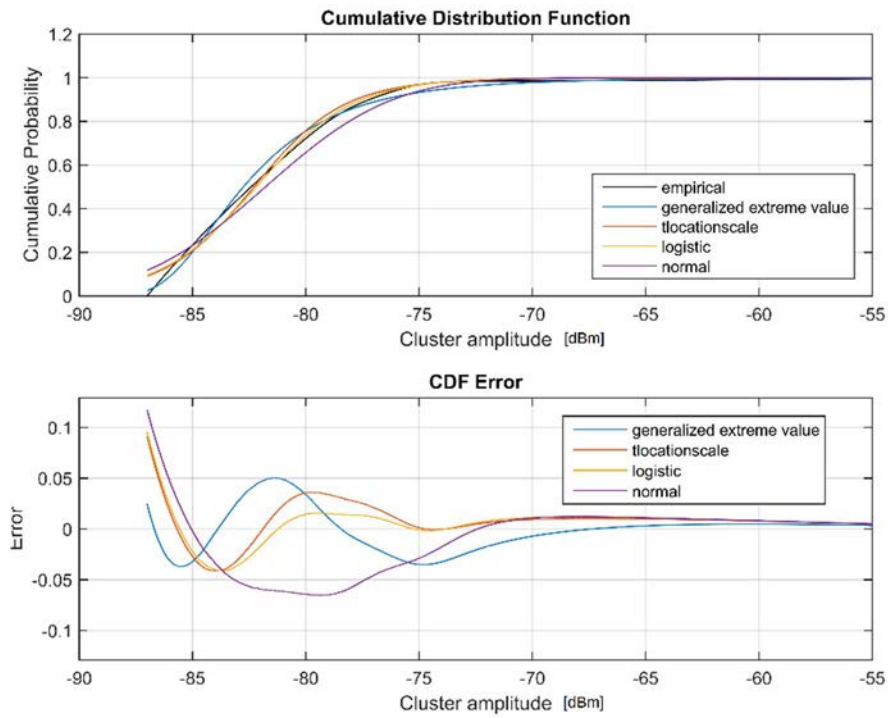


Figure 61: Cluster amplitude - Ch #6

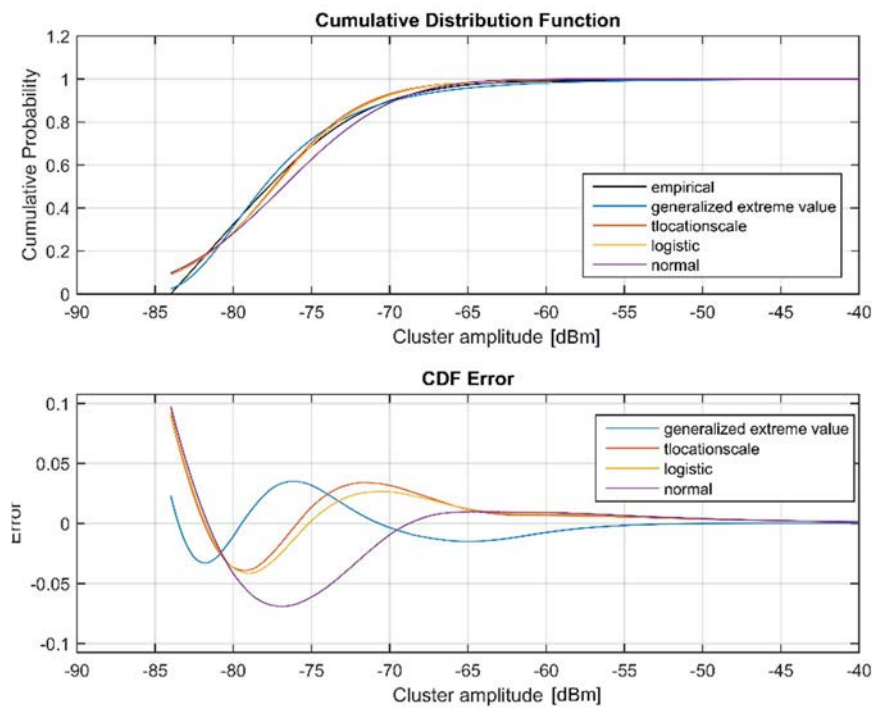


Figure 62: Cluster amplitude - Ch #1

6.4.4 Conclusions

The three parameters (cluster dimension, interarrival time and cluster amplitude) can be used to build a MATLAB function [i.12] that simulates the best case (Ch #6) and worst case (Ch #1) of interference in the ISM band. The block can be used to simulate the realistic interference caused in the studied environments, thus allowing an evaluation of the performance of a WBAN system in the real use case scenario. The statistical parameters of the interference clusters have been used to build a MATLAB simulator [i.12]. The simulator creates a cluster-based interference vector which follows the statistics of the selected scenario: low, moderate or high interference.

6.5 Extracting the mathematical model of the interference

The statistical parameters of the interference clusters have been used to build a MATLAB simulator [i.12]. The simulator creates a cluster-based interference vector which follows the statistics of the selected scenario: low or high interference.

In this clause, a cluster-based stochastic model of the aggregate interference is derived. In particular, two channels have been evaluated: the best and the worst one among all the measurement campaigns. Channel 6 (2 437 MHz) of Measurement Campaign (MC) no. 1 is the best one (Low Interference, (LI)) and Channel 1 (2 412 MHz) of MC no. 2 is the worst one (High Interference, (HI)).

The statistical model of the interference starts modelling three characteristics of the interference: clusters dimension, interarrival time of the clusters and cluster amplitude. A cluster is defined as a group of consecutive samples that overcome the threshold of the noise level.

Figures 63 and 64 show the occurrences of the dimension of the clusters over one week for channel 6 (low interference) and channel 1 (high interference), respectively. The maximum dimension of cluster in channel 1 is 80 consecutive samples, while in channel 6 is only 7.

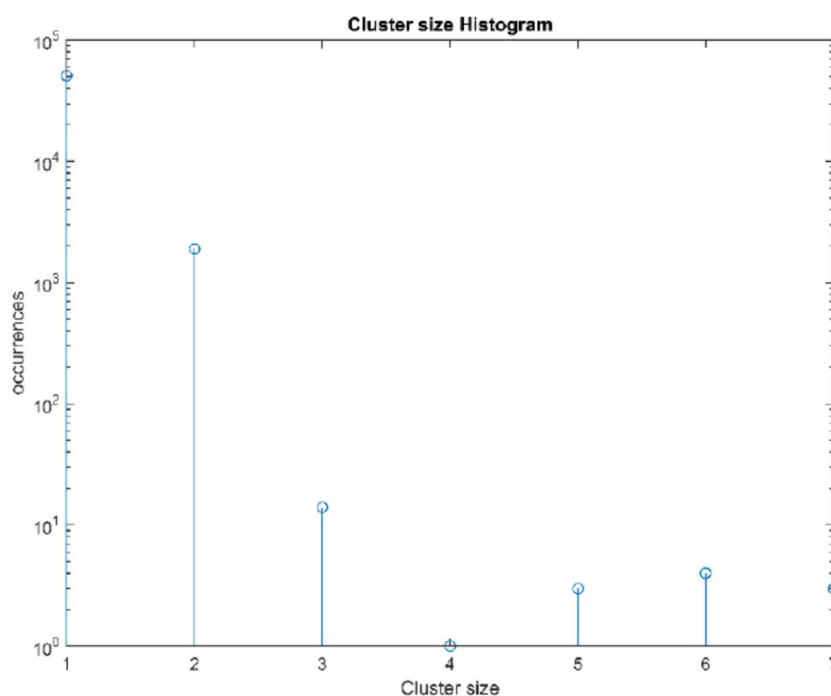
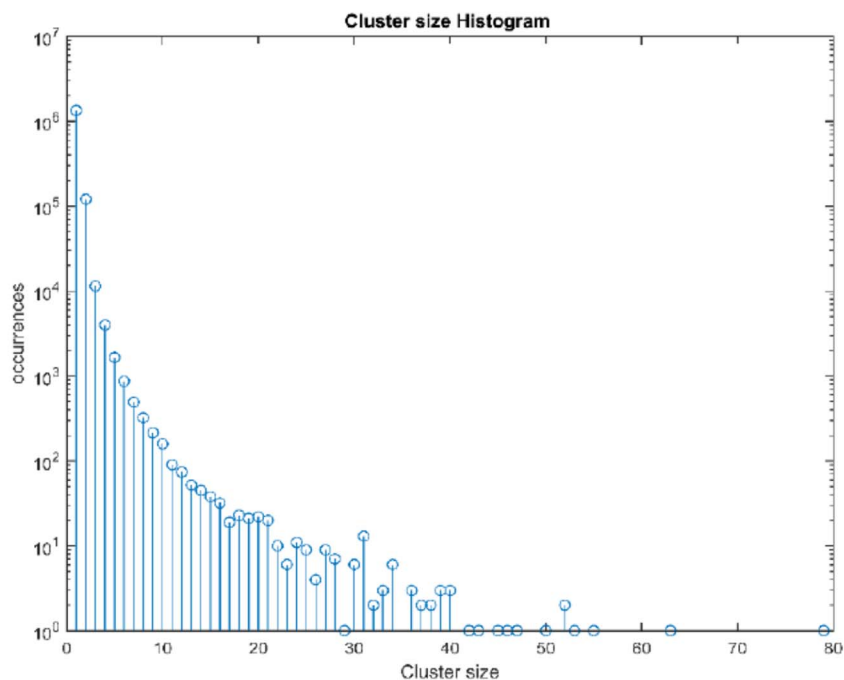


Figure 63: Occurrences of the dimension of the clusters; Channel 6 (Low Interference)



**Figure 64: Occurrences of the dimension of the clusters;
Channel 1 (High Interference)**

The best fitting distribution for the dimension of the cluster is Pareto for both Channel 1 and 6, as depicted in Figures 65 and 66. Generalized Pareto distribution is:

$$f(x|k, \sigma, \theta) = \frac{1}{\sigma} \left(1 + k \left(\frac{x - \theta}{\sigma} \right) \right)^{-1-1/k} \quad (22)$$

where k is the shape parameter, σ is the scale parameter and θ is the threshold parameter. Channel 6 (LI) shows $k = 4,8$, $\sigma = 2,5e-15$ and $\theta = 1$, while Channel 1 (HI) shows $k = 2,43$, $\sigma = 2,34e-15$ and $\theta = 1$. The most frequent cluster size in Channel 6 (LI) is 1 sample.

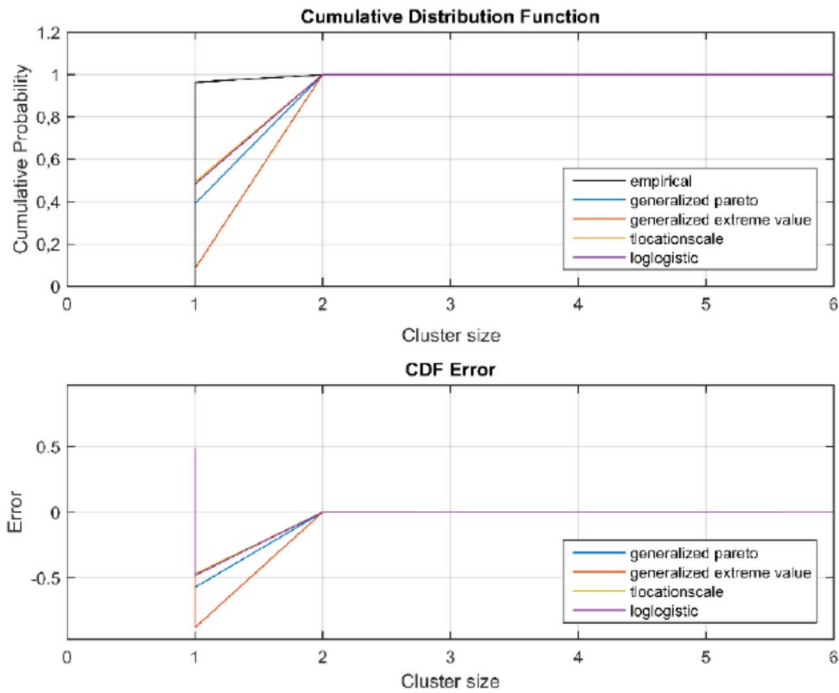


Figure 65: Best fitting CDF and CDF error of the dimension of the clusters; Channel 6 (Low Interference)

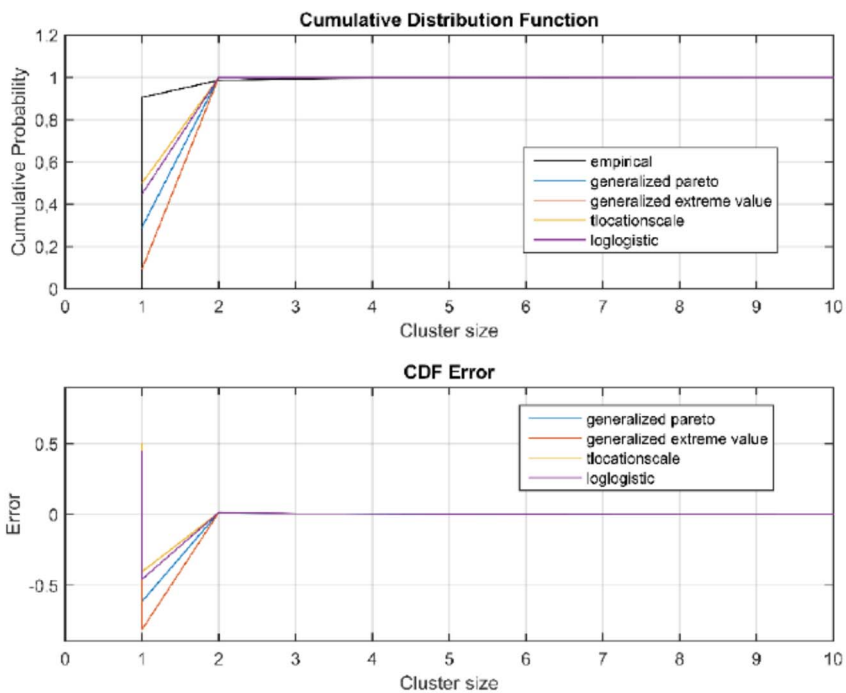
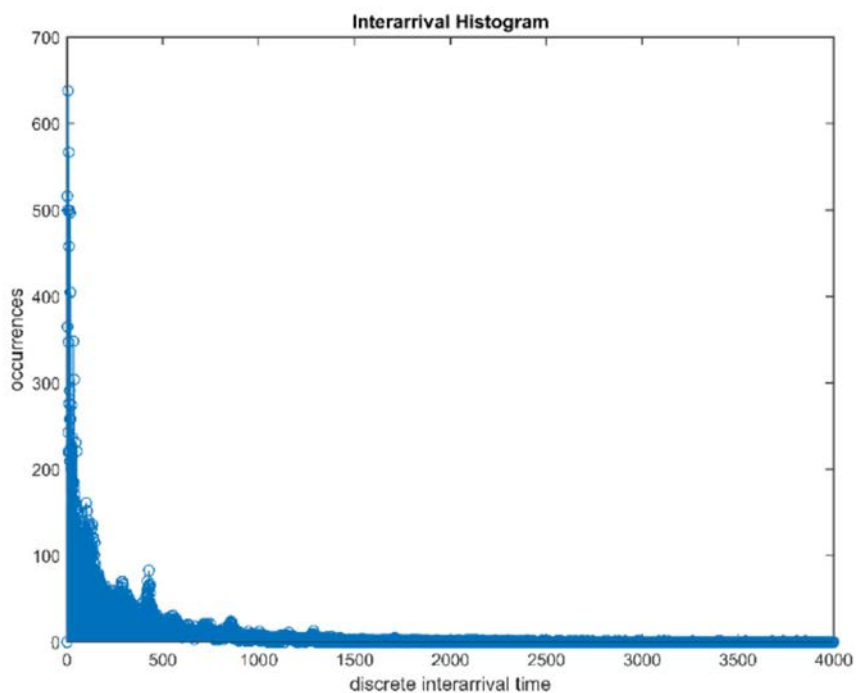
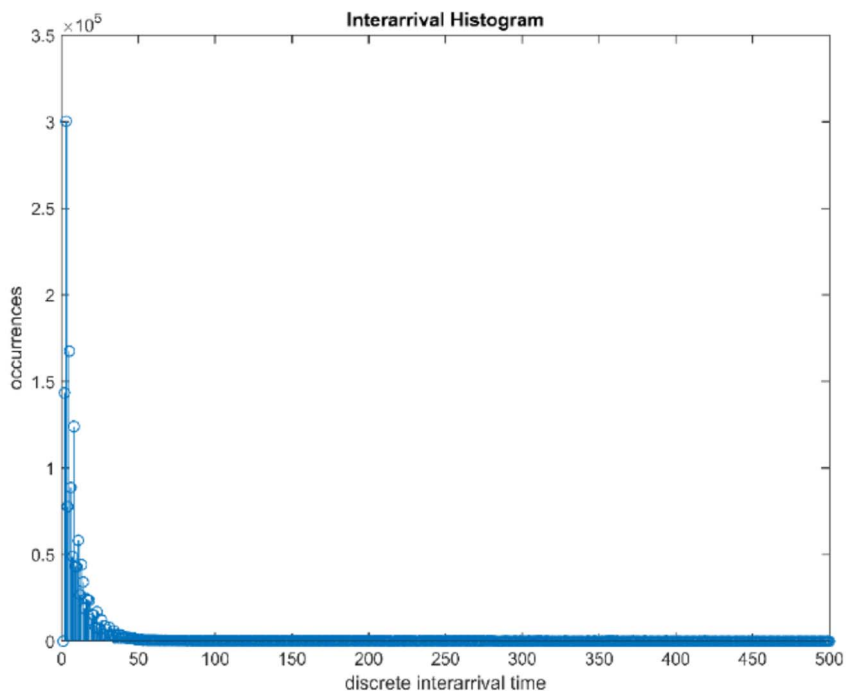


Figure 66: Best fitting CDF and CDF error of the dimension of the clusters; Channel 1 (High Interference)

Figures 67 and 68 show the occurrences of the inter-arrival time of the clusters over one week for channel 6 (Low Interference) and channel 1 (High Interference), respectively. In channel 1 (HI) the interarrival time is very low, i.e. interference clusters occur very frequently. This means almost continuous interference in the band (2 412 MHz). In channel 6 (LI) the interarrival time is much larger, i.e. interference clusters occur sporadically. This means intermittent interference in the band (2 437 MHz). The empirical CDF (black line in Figure 23), related to the interarrival time vector of the HI case, reaches a value equal to 0.7 when an interarrival time is equal to 10 and a value equal to 0.9 when an interarrival time is equal to 20. This means that interarrival times greater than 20 are improbable. The CDF error is remarkable for every distribution considered, but only for the first value of the clusters size.



**Figure 67: Occurrences of the inter-arrival time of the clusters;
Channel 6 (Low Interference)**



**Figure 68: Occurrences of the inter-arrival time of the clusters;
Channel 1 (High Interference)**

This error is determined by the inability of the statistical distributions considered by the MATLAB [i.12] function `allfitdist` to represent perfectly the particular shapes of the empirical cluster size CDF. It is possible that another statistical distribution, not considered by the function, could represent in a better way the empirical cluster size CDF.

Best fitting distribution for the inter-arrival time of clusters is Pareto for Channel 6 (LI), as depicted in Figure 69. The parameters of the distribution in this case are: $k = 0,12$, $\sigma = 373,5$ and $\theta = -2,2e-15$. The CDF error, between the empirical CDF and the CDF of every distribution represented, is in the range $-0,1:0,15$. Best fitting distribution for the interarrival time of clusters is Generalized Extreme Value (GEV) for Channel 1 (HI), as depicted in Figure 70. The parameters of the distribution in this case are: $k = 0,55$, $\mu = 4,7$ and $\sigma = 3,42$. The error between the empirical CDF and any other CDF of fitting distributions is in the range $-0,14:0,12$.

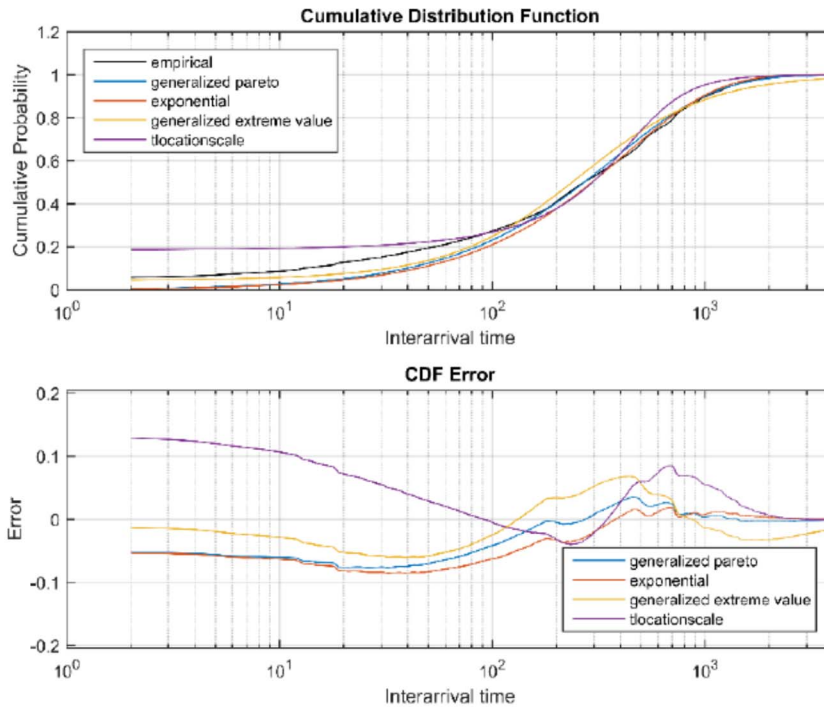


Figure 69: Best fitting CDF and CDF error of the inter-arrival time of the clusters; Channel 6 (Low Interference)

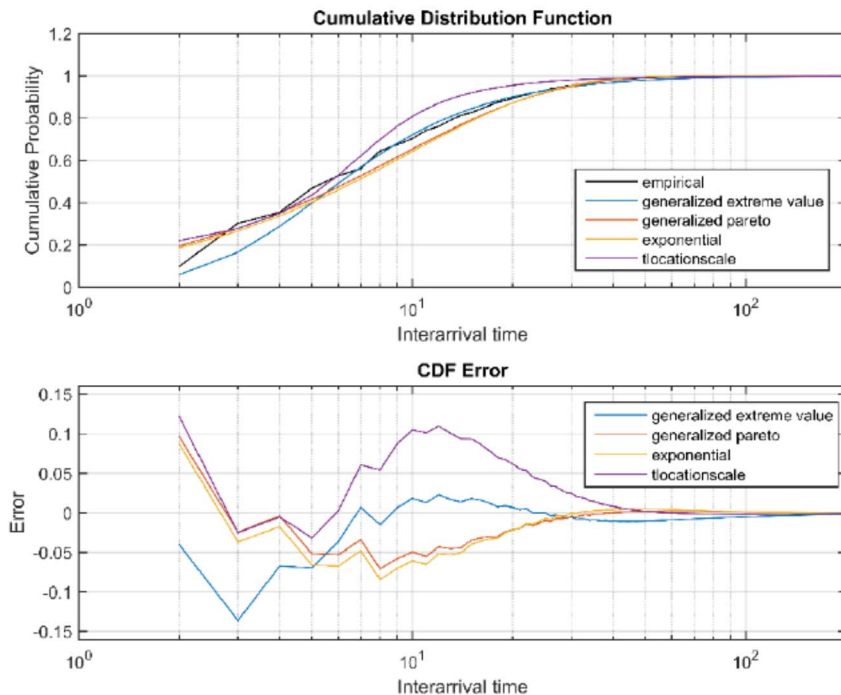
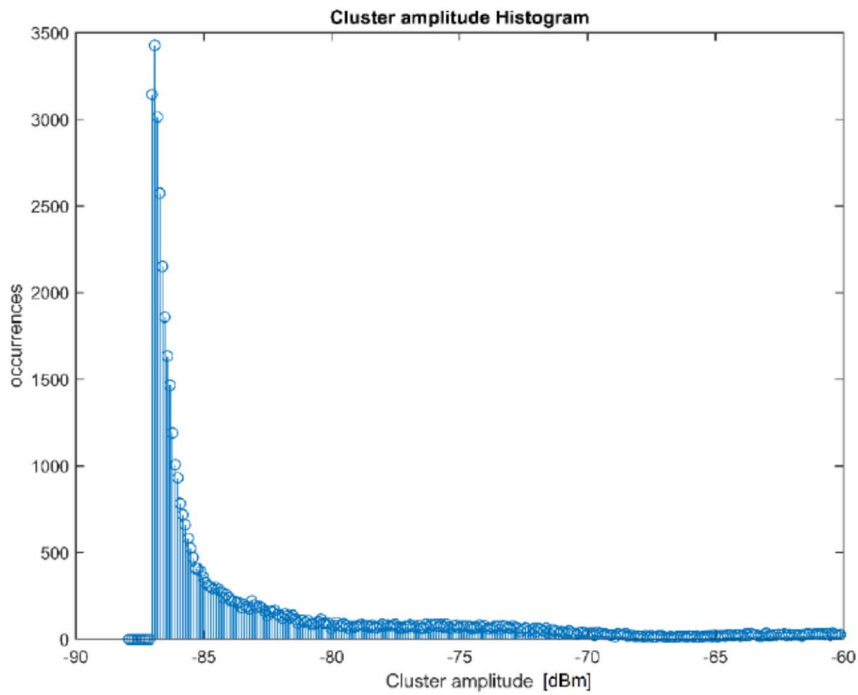
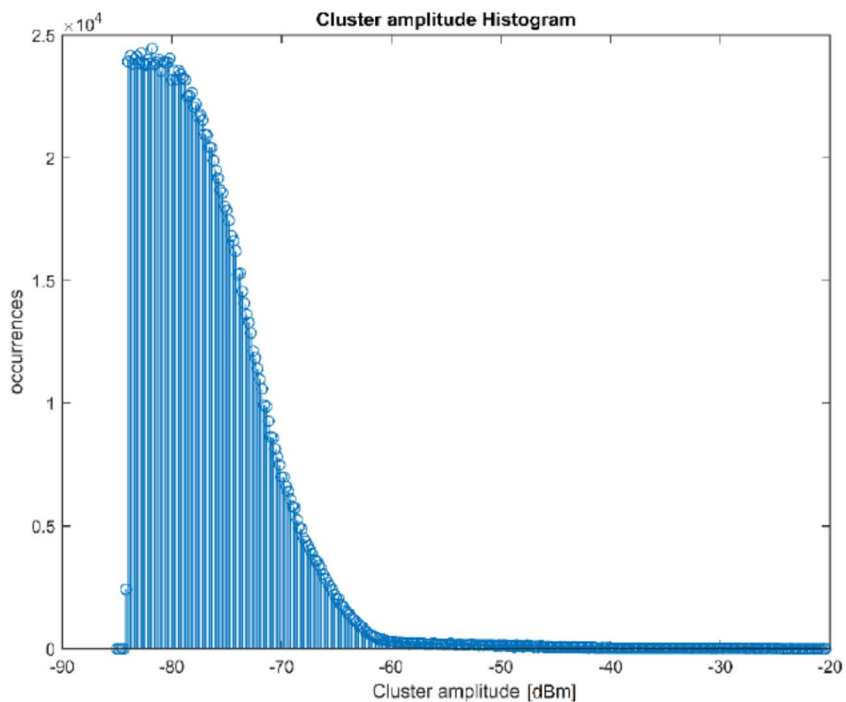


Figure 70: Best fitting CDF and CDF error of the inter-arrival time of the clusters; Channel 1 (High Interference)

Figures 71 and 72 show the occurrences of the amplitude of the clusters over one week for channel 6 (low interference) and channel 1 (high interference), respectively. In Channel 6 (LI) the amplitude of the clusters ranged from -87 to -85 dBm, while in Channel 1 (HI) ranged from -84 to -62 dBm. The best fitting distribution for the amplitude of the clusters is the GEV for both Channel 6 and Channel 1, as depicted in Figures 73 and 74. The GEV representing Channel 6 (LI) has the following parameters: $k = 0:14$, $\mu = -83,7$ and $\sigma = 2,7$. The CDF error is in the range $-0,06:0,12$. The GEV representing Channel 1 (HI) has the following parameters: $k = 0:12$, $\mu = -79,4$ and $\sigma = 3,7$. The CDF error is in the range $-0,07:0,1$, for every distribution represented.



**Figure 71: Occurrences of the amplitude of the clusters;
Channel 6 (Low Interference)**



**Figure 72: Occurrences of the amplitude of the clusters;
Channel 1 (High Interference)**

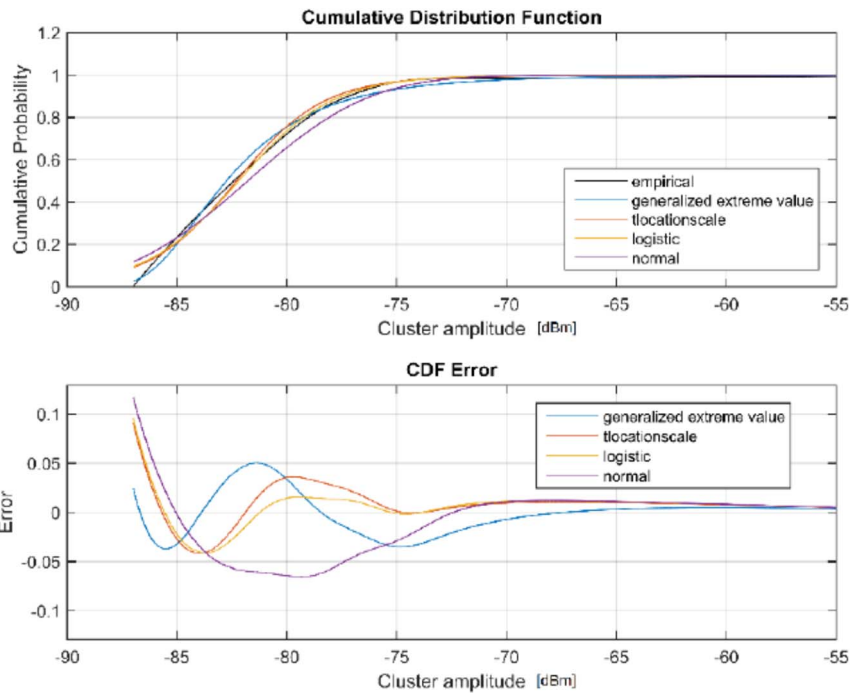


Figure 73: Best fitting CDF and CDF error of the amplitude of the clusters; Channel 6 (Low Interference)

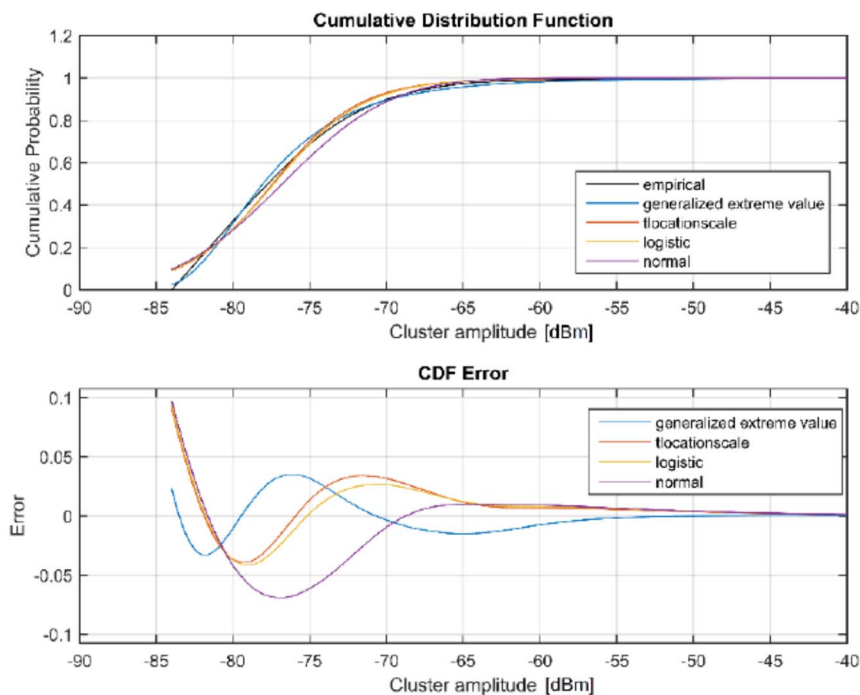


Figure 74: Best fitting CDF and CDF error of the amplitude of the clusters; Channel 1 (High Interference)

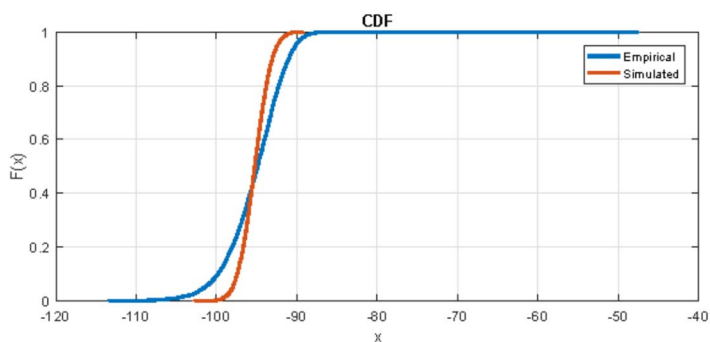
Cluster-Based Interference Simulator

The statistical parameters of the interference clusters have been used to build a MATLAB simulator [i.12]. The simulator creates a cluster-based interference vector which follows the statistics of the selected scenario: low, moderate or high interference.

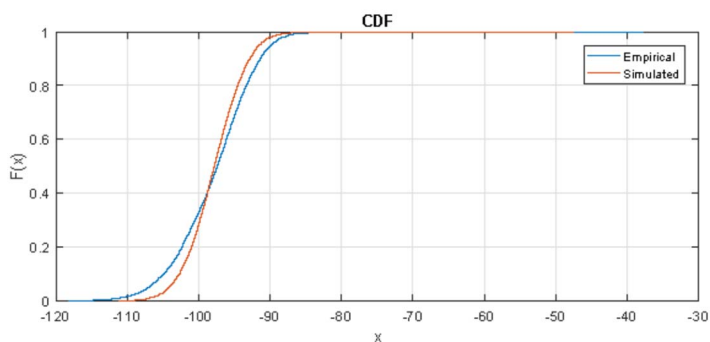
In order to measure the accuracy of the cluster-based statistical model of the interference, the two-sample Kolmogorov-Smirnov (KS) test is applied to the empirical data and the simulated data. The Kolmogorov-Smirnov test is a nonparametric hypothesis test that evaluates the difference between the CDFs of the distributions of the two sample data vectors over the range of x in each data set. The two-sided test uses the maximum absolute difference between the CDFs of the distributions of the two data vectors. The test statistic is:

$$D = \max_x (CDF_1(x) - CDF_2(x)) \quad (23)$$

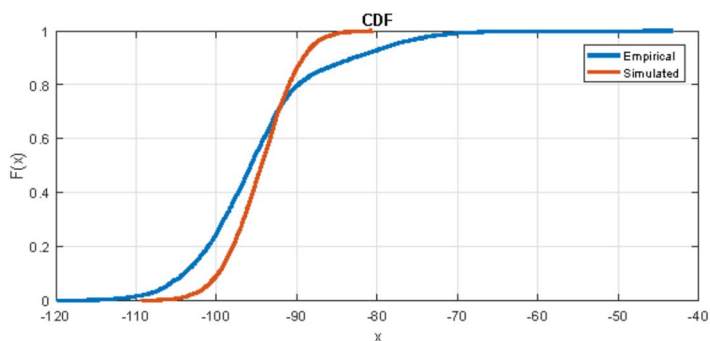
where $CDF_1(x)$ is the proportion of x_1 values less than or equal to x and $CDF_2(x)$ is the proportion of x_2 values less than or equal to x . Figure 75 shows the CDFs of the empirical and simulated data for the low, moderate and high interference scenarios. The KS test always rejects the null hypothesis with a significance level of 5 %.



(a) Low interference scenario.



(b) Moderate interference scenario.



(c) High interference scenario.

Figure 75: CDFs of the empirical and the simulated data

6.6 Further investigations: a more accurate statistical model of the interference

6.6.0 Introduction

The following results are extrapolated from the journal paper [i.18]:

In order to better characterize the aggregate interference in a hospital environment for the largely used 2,35 GHz to 2,50 GHz band based on a network experimentation representing three one-week-long measurement campaigns, further investigations are carried out and two more accurate statistical models of the aggregate interference have been proposed [i.18].

Leveraging on these measurements, the spectrum occupancy is quantified according to three metrics, namely CO, FBO and SRO. Focusing on the two statistical models:

- the first model describes the aggregate interference (plus noise) over the entire time-frequency intervals;
- the second model describes the aggregate interference (without noise) by grouping the interference samples in clusters.

The results show that mission-critical medical services in the ISM band can be severely hampered by the interference, calling for the use of reserved sub-bands or the use of interference detection and mitigation techniques. The proposed models also serve as the basis for simulating network behaviour and designing medical devices in wireless hospital environments.

6.6.1 Accurate statistical models of the interference

6.6.1.0 Introduction

To characterize the aggregate interference in a hospital environment, two statistical models in the 2,35 GHz to 2,50 GHz band are proposed. The first model describes the aggregate interference (plus noise) over the entire time-frequency intervals; while the second model describes the aggregate interference (without noise) by grouping the interference samples in clusters. Each proposed model is selected among the candidate distributions, like the one that best fits the measurement data according to the Bayesian Information Criterion (BIC) [i.25] described in the following.

Let $\check{f}_x(\cdot | \theta)$ denote a candidate distribution for each element of the random sample with corresponding joint distribution $\check{f}_x(\cdot | \theta)$ and vector parameter θ of dimension d . For a given observed vector \mathbf{x} of length n , the cost associated with $\check{f}_x(\cdot | \theta)$ is given by:

$$\zeta_{\text{BIC}}(\mathbf{x}) = -2 \ln(\check{f}_x(\mathbf{x} | \hat{\theta})) + d \ln(n) \quad (24)$$

where $\hat{\theta}$ is a maximum likelihood (ML) estimate of θ , i.e.:

$$\hat{\theta} = \arg \max_{\tilde{\theta}} \check{f}_x(\mathbf{x} | \tilde{\theta}) \quad (25)$$

Among all the candidate distributions, the best fit distribution $f_x(\cdot | \theta)$ with corresponding joint distribution $f_x(\cdot | \theta)$ that minimizes the BIC in (24) is selected.

The similarity of the selected distribution with the empirical distribution based on measurement data can be quantified using the Jensen-Shannon Divergence (JSD) [i.26]. Let p_1 and p_2 be two Probability Density Function (PDF) representing a RV x taking values on a set χ , then the JSD is defined as:

$$\mathbb{J}\{p_1 || p_2\} = \frac{1}{2} \mathbb{D}\{p_1 || q\} + \frac{1}{2} \mathbb{D}\{p_2 || q\} \quad (26)$$

where $q = (p_1 + p_2)/2$ and $D\{p_1||p_2\}$ is the Kullback–Leibler divergence, defined as:

$$D\{p_1||p_2\} = \int_{-\infty}^{\infty} p_1(x) \log \left(\frac{p_1(x)}{p_2(x)} \right) dx. \quad (27)$$

6.6.1.1 Time–Frequency Statistical Model of the Interference

The data set measured in the daily surgery ward was chosen to determine the time–frequency distribution of the aggregate interference in different interference regimes.

NOTE: The daily surgery data set was chosen since it was the largest one containing the full dynamic range of the interference, and it has the same interference characteristics as the other two wards.

Several candidate distributions have been considered including: Burr; exponential; extreme value; Gaussian; Generalized Extreme Value (GEV); logistic; log–normal; t –location scale; and Weibull. The selection is performed using an algorithm developed based on [i.27]. Table 8 shows the selected distribution and the associated parameters for different scenarios in the delay surgery ward. The four best-fit distributions are listed in the following, where x is a RV representing the received power in time and frequency.

The GEV distribution [i.28] is given by:

$$f_x(x|k, \mu, \sigma) = \frac{1}{\sigma} \exp \left\{ - \left(1 + k \frac{x - \mu}{\sigma} \right)^{-1/k} \right\} \times \left(1 + k \frac{x - \mu}{\sigma} \right)^{-1-1/k} \quad (28)$$

where k is the shape parameter, μ is the location parameter, and σ is the scale parameter.

Table 8: Selected distributions and associated parameters

Scenario	Selected Distribution	Distribution Parameters
Day 1 Spectrum Variation	GEV	$k = 0.6676; \sigma = 2.9557; \mu = -85.9427$
Day 2 Spectrum Variation	GEV	$k = 0.6370; \sigma = 2.8504; \mu = -85.5746$
Day 3 Spectrum Variation	GEV	$k = 0.7941; \sigma = 2.8023; \mu = -85.7233$
Day 4 Spectrum Variation	GEV	$k = 0.8568; \sigma = 2.6080; \mu = -85.9357$
Day 5 Spectrum Variation	GEV	$k = 0.7900; \sigma = 2.7385; \mu = -85.8011$
Day 6 Spectrum Variation	GEV	$k = 0.8520; \sigma = 3.0775; \mu = -85.6074$
Day 7 Spectrum Variation	GEV	$k = 0.7812; \sigma = 2.9172; \mu = -85.6607$
Whole Week Spectrum Variation	GEV	$k = 0.7812; \sigma = 2.8348; \mu = -85.9843$
Whole Week IEEE 802.11b/g Ch. 1	Burr type XII	$\alpha = 5.7691; c = 43.5808; k = 0.2567$
Whole Week IEEE 802.11b/g Ch. 6	t –location scale	$\mu = 5.3937; \sigma = 0.3650; \nu = 1.9946$
Whole Week IEEE 802.11b/g Ch. 11	logistic	$\mu = -0.0094; \sigma = 0.0290$
Whole Week IEEE 802.11n Ch. 3	GEV	$k = 0.2759; \sigma = 0.0380; \mu = 0.0711$
Whole Week IEEE 802.11n Ch. 9	logistic	$\mu = 0.0563; \sigma = 0.0047$
Whole Week FBO Variation	t –location scale	$\mu = 0.8664; \sigma = 0.0360; \nu = 2.4698$
Whole Week SRO (IEEE 802.11b/g)	GEV	$k = 0.4101; \sigma = 0.0022; \mu = 0.0055$
Whole Week SRO (IEEE 802.11n)	t –location scale	$\mu = 3.8262; \sigma = 0.1370; \nu = 2.2628$

The Burr type XII distribution [i.28] is given by:

$$f_x(x|\alpha, c, k) = \frac{kc(x/\alpha)^{c-1}}{\alpha(1+(x/\alpha)^c)^{k+1}} \quad (29)$$

where c and k are the shape parameters, and α is the scale parameter. The t –location scale distribution [i.28] is given by:

$$f_x(x|\mu, \sigma, \nu) = \frac{\Gamma(\frac{\nu+1}{2})}{\sqrt{\nu} \sqrt{\pi} \Gamma(\nu/2)} \left(\frac{\nu + \frac{(x-\mu)^2}{\sigma}}{\nu} \right)^{-\frac{\nu+1}{2}} \quad (30)$$

where $\Gamma(\cdot)$ represents the gamma function, μ is the location parameter, σ is the scale parameter, and ν is the shape parameter. The logistic distribution [i.28] is given by:

$$f_x(x|\mu, \sigma) = \frac{e^{-\frac{x-\mu}{\sigma}}}{\sigma \left(1 + e^{-\frac{x-\mu}{\sigma}}\right)^2} \quad (31)$$

where μ is the location parameter and σ is the scale parameter.

Two additional scenarios of interest have been considered, namely low and high interference, for the popular IEEE 802.11b and IEEE 802.11g [i.31] systems in the daily surgery ward. It was found that the stable distribution is the best fit for these two scenarios. The characteristic function of a stable distribution [i.28] is given by:

$$\Phi_x(x|\alpha, \beta, \gamma, \delta) = \exp\{ix\gamma - |\delta x|^\alpha (1 - i\beta \operatorname{sgn}(x)\phi)\} \quad (32)$$

where x is a RV representing the received power in time and frequency, i is the imaginary unit, α is the first shape parameter, β is the second shape parameter, γ is the scale parameter, and δ is the location parameter, and

$$\phi = \begin{cases} \tan(\pi\alpha/2) & \text{for } \alpha \neq 1 \\ -(2/\pi) \log|x| & \text{for } \alpha = 1. \end{cases} \quad (33)$$

These results agree with the theory of statistical distribution for the aggregate interference available in literature and detailed in [i.19], [i.20], [i.21], [i.22], [i.23] and [i.24].

Table 9 shows the BIC and JSD values for the six best statistical distributions in low and high interference scenarios, for the popular IEEE 802.11b [i.30] and IEEE 802.11g [i.31] systems in the daily surgery ward. The stable distribution is always the best fit distribution to the empirical data. The parameters of the best fitting (Stable) distribution are summarized in Table 10.

Table 9: BIC and JSD values for high and low interference scenarios

Scenario	Distribution	BIC	JSD
Low	stable	3.0928×10^4	7.5753×10^{-4}
	logistic	3.1005×10^4	8.0385×10^{-4}
	t-location scale	3.1060×10^4	8.0602×10^{-4}
	Gaussian	3.1217×10^4	7.6444×10^{-4}
	GEV	3.1795×10^4	1.0131×10^{-3}
	extreme value	3.5839×10^4	2.2964×10^{-3}
High	stable	3.4938×10^4	1.7755×10^{-3}
	Burr type XII	3.4959×10^4	1.9803×10^{-3}
	GEV	3.4963×10^4	2.0030×10^{-3}
	t-location scale	3.5099×10^4	2.0984×10^{-3}
	logistic	3.5131×10^4	1.9824×10^{-3}
	Gaussian	3.5425×10^4	1.9814×10^{-3}

Table 10: Parameters of the Stable distribution for the low and high interference scenarios

	α	β	γ	δ
Low	1.818	-0.938	2.278	-94.755
High	1.707	0.934	4.967	-96.550

6.6.1.2 Cluster-Based Statistical Model of the Interference

In this clause, a cluster-based statistical model of the aggregate interference is developed for two scenarios of interest, namely low and high interference, for the popular IEEE 802.11b [i.30] and IEEE 802.11g [i.31] systems over all the three measurement campaigns.

NOTE: For a given channel, a cluster is defined as a group of consecutive samples above the threshold.

In particular, channel 6 (2 437 GHz) showed low interference in the X-ray and radiology ward, while channel 1 (2 412 GHz) showed high interference in the accident and emergency ward. The cluster-based statistical model relies on the distributions of cluster size, cluster interference sample, and cluster inter-arrival time. For a given channel: the cluster size is the cardinality of a cluster; the cluster interference sample is the value of a sample inside a cluster; and the cluster inter-arrival time is the difference between the first sweep index of a sample in a cluster and the last sweep index of a sample in the previous cluster.

Figure 76 shows the empirical Probability Mass Function (PMF) of the cluster size. It can be observed that the low interference scenario exhibits a smaller variability of the cluster size compared to the high interference scenario. In particular, the maximum cluster size is 14 and 79 samples in the low and high interference scenarios, respectively. The best fit distribution for the cluster size in both low and high interference scenarios is geometric [i.28] given by:

$$f_x(x|p) = p(1-p)^{x-1} \quad (34)$$

where x is a RV representing the cluster size for the specific channel and p is the success probability parameter. The associated parameter is $p = 0,9755$ for the low interference scenario, and is $p = 0,8896$ for the high interference scenario.

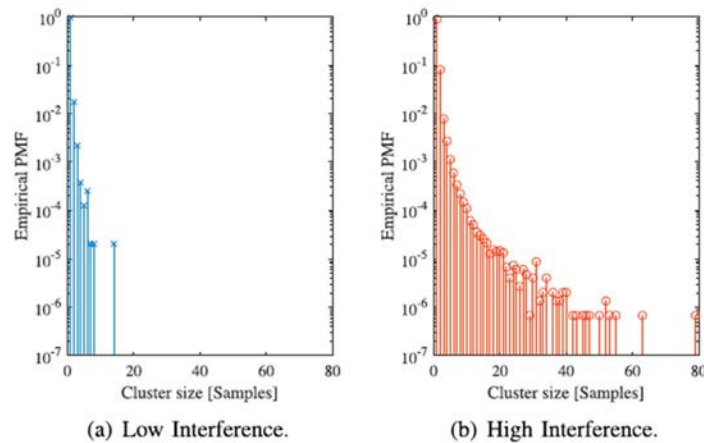


Figure 76: Empirical PMF of the cluster size in low and high interference scenarios

Figure 77 shows the empirical PDF of the cluster interference sample. It can be observed that the cluster interference samples range from 84 to 19 dBm and from 84 to 17 dBm in the low and high interference scenarios, respectively. While the ranges are similar in the two scenarios, it can be observed from the data that in the high interference scenario, there are about 30 times larger number of samples occupying the channel than in the low interference scenario. Note that the empirical PDFs are obtained by normalizing over such numbers of samples. The best fit distribution for cluster interference sample in both low and high interference scenarios is GEV given by (28), where x is a RV representing the cluster interference sample for the specific channel. The associated parameters are $k = 0,65$, $\sigma = 6,30$, and $\mu = 78,41$ for the low interference scenario, and are $k = 0,12$, $\sigma = 3,73$, and $\mu = 79,44$ for the high interference scenario.

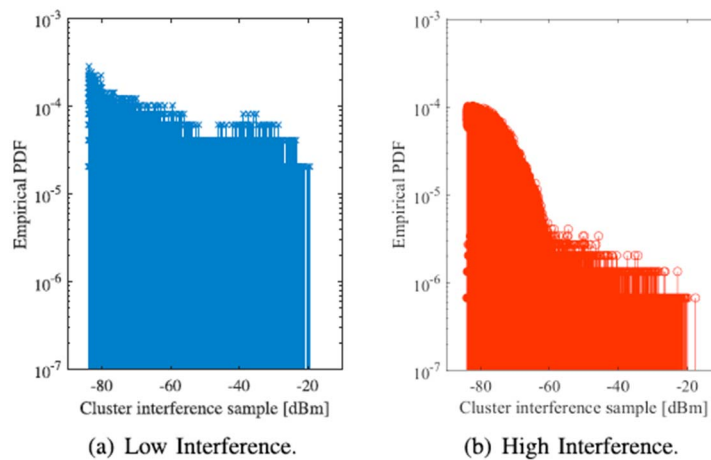


Figure 77: Empirical PDF of the cluster interference sample in low and high interference scenarios

Figure 78 shows the empirical PMF of the cluster inter-arrival time. It can be observed that the low interference scenario exhibits a larger variability of the cluster inter-arrival time compared to the high interference scenario. In particular, the maximum inter-arrival time is around 4 200 and 520 samples in the low and high interference scenarios, respectively.

The best fit distribution for the cluster inter-arrival time in both low and high interference scenarios is geometric [i.28] given by (34), where x is a RV representing the cluster inter-arrival time for the specific channel and p is the success probability parameter. The associated parameter is $p = 0,0037$ for the low interference scenario and is $p = 0,1027$ for the high interference scenario.

The similarity between the empirical distributions (of data generated from the cluster-based statistical model and of data gathered from measurements) is quantified using the JSD in (26). In particular, Table 11 shows the JSD values for the low and high interference scenarios.

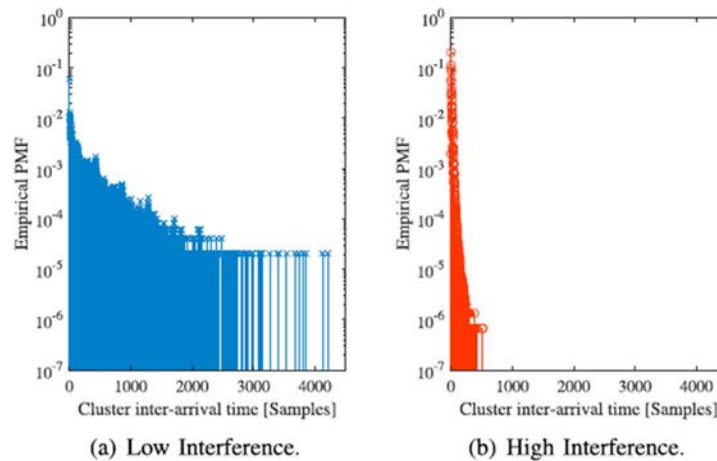


Figure 78: Empirical PMF of the cluster inter-arrival time in low and high interference scenarios

Table 11: Similarity between the empirical distributions of generated data and of measured data

Scenario	JSD
Low	6.0594×10^{-4}
High	1.8858×10^{-6}

Point process theory is applied not only for modelling interference in wireless networks but also, e.g. to characterize stochastic sampling in wireless sensor networks [i.29].

7 SmartBAN communication system simulator

7.0 Introduction

The system level simulator is implemented by using MATLAB R2016a with Simulink (v8.7), Communication System (v6.2), Stateflow (v8.7) and SimEvent (v5.0) Toolboxes [i.12]. Communication Toolbox includes blocks for modelling the PHY layer of a node and hub, SimEvent contains tools for event-based simulation, whereas Stateflow is for modelling the decision logic of packet retransmission.

The transceiver structure follows the technical specifications for PHY [i.1] and MAC [i.11].

7.1 Getting started

At first, it is needed to download the simulator file named *SmartBAN_simulator.zip*. Then it has to unzip the file and get:

```

\Results
\Results\Plot_Results.m
initMask.m
myAWGN.m
myBCH.m
myBCHdecoder.m
myFadingChannel.m

```


myInterference.m

myRepetition.m

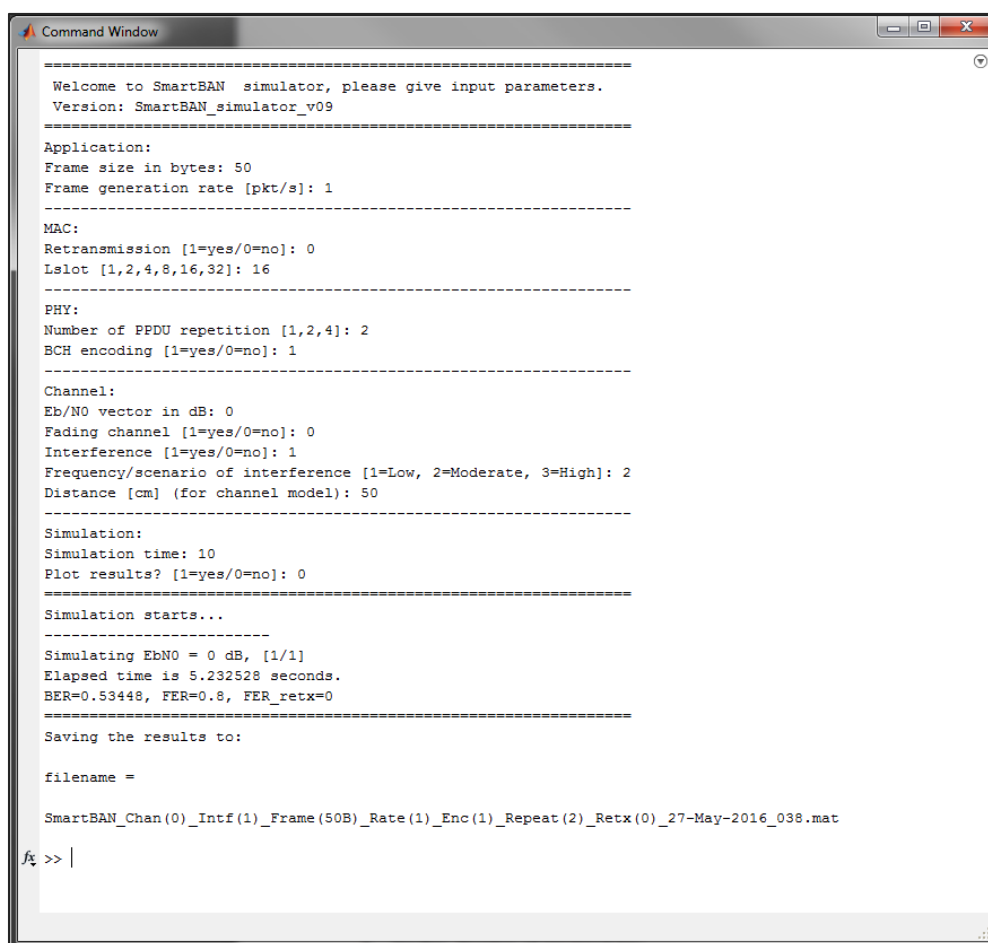
run_SmartBan.m

SmartBAN_simulator.mdl

The *Results* -folder is for saving simulation results. There is also a script for plotting the results named as *Plot_Results.m*. The next seven files are used in simulations, the last one is the simulator model and *run_SmartBan.m* is for running the simulator from the command line. By typing the following, it starts simulation:

```
>> run_SmartBan
```

The simulator asks simulation parameters, as shown in Figure 79 The Simulink model of the SmartBAN simulator is shown in Figure 80



```

Command Window
=====
Welcome to SmartBAN simulator, please give input parameters.
Version: SmartBAN_simulator_v09
=====
Application:
Frame size in bytes: 50
Frame generation rate [pkt/s]: 1
=====
MAC:
Retransmission [1=yes/0=no]: 0
Lslot [1,2,4,8,16,32]: 16
=====
PHY:
Number of PPDU repetition [1,2,4]: 2
BCH encoding [1=yes/0=no]: 1
=====
Channel:
Eb/N0 vector in dB: 0
Fading channel [1=yes/0=no]: 0
Interference [1=yes/0=no]: 1
Frequency/scenario of interference [1=Low, 2=Moderate, 3=High]: 2
Distance [cm] (for channel model): 50
=====
Simulation:
Simulation time: 10
Plot results? [1=yes/0=no]: 0
=====
Simulation starts...
-----
Simulating EbN0 = 0 dB, [1/1]
Elapsed time is 5.232528 seconds.
BER=0.53448, FER=0.8, FER_retx=0
=====
Saving the results to:

filename =

SmartBAN_Chan(0)_Intf(1)_Frame(50B)_Rate(1)_Enc(1)_Repeat(2)_Retx(0)_27-May-2016_038.mat

fx >> |

```

Figure 79: User interface of the simulator

When simulation is finished the results are saved to *\Results* -folder to the file *SmartBAN_Chan(0)_Intf(1)_Frame(50B)_Rate(1)_Enc(1)_Repeat(2)_Retx(0)_27-May-2016_038.mat*. The filename is updated automatically based on the parameters used and time of simulation to make it easier to distinguish different result files.

The file contains *outputs* -structure including:

- *BERvec*: Bit error rate vector, one value for each E_b/N_0 value, computed from MPDUs
- *FERvec*: Frame error rate vector, one value for each E_b/N_0 value, computed from MPDUs
- *FERretxvec*: Frame error rate vector for retransmission scheme, one value for each E_b/N_0 value, computed from MPDUs

- *SimBits*: Number of simulated bits, computed from MPDUs
- *SimFrames*: Number of simulated frames, computed from MPDUs
- *EbN0vec*: Eb/N0 vector
- *params*: Simulation parameters
- *model*: Simulator model
- *SimTime*: Simulation time (duration)
- *SimDate*: Date of simulation
- *uniqueID*: Unique identification number for a file

The results can be plotted by selecting 'yes' before starting simulations or typing:

```
>> Plot_Results('filename')
```

This will save a figure as a JPG file.

The simulator can also be opened in Simulink by double-clicking the filename or typing:

```
>> open_system('model_name')
```

The simulator parameters can be changed by double-clicking the *Simulation parameters* -block (Figure 80). If this simulation approach is used, transmitted frames, errors, retransmission, etc. can be monitored, but the results should be saved manually.

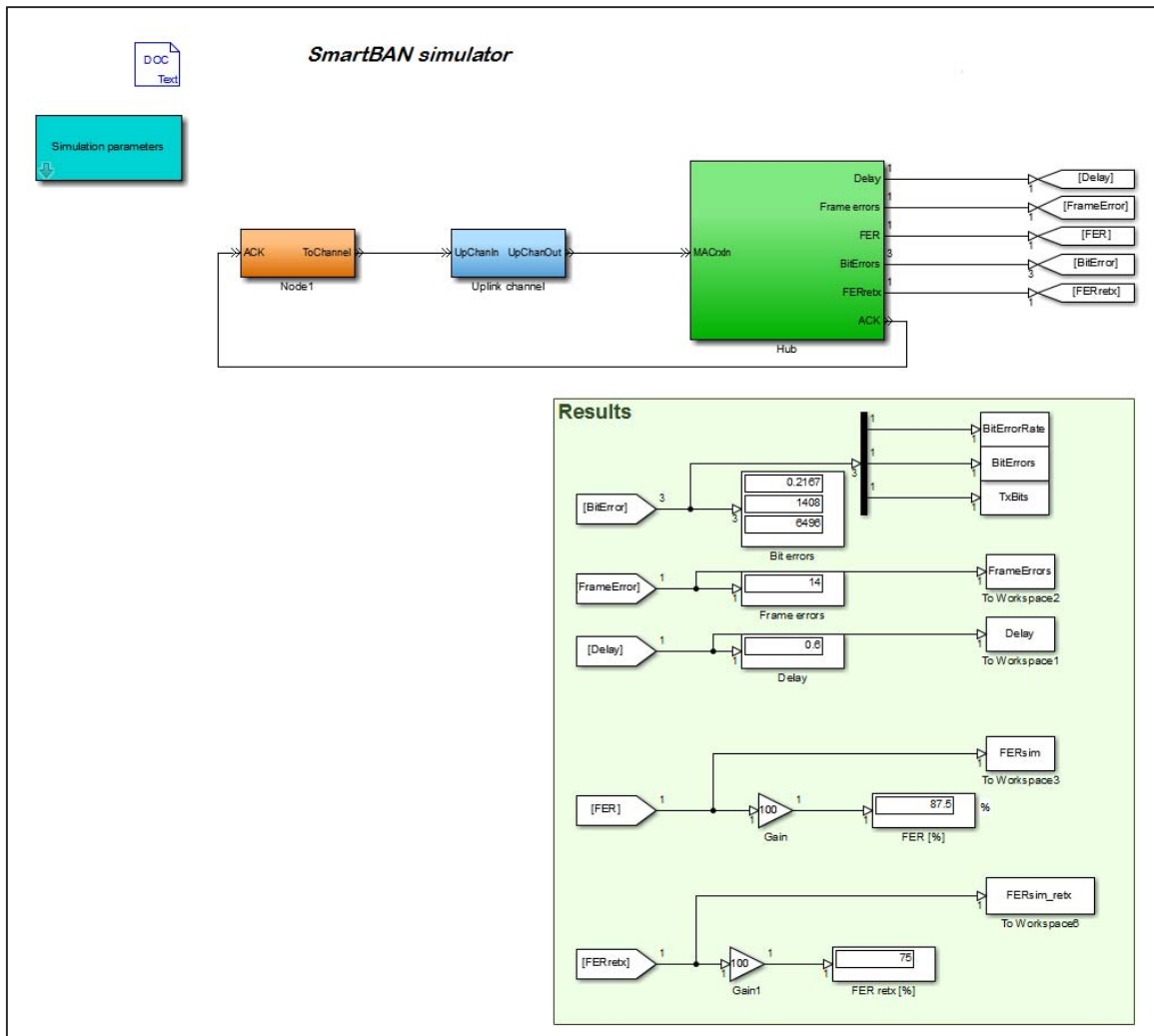


Figure 80: Simulink model of the simulator

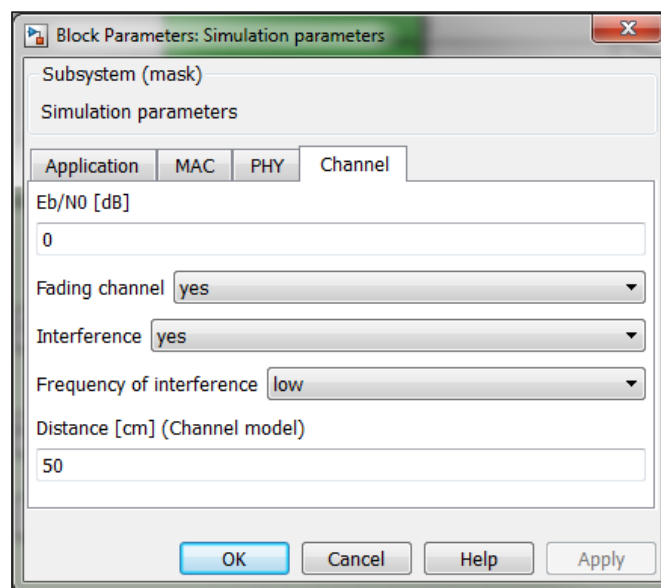


Figure 81: Graphical user interface of the simulation parameters

7.2 Simulator model

7.2.0 Introduction

The simulator model is introduced in details in this clause.

7.2.1 Node

The simulation model for node is shown in Figure 79.

Random bits form a MPDU having a size defined by the given frame size. The size of the frame is limited by a slot time T_s , which is equal to $T_{\min} \times L_{\text{slot}}$ as defined in [i.11] and the PPDU repetition. Next, the 'dummy' bits, i.e. zeros are appended as parity bits and header. Each frame has given a unique sequence number and a node number. The frame generation rate defines how often the frame is generated. The distribution of frame generation interval can be also adjusted. These features were designed keeping in mind further development of the simulator where multiple nodes, and hence, medium access is implemented.

The *Admission control* -block is for admitting a new frame to proceed where permission is given by the transmitter logic.

The lower part of the transmitter structure is for the retransmission procedure. All frames are replicated and saved to a buffer. Based on *FrameError* in the received acknowledgement frame, the frame is discarded, i.e. the port switch p has the value of 2. The frame is retransmitted only once, therefore the port switch q is set to 1. T_x and $Retx$ are the gate release triggers deciding if a new frame or old frame proceeds.

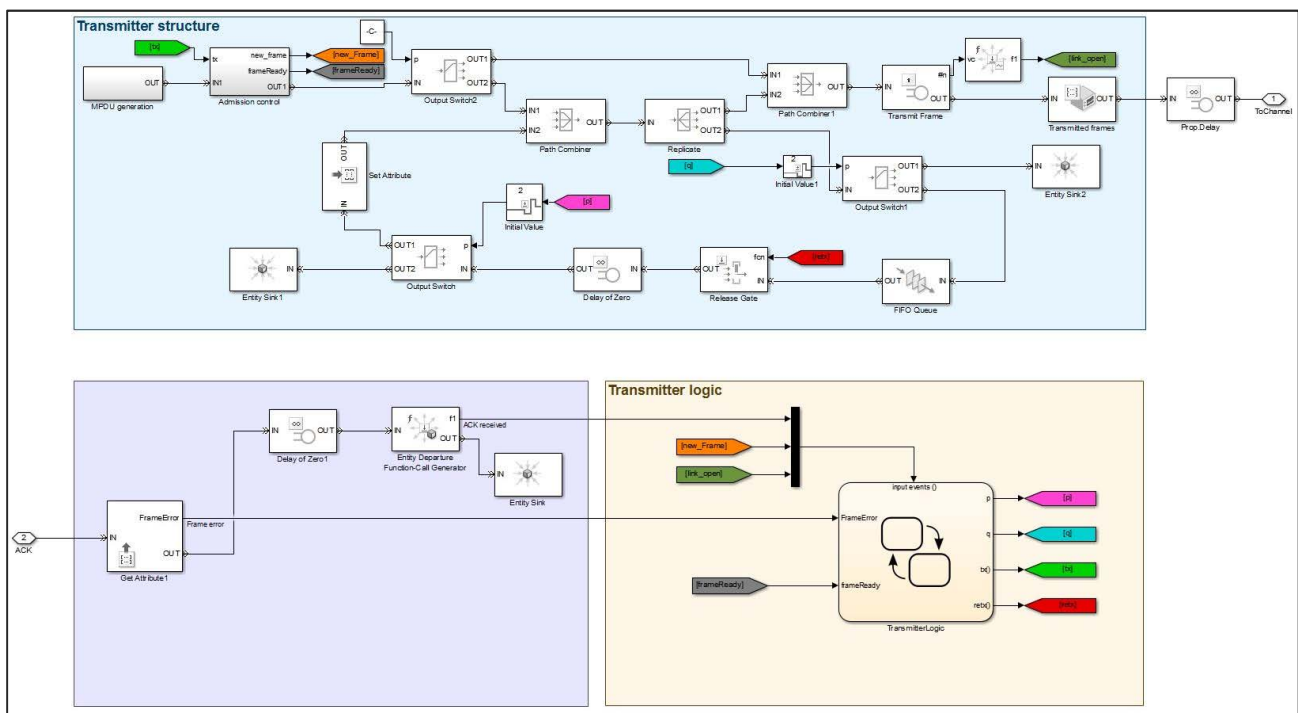


Figure 82: Node model

7.3 Hub

7.3.0 Introduction

The hub contains a full PHY layer transceiver chain including the noise and fading channel. This approach solves issues using SimEvents and Communication System blocks together. Hub model is shown in Figure 83.

- *Fading channel*: Option to have a fading channel on or off.
- *Interference*: Option to have an interference on or off.
- *Interference frequency/scenario*: Low, moderate or high, see clause 6.4 for details.
- *Distance*: The channel model use pathloss to define fading process, distance in centimetres.
- *Simulation time*: Duration of the simulation.
- *Plotting*: Option to plot a figure.

7.4 PHY layer

7.4.0 Introduction

The physical layer model, shown in Figure 84, follows the technical specification of SmartBAN PHY [i.1]. For definitions of applied MATLAB functions, objects and blocks, see MATLAB Help [i.12].

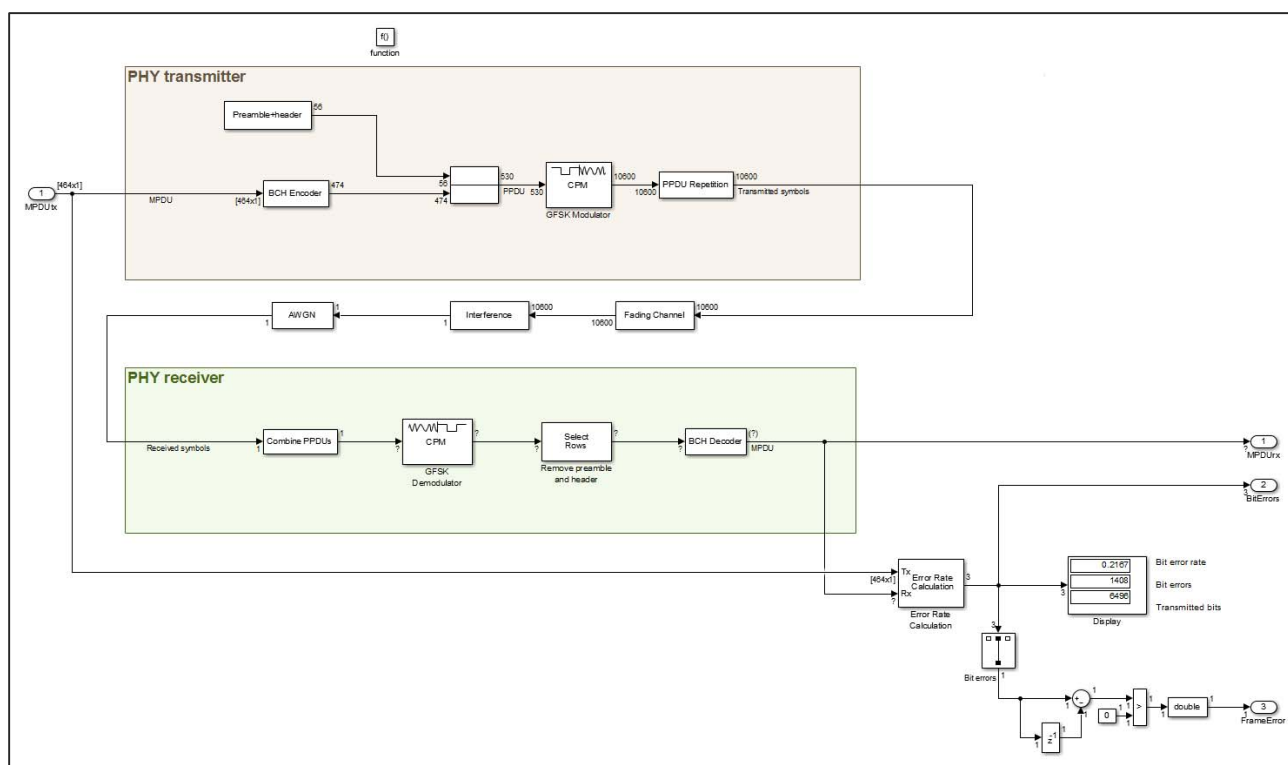


Figure 84: PHY layer model

7.4.1 PHY transmitter

The generation of a transmitted PPDU is as follows:

- *BCH Encoder*: MPDU is encoded as defined in clause 7.3.2 of ETSI TS 103 326 [i.1]. Due to the delay of the GFSK demodulator, additional zeros are appended which are removed before the decoding process.
- *Preamble+header*: PSDU is formed by appending random bits as PLCP header and preamble.
- *GFSK Modulator*: The modulator generates symbols according to clause 7.2 of ETSI TS 103 326 [i.1]. It uses 20 samples per symbol, pulse length of 1, modulation index (h) of 0,5 and bandwidth-time product (BT) of 0,5.
- *PPDU Repetition*: PPDU is repeated by 1, 2 or 4 times as given in clause 7.3.1 of ETSI TS 103 326 [i.1].

7.4.2 Channel, interference and noise

7.4.2.0 Introduction

The transmitted signal goes through a fading channel, if it is selected. The channel is assumed as constant for each PPDU. After that, interference and noise are added to the signal. The applied channel model is the IEEE 802.15.6 [i.16] body surface to body surface CM3 (Scenario S4 & S5) for 2,4 GHz [i.13], where flat small-scale fading is represented by a Ricean distribution with K factor:

$$K_{\text{dB}} = K_0 - m_K PL_{\text{dB}} + \sigma_K n_K, \quad (35)$$

where:

- $K_0 = 30,6$ dB;
- $m_K = 0,43$ dB/cm;
- $\sigma_K = 3,4$ dB.

Pathloss (PL_{dB}) is given by:

$$PL_{\text{dB}} = -10\log_{10}(P_0 e^{-m_0 d} + P_1) + \sigma_P n_P \text{ [dB]}, \quad (36)$$

where:

- $P_0 = -25,8$ dB;
- $m_0 = 2,0$ dB/cm;
- $P_1 = -71,3$ dB;
- $\sigma_P = 3,6$ dB;
- $d =$ distance.
- Calculated pathloss of the IEEE 802.15.6 [i.16] CM for $d = 45$ cm is shown in Figure 82.

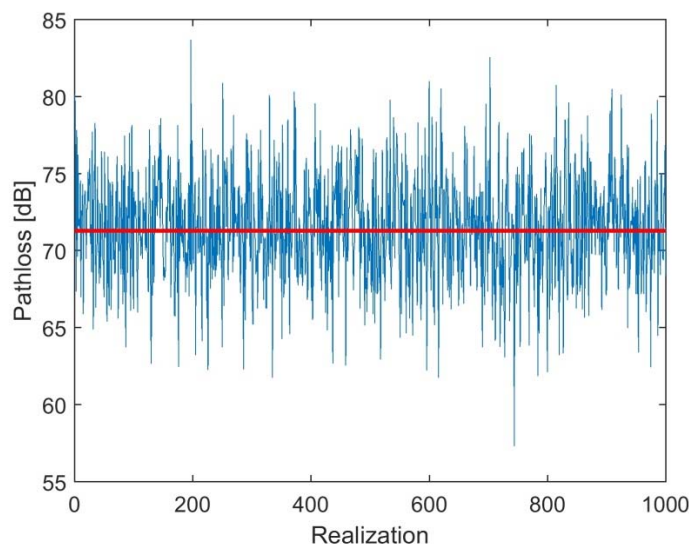


Figure 85: Pathloss of the IEEE 802.15.6 [i.16] CM for $d = 45$ cm

7.4.2.1 Interference

The generated interference vector is added with the signal in this block. The frequency or scenario is either low, moderate or high as selected at the beginning of the simulation. These models are discussed in clause 6 in detail.

Figure 86 illustrates one interference realization for each interference scenario. 12 000 samples correspond to one transmitted PPDU with 50 octets frame body size.

The interference matrix having 100 realizations used in the simulation is generated in the `initMask.m` function. For high interference frequency, a pre-generated interference matrix saved into `IntfMatrix_HIGH_100real.mat` is used. The MAC frame size for high interference frequency is only 50 octets. The use of pre-generated interference matrices in the simulations is justified by high memory allocation and processing time of interference generation, especially when using high interference frequency.

An interference level is adjusted so that path loss given in equation (36) and the signal transmission power of -10 dBm, as defined in [i.16], are met.

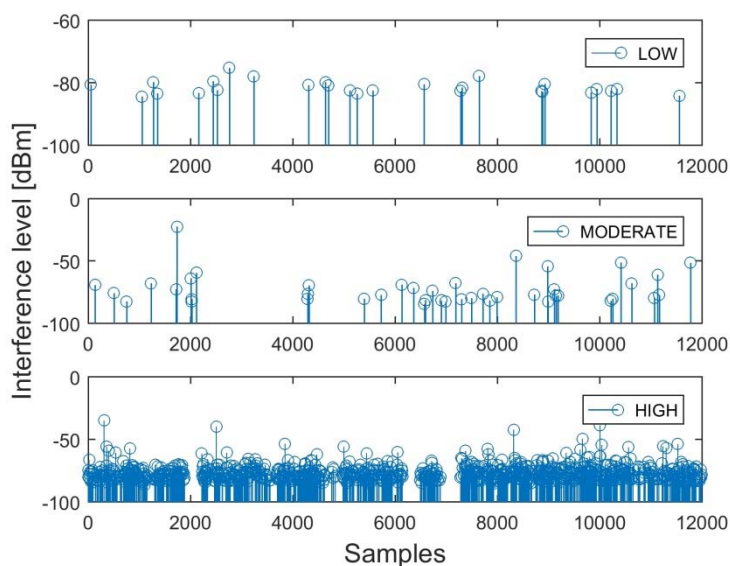


Figure 86: Interference realizations

7.4.3 PHY receiver

The signal is received as follows:

- 1) *Combine PPDUs*: Received PPDUs are combined by using the Equal Gain Combining (EGC) method, where perfect channel phase estimation is assumed.
- 2) *GFSK Demodulator*: The demodulator is an optimum one where a correlator is followed by a Maximum-Likelihood Sequence Detector (MLSD). The Viterbi algorithm is used to perform MLSD. The demodulator has the traceback depth parameter D influencing the output delay, which is the number of zero symbols that precede the first meaningful demodulated value in the output. The "five-time-constraint-length" rule is used to estimate the optimal traceback depth [i.1]. It corresponds to $5 \times \log_2(\text{numStates})$, where:

$$\text{numStates} = \begin{cases} p \cdot M^{(L-1)}, & \text{for even } m \\ 2p \cdot M^{(L-1)}, & \text{for odd } m, \end{cases} \quad (37)$$

where: m is the numerator of modulation index;
 p is the denominator of the modulation index;
 M is the M-ary number;
 L is the pulse length.

- 3) *Remove Preamble and Header*: The block removes the preamble and PLCP header.
- 4) *BCH Decoder*: The block decodes the input signal.

- 5) *Error Rate Calculation*: It calculates the transmitted bits, bit errors and bit error rate. The frame error rate is also calculated.

7.5 MAC - Frame retransmission

A user can select if a frame retransmission is enabled or not. If a frame is corrupted, i.e. having $FrameError=1$, then the frame is retransmitted once. *ReceiverLogic* --chart sends an ACK-frame including an indication of frame error introduced in Figure 87 The chart has the following inputs and outputs:

- p : indicates a port of a switch to be selected. '1' is for discard, '2' for retransmission and '3' for reception.
- $send_ack$: a generated event for ACK frame.
- $FrameError$: indicates if a frame is corrupted or not.
- $FrameRetransmitted$: parameter indicating if a frame is retransmitted or not.

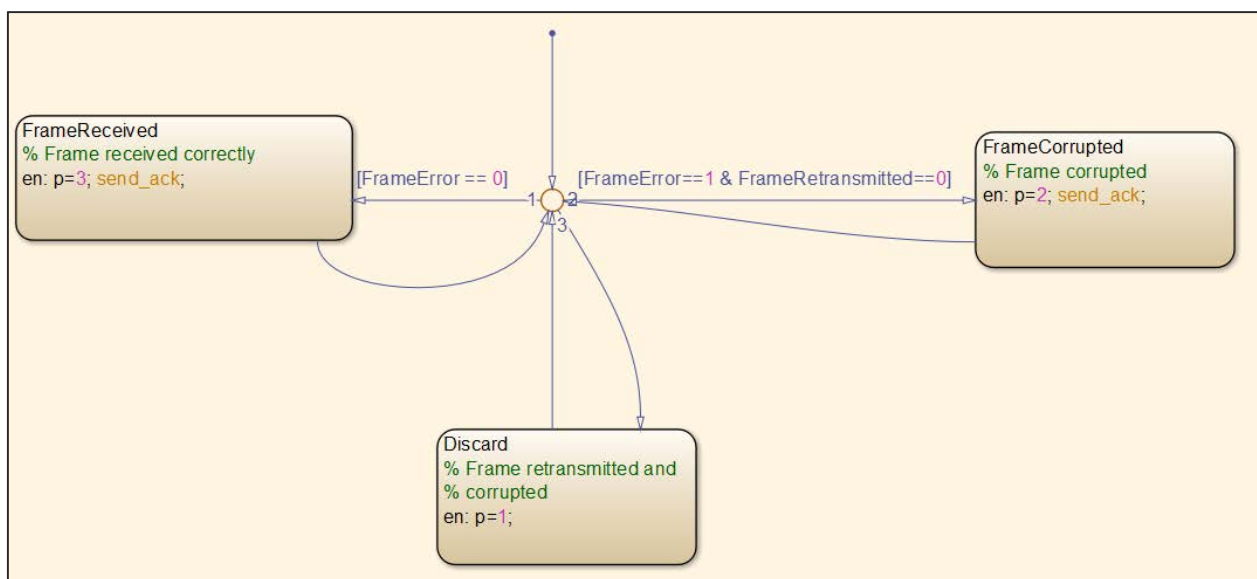


Figure 87: Receiver logic

TransmitterLogic -chart, shown in Figure 88 decides if a new frame transmission or retransmission takes place. Decision logic is as follows:

- At the beginning of a simulation, there is a frame generated. *Transmitting* -state is selected and entry (en) values are given; the frame is replicated ($q = 2$) and saved to a buffer and tx is sent. When the frame has been transmitted transition guards are checked in this order:
 - 1) ACK frame is received (new_ack) and there is no error ($FrameError = 0$). If it is true, discard an acknowledged frame by setting $p = 2$, $q = 2$ and send $retx$ and proceed to a connective junction.
 - 2) ACK frame is received and there is error ($FrameError = 1$), move to *Retransmitting* -state if retransmission is enabled ($Retx = 1$). When entering to the state, release a buffered frame ($p = 1$, $retx$) and do not buffer it again ($q = 1$).
 - 3) Otherwise, move directly to the connective junction.
- Connective junction:
 - 1) Proceed to *Idle* -state if there is no frame to transmit ($FrameReady = 0$).
 - 2) Return to *Transmitting* -state if a frame is ready.

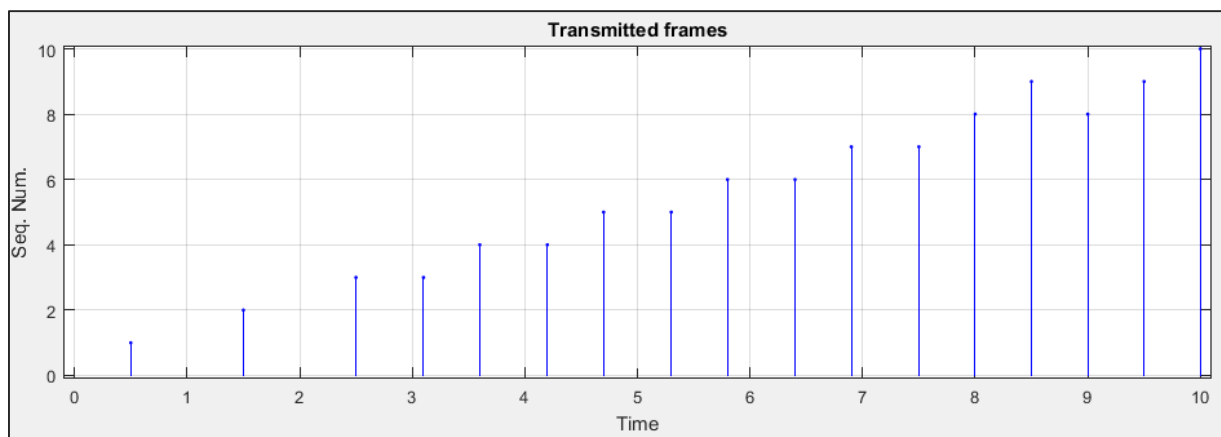


Figure 89: Transmitted frames

7.6 Verification results

For binary Gaussian Frequency Shift Keying (GFSK) with modulation index $h=1/2$, the bit error probability P_b at high E_b/N_0 is closely approximated by [i.14] and [i.15].

$$P_b = Q\left(\sqrt{2 \cdot \frac{E_b}{N_0}}\right). \quad (38)$$

Figure 90 shows the results of the verification simulations. The following conclusion can be drawn: the simulation result (Uncoded, $PPDU_{rep} = 1$) follows the theoretical bit error probability given above. $PPDU_{rep}$ indicates the number of PPDU repetitions.

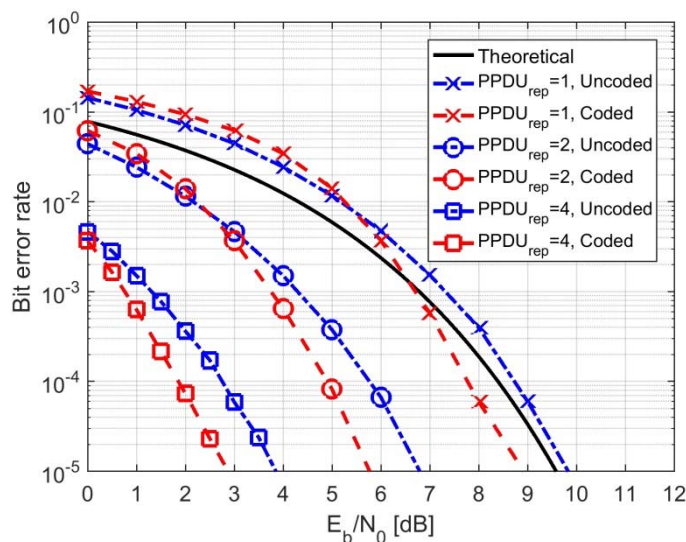


Figure 90: Verification results

8 Simulation results

8.0 Introduction

Simulation results using the simulator described earlier are given in this clause. Clause 8.1 gives the simulation parameters, clause 8.2 includes the results in AWGN channel, clause 8.3 fading channel results and clause 8.4 results with the interference.

8.1 Simulation parameters

Table 12 summarizes the used simulation parameters. Parameters related to the SmartBAN transceiver are directly from the technical specifications, channel parameters are introduced in clause 7.3.2 and interference is discussed in clause 6.

Table 12: Simulation parameters

Parameter	Value(s)	Unit	Explanation
noRepeatPPDU	1,2,4	-	PPDU repetition
Retx	no, yes	-	Retransmission
frameSize	50, 250, 500, 1 000	octets	MAC frame body [octets]
EbN0	-	dB	E_b/N_0 vector
packetGenRate	100	pps	Packet generation rate
NoSamplesPerSymbolGFSK	20	samples	The number of output samples for each bit
PulseLengthGFSK	1	symbols	The length of the frequency pulse shape
TraceBackDepth	10	-	The number of trellis branches used to construct each traceback path
distance	45	cm	Distance for the channel model
Lslot	32	-	Defines the size of Ts, and therefore, limits the size of the MAC frame body
enableChannel	no, yes	-	Enable channel
enableBCH	no, yes	-	Enable encoding, n = 127, k = 113
enableInterference	no, yes	-	Enable interference
freqInterference	low, moderate, high	-	Frequency/ scenario of interference
NoInterferenceRealization	100	-	Number of interference realizations
simuTime	2 000	s	Simulation time
NoSimulatedFrames	40 000	frames	Number of frames to be simulated per E_b/N_0 value

8.2 AWGN channel

The simulation results in the AWGN channel is applied to define the requirement for the receiver sensitivity as in clause 8.9.1 of the IEEE 802.15.6 standard [i.16]. As defined in the standard, it is assumed that PSDU is 255 octets, noise figure is 13 dB and the implementation losses is 6 dB. The total loss is defined as:

$$S_{\text{dBm}} = -174 \text{ dBm} + NF_{\text{dB}} + \frac{E_b}{N_0} + 10 \cdot \log_{10}(R) + I_{\text{dB}} \quad (39)$$

where:

NF_{dB} is the noise figure in dB;

E_b/N_0 is threshold value for FER < 10 % in dB;

R is the data rate;

I_{dB} is the implementation losses in dB.

Figures 91 and 92 represent the simulation results in the AWGN channel for BER and FER, respectively, and Table 13 gives the receiver sensitivity numbers according to the simulation results and equation (39).

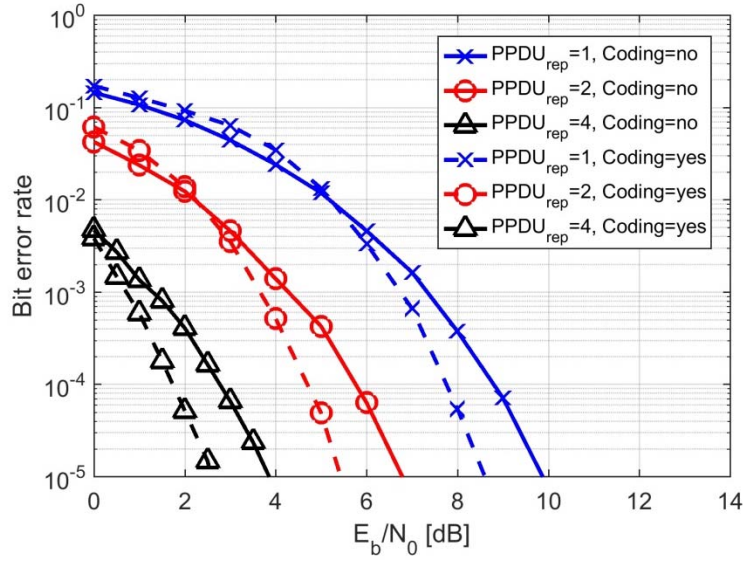


Figure 91: AWGN, BER

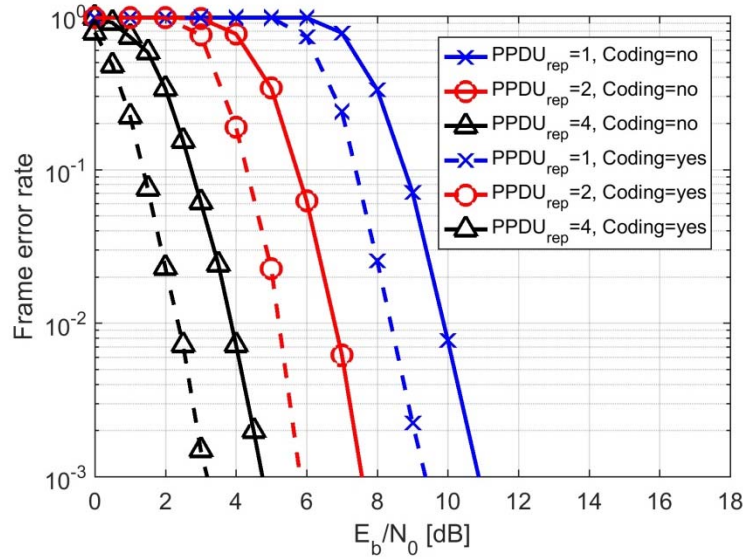


Figure 92: AWGN, FER

Table 13: Receiver sensitivity numbers

Symbol rate (Msymbols/s)	Code rate	Repetition	Information rate (Mbps)	E_b/N_0 , FER =10%	Maximum input level at sensitivity (dBm)
1,0	1	1	1,0	8,8	-86,2
1,0	1	2	0,5	5,8	-92,2
1,0	1	4	0,25	2,8	-98,2
1,0	113/127	1	0,89	7,4	-88,1
1,0	113/127	2	0,44	4,3	-94,3
1,0	113/127	4	0,22	1,4	-100,2

8.3 Fading channel

The simulation results using encoding in the fading channel are presented in Figures 93 to 81. Figure 97 gives the results for BER using 1-, 2- and 4-time PPDU repetition ($PPDU_{rep}$). Next figures illustrate FER for 50-, 250-, 500- and 1 000-octets MAC frame body without and with retransmission (Retx). The 4-time PPDU repetition cannot be applied for 1 000-octets frame body due to the limitation of the packet length given in clause 8.1 of ETSI TS 103 326 [i.1]. Table 14 gives the E_b/N_0 values for the FER level of 1 % and 10 %.

Table 14: E_b/N_0 values for FER=[1, 10] %

FER		10 %		1 %	
Retransmission		w/o Retx	w/ Retx	w/o Retx	w/ Retx
Frame size	$PPDU_{rep}$				
50	1	16	9,4	26,3	15,3
	2	8,8	5,0	13,9	8,6
	4	3,8	1,5	7,3	3,7
250	1	17,7	9,8	27,8	16,2
	2	9,1	5,4	15,0	8,7
	4	4,2	2,4	7,2	4,1
500	1	17,7	10,2	28,2	16,4
	2	9,5	6,4	15,1	9,4
	4	5,3	2,6	7,6	5,3
1 000	1	17,8	10,4	28,3	16,9
	2	9,6	6,4	15,9	9,6

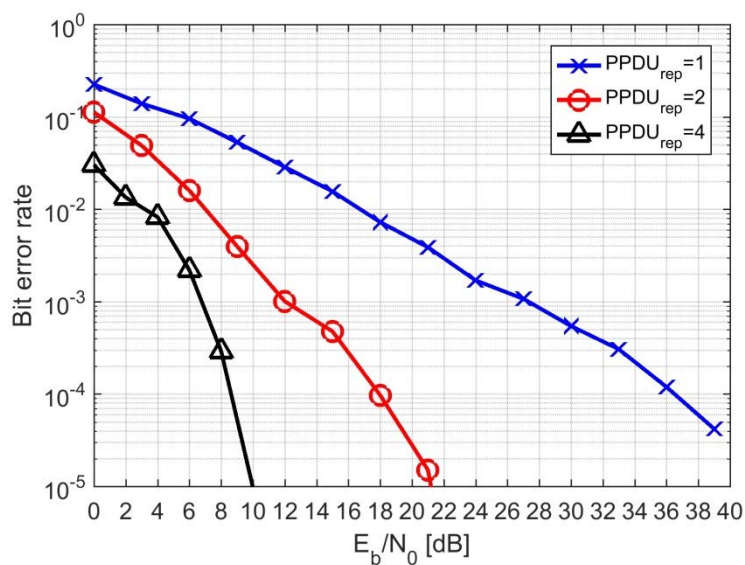


Figure 93: Fading channel, BER

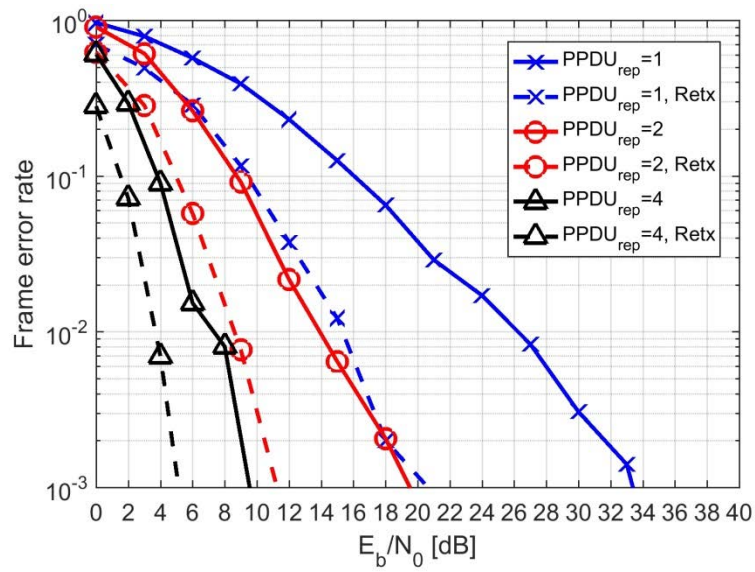


Figure 94: Fading channel, FER, frame size = 50 octets

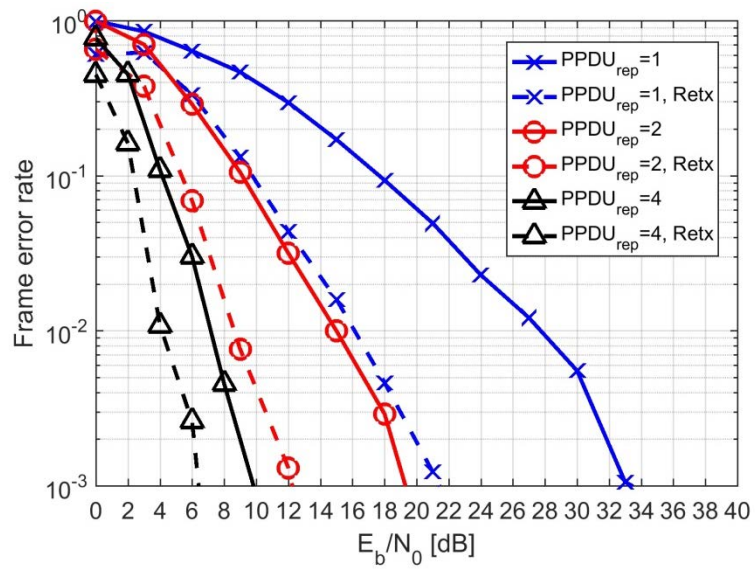


Figure 95: Fading channel, FER, frame size = 250 octets

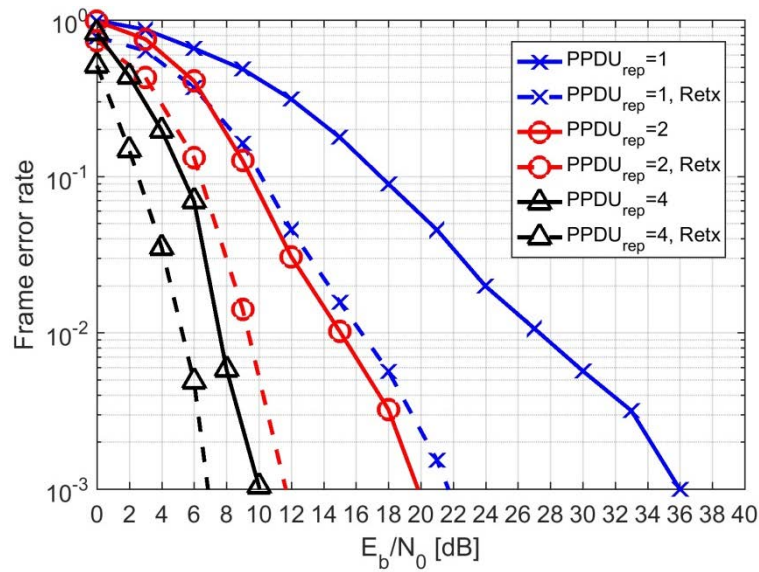


Figure 96: Fading channel, FER, frame size = 500 octets

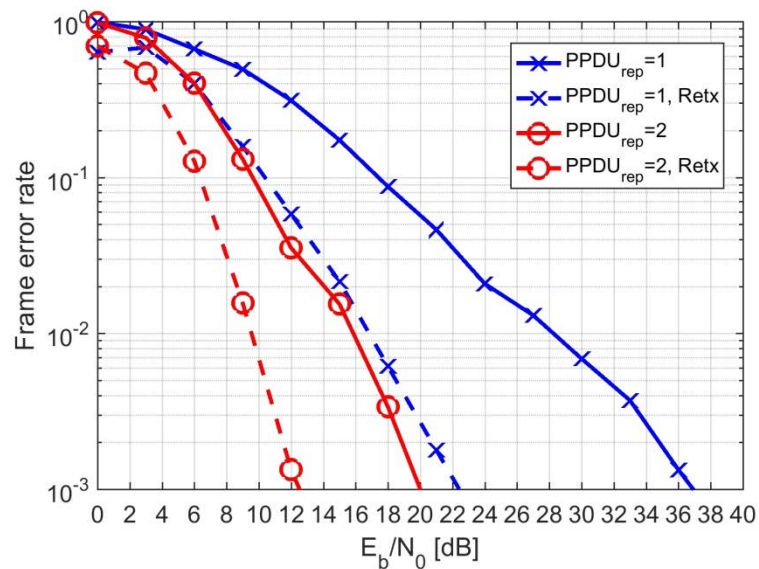


Figure 97: Fading channel, FER, frame size = 1 000 octets

8.4 Fading channel and interference

Figures 98 and 99 present the simulation results using the fading channel and interference. The frame body size of 50 octets was applied. An interference scenario is either low, moderate or high. As results show, the interference has minimal impact on the system performance when the interference scenario is low. Other interference scenarios cause a great distortion to a received signal.

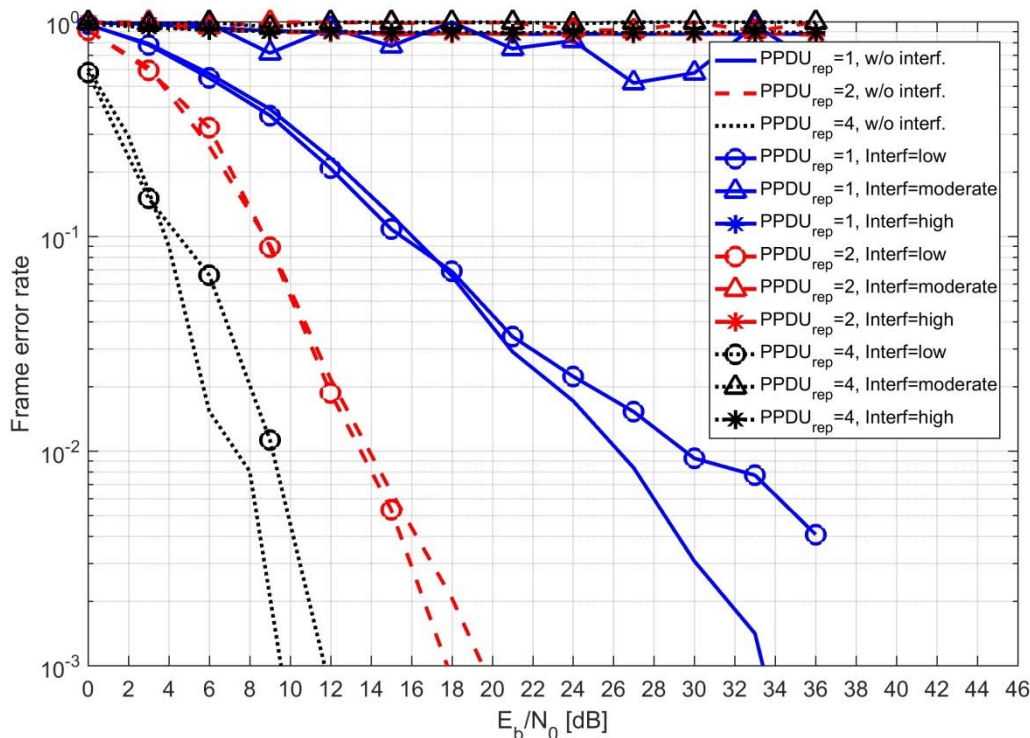


Figure 98: Fading channel and interference, FER, frame size = 50 octets

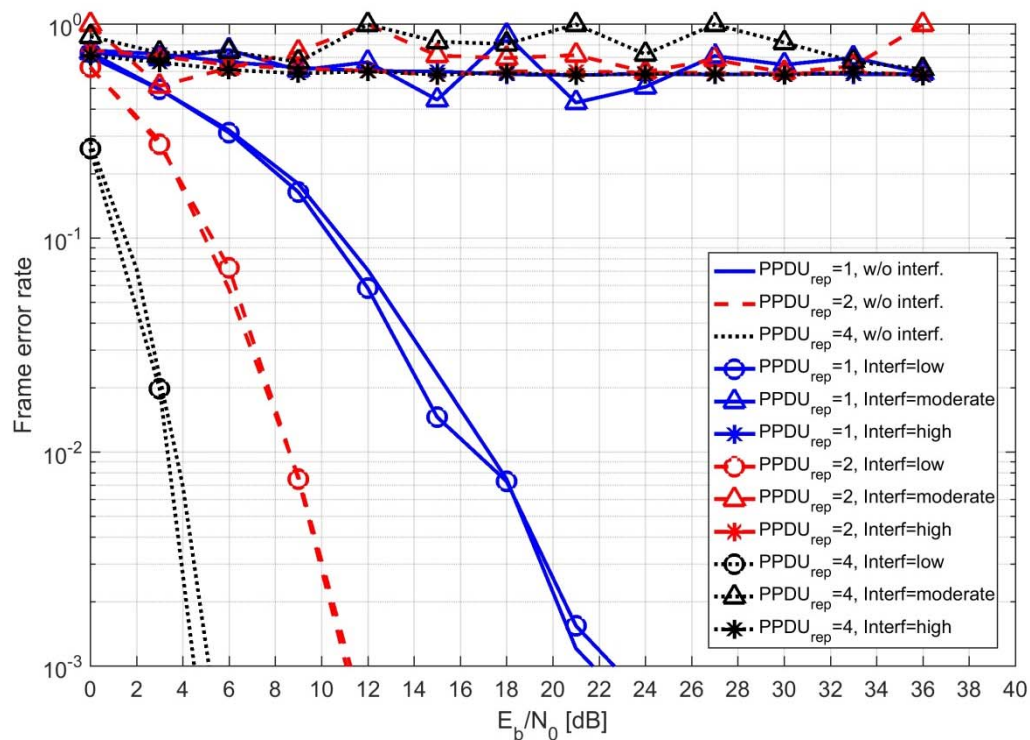


Figure 99: Fading channel and interference, FER with retransmission, frame size = 50 octets

8.5 Discussion

This clause presents the simulation results of the SmartBAN PHY with and without transmission of a PPDU. The SmartBAN receiver was implemented by using optimal solutions. The coherent demodulator applied a correlator followed by the Viterbi implementation of MLSD. In the diversity combining of PPDU, an EGC combinator assuming the perfect channel phase estimation was implemented. These choices give a basis for further receiver design.

The simulator gives a possibility to implement channel access logic and study channel access delay of a SmartBAN system at some level. It requires copies of nodes and a stateflow chart modelling the logic for channel access. Since the simulator is modular, it is straightforward to study other receiver structures. Future work could also include studies using other channel models than the IEEE 802.15.6 [i.16] model.

The system performance in an interfered fading channel needs more detailed studies. Now, the simulations were completed by using the transmitted power of -10 dBm and the IEEE 802.15.6 [i.16] channel model. The average pathloss for 45 cm is -71,3 dB. When comparing the received signal power to the interference levels as illustrated in Figure 98 it is obvious that when the intensity of the interference rises, the system performance falls.

Annex A: Spatial Sample Clustering Algorithm

Spatial Sample Clustering Algorithm is presented here. For more details and the exact method to use the algorithm, please refer to [i.8].

Part 1 Data Declaration (SSC)

Input Data:

- 1: $S(n)$ \leftarrow sample space where n represents the samples.
- 2: RB_{40} \leftarrow Relative bandwidth for IEEE 802.11n
- 3: RB_{20} \leftarrow Relative bandwidth for IEEE 802.11b/g
- 4: RB_{NB} \leftarrow Relative bandwidth for NB Systems
- 5: RB_{Set} \leftarrow Array of relative bandwidths for all systems
- 6: MG_{WB} \leftarrow Max. Gap limit for wideband systems
- 7: MG_{NB} \leftarrow Max. Gap limit for narrowband systems
- 8: MG_{Set} \leftarrow Array of gap limits for all systems
- 9: N \leftarrow Noise threshold for the current sweep given by Med-FCME
- 10: $BinWidth$ \leftarrow Width of one individual sample in whole sample space
- 11: f_{cSet40} \leftarrow A set of legitimate center frequencies (in MHz) of IEEE 802.11n
- 12: f_{cSet20} \leftarrow A set of legitimate center frequencies of (in MHz) IEEE 802.11b/g

Variables:

- 13: EI \leftarrow End index, i.e., index of the last sample
 - 14: ECI \leftarrow 0, Edge check index, i.e., Index of the sample under observation
 - 15: SB_{II} \leftarrow 0, Index of initial signal boundary
 - 16: SB_{FI} \leftarrow 0, Index of final signal boundary
 - 17: $Pivot_{Index}$ \leftarrow 0, Index of the pivot sample
 - 18: $SigCounter$ \leftarrow 0, Signal counter for this sweep
 - 19: $GapCounter$ \leftarrow 0, A counter for keeping track of samples below noise level
 - 20: BW_{Est} \leftarrow 0, Estimated bandwidth in MHz
 - 21: FC_{Est} \leftarrow 0, Estimated center frequency in MHz
 - 22: $Cluster(n)$ \leftarrow An array of size n to hold sample cluster, potentially a signal
 - 23: $map < k, v >$ \leftarrow A key-value pair map where values v are estimated center frequencies and the keys k are system names
 - 24: $Map < K, map < k, v >>$ \leftarrow A map containing $map < k, v >$ as value and keys are sequential integers starting from 1
 - 25: \triangleright Actual algorithm starts from Part 2.
-

Part 2 Wideband Signal Search

Initiate Wideband Signal Search

```

26: while  $ECI < EI$  do
27:   if  $S(ECI) > N$  then
28:      $SB_{II} := ECI$ 
/*Call the LOOPER function*/
29:     LOOPER ( $S(n), SB_{II}, MG_{WB}$ )
/*Looper returns*/
30:      $BW_{Est} \leftarrow$  Estimated bandwidth
31:      $ECI \leftarrow$  Current edge index
32:      $Pivot_{Index} \leftarrow$  Current pivot element
/*Continue and Validate cluster as legitimate Signal*/
33:     Set  $SB_{FI} = ECI$ 
34:     switch  $BW_{Est}$  do
35:       case  $BW_{Est} \geq RB_{40}$ 
/*Mark an IEEE 802.11n signal*/
36:         Increment  $Sig_{Counter}$ 
37:          $FC_{Est} = \operatorname{argmin}|Pivot_{Index} - fc_{Set40}|$ 
38:         Add  $FC_{Est}$  to  $map < k, v >$ 
39:         Set  $K := Sig_{Counter}$ 
40:         and  $V := map < k, v >$ 
41:         Add  $K, V$  to  $Map < K, V >$ 
42:         Mark  $S(n)$  from  $SB_{II}$  to  $SB_{FI}$  as NaN
43:       case  $BW_{Est} \geq RB_{20} \ \&\& \ BW_{Est} < RB_{40}$ 
/*Mark an IEEE 802.11b/g signal*/
44:         Increment  $Sig_{Counter}$ 
45:          $FC_{Est} = \operatorname{argmin}|Pivot_{Index} - fc_{Set20}|$ 
46:         Add  $FC_{Est}$  to  $map < k, v >$ 
47:         Set  $K := Sig_{Counter}$ 
48:         and  $V := map < k, v >$ 
49:         Add  $K, V$  to  $Map < K, V >$ 
50:         Mark  $S(n)$  from  $SB_{II}$  to  $SB_{FI}$  as NaN
51:       case None of the above
52:         Cluster invalid, false alarm
53:     else
54:       Increment  $ECI$ 
55:     end if
56:   end while
57:
58: Reset all counters except  $Sig_{Counter}$ 
59:   ▷ Send the modified  $S(n)$  in which, wideband signal cluster/clusters (if any) are marked
   NaN, for Narrowband search.

```

Part 3 Narrowband Signal Search

Initiate Narrowband Signal Search

```

60: while  $ECI < EI$  do
61:   if  $S(ECI) > N$  then
62:      $SB_{II} := ECI$ 
/*Call the LOOPER function*/
63:     LOOPER ( $S(n), SB_{II}, MG_{NB}$ )
/*Looper returns*/
64:      $BW_{Est} \leftarrow$  Estimated bandwidth
65:      $ECI \leftarrow$  Current edge index
66:      $Pivot_{Index} \leftarrow$  Current pivot element
/*Continue and Validate cluster as legitimate Signal*/
67:     if  $BW_{Est} \geq RB_{NB}$  then
68:       Increment  $Sig_{Counter}$ 
69:        $FC_{Est} = Pivot_{Index}$ 
70:       Add  $FC_{Est}$  to  $map < k, v >$ 
71:       Set  $K := Sig_{Counter}$ 
72:       and  $V := map < k, v >$ 
73:       Add  $K, V$  to  $Map < K, V >$ 
74:     end if
75:   else
76:     Increment  $ECI$ 
77:   end if
78: end while
79:

```

▷ Return the $Map < K, V >$ to the main Script.

Part 4 LOOPER Function

```

80: function LOOPER( $S(n), SB_{II}, MaxGap$ )
81:    $Sample_{Counter} = 0$ 
82:   while  $Gap_{Counter} \leq MaxGap \parallel ECI \neq EI$  do
83:     for ( $j = SB_{II}; j \leq ECI; j++$ ) do
84:       if  $S(j) > N$  then
85:         Increment  $Sample_{Counter}$ 
86:         Add  $S(j)$  to  $Cluster(j)$ 
87:         Mark  $Pivot_{Index} = argmax|Cluster|$ 
88:         Set  $Gap_{Counter}=0$ 
89:       else if  $S(j) < N$  then
90:         Increment  $Gap_{Counter}$ 
91:       end if
92:       if  $Gap_{Counter} == MaxGap$  then
/*Edge check index becomes the current sample index*/
93:         Set  $ECI = j$ 
/*Bandwidth estimate of the cluster in MHz*/
94:          $BW_{Est} = \frac{Sample_{Counter} \times BinWidth}{10e6}$ 
95:         Break
96:       end if
97:     end for
98:   end while
99:   return  $BW_{Est}, ECI, Pivot_{Index}$ 
100: end function

```

History

Document history		
V1.1.1	December 2016	Publication
V1.1.2	June 2021	Publication